

PROJECT ADMINISTRATION DATA SHEET

ORIGINAL

REVISION NO. _____

Project No. G-35-651 (R6020-OA0)

GTRC ~~XXX~~

DATE 8 / 28 / 85

Project Director: Tim Long *LOLAND TIMOTHY LONG*

School ~~XXX~~

Geo Sci

Sponsor: U. S. Nuclear Regulatory Commission

Type Agreement: Contract No. NRC-04-85-122

Award Period: From 8/1/85 To 7/31/88 (Performance) 7/31/88 (Reports)

Sponsor Amount:

This Change

Total to Date

Estimated: \$ 100,000

\$ 278,921

Funded: \$ 100,000

\$ 100,000 (Through 7/31/86)

Cost Sharing Amount: \$ may be added later

Cost Sharing No: G-35-324

Title: Georgia/Alabama Regional Seismographic Network

ADMINISTRATIVE DATA

OCA Contact

Brian J. Lindberg

X4820

1) Sponsor Technical Contact:

2) Sponsor Admin/Contractual Matters:

~~Dr. Andrew Murphy~~ *qu Long* DR. ERNST ZURFLUEH

Ronald D. Thompson

U. S. Nuclear Regulatory Commission

Contracting Officer

Mail Stop: 1130-SS

Division of Contracts

Washington, DC 20555

U. S. Nuclear Regulatory Commission

(301) 427-4078

Mail Stop: AR-2223

Washington, DC 20555

Defense Priority Rating: N/A

Military Security Classification: N/A

(or) Company/Industrial Proprietary: N/A

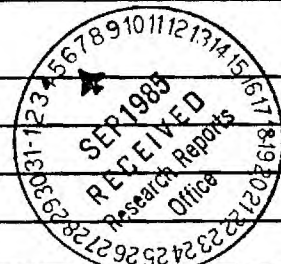
RESTRICTIONS

See Attached N/A Supplemental Information Sheet for Additional Requirements.

Travel: Foreign travel must have prior approval - Contact OCA in each case. Domestic travel requires sponsor approval where total will exceed greater of \$500 or 125% of approved proposal budget category.

Equipment: Title vests with GIT

COMMENTS:



COPIES TO:

SPONSOR'S I. D. NO. 02.106.000.86.001

Project Director
Research Administrative Network
Research Property Management
Accounting

Procurement/GTRI Supply Services
Research Security Services
Reports Coordinator (OCA)
Research Communications (2)

GTRC
Library
Project File
Other Jones

GEORGIA INSTITUTE OF TECHNOLOGY
OFFICE OF CONTRACT ADMINISTRATION

NOTICE OF PROJECT CLOSEOUT

Closeout Notice Date 03/04/91
Original Closeout Started 08/29/90

Project No. G-35-651 _____ Center No. R6020-0A0 _____

Project Director LONG L T _____ School/Lab E & A SCI _____

Sponsor NUCLEAR REGULATORY COMM/GENERAL _____

Contract/Grant No. NRC-04-85-122 _____ Contract Entity GTRC

Prime Contract No. _____

Title GA/AL REGIONAL SEISAMOGRAPHIC NETWORK _____

Effective Completion Date 900731 (Performance) 901031 (Reports)

Closeout Actions Required:	Y/N	Date Submitted
Final Invoice or Copy of Final Invoice	Y	_____
Final Report of Inventions and/or Subcontracts	N	_____
Government Property Inventory & Related Certificate	Y	_____
Classified Material Certificate	N	_____
Release and Assignment	Y	_____
Other _____	N	_____
Comments _____		

Subproject Under Main Project No. _____

Continues Project No. _____

Distribution Required:

Project Director	Y
Administrative Network Representative	Y
GTRI Accounting/Grants and Contracts	Y
Procurement/Supply Services	Y
Research Property Management	Y
Research Security Services	N
Reports Coordinator (OCA)	Y
GTRC	Y
Project File	Y
Other _____	N
_____	N

Georgia/Alabama Regional Seismographic Network

Final Report
August 1985–October 1990

Prepared by L. T. Long

**School of Earth and Atmospheric Sciences
Georgia Institute of Technology**

**Prepared for
U.S. Nuclear Regulatory Commission**

AVAILABILITY NOTICE

Availability of Reference Materials Cited in NRC Publications

Most documents cited in NRC publications will be available from one of the following sources:

1. The NRC Public Document Room, 2120 L Street, NW, Lower Level, Washington, DC 20555
2. The Superintendent of Documents, U.S. Government Printing Office, P.O. Box 37082, Washington, DC 20013-7082
3. The National Technical Information Service, Springfield, VA 22161

Although the listing that follows represents the majority of documents cited in NRC publications, it is not intended to be exhaustive.

Referenced documents available for inspection and copying for a fee from the NRC Public Document Room include NRC correspondence and internal NRC memoranda; NRC Office of Inspection and Enforcement bulletins, circulars, information notices, inspection and investigation notices; Licensee Event Reports; vendor reports and correspondence; Commission papers; and applicant and licensee documents and correspondence.

The following documents in the NUREG series are available for purchase from the GPO Sales Program: formal NRC staff and contractor reports, NRC-sponsored conference proceedings, and NRC booklets and brochures. Also available are Regulatory Guides, NRC regulations in the *Code of Federal Regulations*, and *Nuclear Regulatory Commission Issuances*.

Documents available from the National Technical Information Service include NUREG series reports and technical reports prepared by other federal agencies and reports prepared by the Atomic Energy Commission, forerunner agency to the Nuclear Regulatory Commission.

Documents available from public and special technical libraries include all open literature items, such as books, journal and periodical articles, and transactions. *Federal Register* notices, federal and state legislation, and congressional reports can usually be obtained from these libraries.

Documents such as theses, dissertations, foreign reports and translations, and non-NRC conference proceedings are available for purchase from the organization sponsoring the publication cited.

Single copies of NRC draft reports are available free, to the extent of supply, upon written request to the Office of Information Resources Management, Distribution Section, U.S. Nuclear Regulatory Commission, Washington, DC 20555.

Copies of industry codes and standards used in a substantive manner in the NRC regulatory process are maintained at the NRC Library, 7920 Norfolk Avenue, Bethesda, Maryland, and are available there for reference use by the public. Codes and standards are usually copyrighted and may be purchased from the originating organization or, if they are American National Standards, from the American National Standards Institute, 1430 Broadway, New York, NY 10018.

DISCLAIMER NOTICE

This report was prepared as an account of work sponsored by an agency of the United States Government. Neither the United States Government nor any agency thereof, or any of their employees, makes any warranty, expressed or implied, or assumes any legal liability of responsibility for any third party's use, or the results of such use, of any information, apparatus, product or process disclosed in this report, or represents that its use by such third party would not infringe privately owned rights.

Georgia/Alabama Regional Seismographic Network

Final Report
August 1985–October 1990

Manuscript Completed: November 1990
Date Published: November 1990

Prepared by
L. T. Long

School of Earth and Atmospheric Sciences
Georgia Institute of Technology
Atlanta, GA 30332

Prepared for
Division of Engineering
Office of Nuclear Regulatory Research
U.S. Nuclear Regulatory Commission
Washington, DC 20555
NRC FIN D1598
Under Contract No. NRC-04-85-122

EXECUTIVE SUMMARY AND ABSTRACT

OBJECTIVE:

The objective of this study was to contribute data and analyses conducive to the development of criteria for establishing earthquake hazard potential in the southeastern United States.

TASKS:

The first task was to provide support for the installation and maintenance of the Georgia/Alabama Regional Seismographic Network. The network is an educational and research component of the School of Earth and Atmospheric Sciences at The Georgia Institute of Technology. During this project, the seismic network consisted of seven stations in Alabama, five stations in southeastern Tennessee, two stations in South Carolina and five to eight stations in Georgia. The seismic net included three three-component short-period stations. All data were telemetered to Georgia Tech in Atlanta, Georgia, for recording on analog recorders and event recorded on a digital computer.

The second task was to monitor the seismic activity in southeastern Tennessee, northern Alabama, and Georgia. The data were used and continue to be used in appropriate topical studies.

RESULTS:

The Georgia/Alabama regional Seismographic Network has enhanced the understanding of seismicity in the southeastern United States by (1) identifying and defining mechanisms for distinct types of earthquakes, (2) contributing data to other investigators, and (3) supporting topical studies on seismological problems related to the propagation and generation of seismic waves.

(1) Studies made possible by the Georgia/Alabama Regional Seismographic Network have led to the development of a theory to explain major intraplate earthquakes. The model for major intraplate earthquakes explains how tectonic plate stress can be converted or concentrated for release in major intraplate earthquakes. The process starts by a decrease in the strength of the lower crust (most likely by a change in the fluid regime) and a subsequent weakening of the stress channel, the mid-crustal zone of high strength subject to forces at plate boundaries. The decrease in strength allows deformation in a central core (the weakened zone) and a concentration of stress on the boundary of this core. Further weakening and the concentration of stress at the edge of the core can lead to a major earthquake. Following a major

earthquake, the area remains active in an extended aftershock sequence. The mechanism is explained in Long (1988) and is given in this report.

In this study, we have related the focal mechanisms of earthquakes in southeastern Tennessee to theoretical computations of stress in and around a weak zone consistent with the model of Long (1988). **There is a strong implication in the analyses and data from this and related studies that a major earthquake has occurred (or could occur) in the southeastern Tennessee seismic zone.** We base this conclusion on the following observations:

1) Focal mechanism of small earthquakes in southeastern Tennessee correlate with a pattern of stress consistent with a weak zone in a compressed plate.

2) The pattern of epicenters extending in a northeast-southwest direction in southeastern Tennessee is very similar in shape and size to the New Madrid seismic zone.

3) Travel time residuals suggest anomalously low velocity in a zone southwest of Knoxville.

4) Coda decay in local earthquakes suggest anomalously low Q in a zone southwest of Knoxville.

5) The seismicity underlies a sedimentary basin which penetrates to depths of seven kilometers into the crust.

6) The earthquakes occur at depths of 8 to 20 km, and can not be explained by surface phenomena.

7) The gravity and magnetic data suggest that the crust responsible for the seismicity is a Precambrian rift, analogous in structure and composition to the crust underlying the New Madrid seismic zone.

The existence of nuclear power plants within a radius of 400 km from southeastern Tennessee conveys a need for careful monitoring of the seismicity of southeastern Tennessee.

The potential existence of a crustal zone capable of supporting a major intraplate earthquake in the southeastern United States may be limited to southeastern Tennessee (and Charleston, South Carolina). Other areas of observed seismicity, such as the Piedmont of Georgia and South Carolina, are populated by a distinctly different type of earthquake. Earthquakes in the Piedmont crystalline province are shallow (less than 5 km deep), are consistent with failure along existing joints, are predominantly associated with reservoir impoundment, and with this mechanism may have a practical upper magnitude limit of 5.7.

The seismicity of Alabama, apart from events in northeastern Alabama associated with the southeastern Tennessee seismicity, is largely induced by coal mining practices, such as the longwall method of extraction, and are typically shallow collapse events.

(2) The network data have been routinely made available to the community and published in the SEUSSN Bulletin.

(3) Topical studies at Georgia Tech have used the network data as a basis for numerous observational studies and for comparisons with theoretical exercises. Topical studies include: (1) an investigation of a strata collapse behind a longwall in an Alabama coal mine, (2) a study of reservoir induced events in the Richard B. Russell reservoir area showing correlation of the events with the Middleton-Loundesville Fault Zone, and (3) focal mechanisms in southeastern Tennessee showing a pattern of stress orientation consistent with a weak zone in a stressed crust as the cause of the southeastern Tennessee seismicity.

TABLE OF CONTENTS

	<u>page</u>
Executive Summary and Abstract	iii
Table of Contents	vi
List of Figures	vii
List of Tables.....	x
Georgia/Alabama Regional Seismographic Network	1
Objectives.....	1
Summary of Results and Findings	2
Network maintenance and seismic monitoring	2
Graphical representation of operational status	2
Recorded seismicity.....	2
Continuation of network studies.....	3
Abstracts of Presentations	4
Results of topical Studies	21
The mechanism of Major Intraplate Earthquakes.....	21
Finite Difference Applications.....	24
Reservoir Induced Seismicity.....	24
Coda Synthesis and Inversion.....	24
Mining Events.....	25
Appendix A. Modeling the seismic P coda as the response of a discrete-scatterer medium	32
Appendix B. A model for major intraplate continental earthquakes	73
Appendix C. A local weakening of the brittle-ductile transition can explain some intraplate seismic zones.....	88

LIST OF FIGURES

	<u>page</u>
Figure 1. Seismic stations maintained or monitored	26
Figure 2a-d. Graphical representation of station coverage for reporting period.....	27
Figure 3. Seismic events reported and located by the seismic network.....	31
Appendix A	
Figure 1. Relation among scattering angle, emergent angle and location of source, scatterer, and receiver....	56
Figure 2. System response of Georgia Tech seismic network	57
Figure 3. Scatterer based polar coordinate system	58
Figure 4. Coordinate system used to determine polarization of the scattered S-wave	59
Figure 5. Radiation patterns for granite scatterer embedded in sandstone host.....	60
Figure 6. Radiation patterns for basalt scatterer embedded sandstone host.....	61
Figure 7. Scattered responses for granite scatterer in sandstone host.....	62
Figure 8. Combined response for attenuation and scattering.....	63
Figure 9. One-scatterer model and synthetic seismogram...	64
Figure 10. Alabama blast model.....	65
Figure 11. Comparison of observed blast, emergent onset, with synthetic seismograms.....	66
Figure 12. Comparison of observed blast, impulsive onset, with synthetic seismograms.....	67
Figure 13. Schematic model for horizontal layer of scatterers.....	68

Figure 14. Model and synthetic seismogram for horizontal layer of scatterers.....	69
Figure 15. Earthquake model.....	70
Figure 16. Synthetic seismograms generated using earthquake model.....	71
Figure 17. P-wave codas of earthquakes recorded in Tennessee.....	72

Appendix B

Figure 1. Illustration of the five phases of a major intraplate earthquake.....	86
Figure 2. Pattern of seismicity and focal mechanisms for southeastern Tennessee; a possible example of phase 3. Pattern of seismicity for New Madrid; a possible example for phase 5.....	87

Appendix C

Figure 1. Seismicity of southeastern Tennessee.....	107
Figure 2. Focal mechanism solutions and epicenters in the central zone.....	108
Figure 3. Dip of the B axis of the focal mechanism solution for the central zone.....	109
Figure 4. Difference between the dip of the tension axis and the dip of the pressure axis.....	110
Figure 5. Model for a single circular zone of weakening in a horizontal crustal plate.....	111
Figure 6. Stress surrounding a weak circular zone in a horizontal crustal plate.....	112
Figure 7. Deviatoric stresses surrounding a weak zone in a horizontal crustal plate.....	113
Figure 8. Dilatation surrounding a weak zone in a horizontal crustal plate.....	114
Figure 9. Deviatoric stress for two circular zones of weakened crust aligned parallel to the applied stress....	115

Figure 10. Deviatoric stress for two circular zones of weakened crust aligned perpendicular to the applied stress.....	116
Figure 11. Deviatoric stress for two circular zones of weakened crust aligned at 45 degrees to the direction of applied stress.....	117
Figure 12. Geologic model for a vertical profile across a zone of weakness in the crust.....	118
Figure 13. Deviatoric stress in a vertical section across a zone of weakness in the crust.....	119
Figure 14. Model for crustal stress surrounding a zone of weakness in the lower crust.....	120

LIST OF TABLES

Appendix A

Table 1. Properties for typical geologic materials..... 56

Appendix B

Table 1. Conventional Paradigms and Alternates..... 77

Appendix C

Table 1. Earthquake locations and focal mechanisms..... 106

GEORGIA/ALABAMA REGIONAL SEISMOGRAPHIC NETWORK

Objectives

The objective of this study was to contribute data and analyses conducive to the development of criteria for establishing earthquake hazard potential in the southeastern United States. The main tasks were to install and maintain a seismic network and to monitor the seismic activity in eastern Tennessee, northern Alabama, and Georgia. The data were contributed to the southeastern U. S. regional bulletin. Also, available information was used in appropriate topical studies.

Specific objectives for network maintenance and seismic monitoring were as follows:

- * Install or provide about 16 short-period seismograph stations deployed in Tennessee, Alabama, and Georgia. This network was to be operated with a maximum of 5 percent downtime.
- * Obtain and/or reaffirm use permits and telemetry service to convey the data to a central recording point.
- * Provide all seismic phase readings and hypocenter locations to the Southeast U. S. Seismographic Network Bulletin.
- * Provide a recording medium with on-line digital recording at the Central Recording Facility.
- * Report any significant earthquake within the study region to the Nuclear Regulatory Commission within 24 hours.
- * Relocate and/or establish new seismograph stations as it becomes necessary after approval of the Nuclear Regulatory Commission.

Objectives for topical studies are as follows:

- * Study the spatial and temporal distributions, including earthquake recurrence rates, of seismicity and relate them to structural features.
- * Identify parameters that influence seismic processes within the network area and use these in defining seismogenic/tectonic provinces.
- * Study crustal and upper mantle velocity structure in the United States based on the current data from the network.
- * Study the magnitudes of historic events using magnitude-felt area

relationships and obtain the magnitude-frequency relationships.

* Evaluate the relative significance of results obtained in each of the above analyses as they impact the determination of seismic hazards.

Summary of Results and Findings

Network maintenance and seismic monitoring

During the period of 1 August, 1985, to 31 July, 1989, the Georgia/Alabama Regional Seismic Net recorded data from 22 stations located as shown in figure 1. The Clarks Hill Reservoir Area and the area of Lake Richard B. Russell were monitored by five stations. The state of Georgia was monitored by five additional stations. Seven stations were located in Alabama and five in southeastern Tennessee. The Alabama, Tennessee and northwest Georgia stations constitute coverage for the termination of the Southern Appalachian seismic zone. System calibration was maintained by periodic laboratory evaluation of individual stations. During June 1989 a recalibration of all stations was completed.

Graphical representation of operational status

Downtime was a strong function of season, principally because of failures induced by lightning or corrosion. Georgia and the southeastern United States experience the second highest lightning strike incidence in the United States. Downtime at station CH6 was due to lumbering activity. The phone line service provided by Georgia Power was terminated in 1988 and station TVG will be down until alternatives are found or until a local net is reinstalled near TVG in 1991 to monitor the filling of the reservoir. The graphical representation of the operational status of the network is given in the form of the daily log of recording and is given in figure 2a-d.

Recorded Seismicity

The earthquakes recorded on the Georgia/Alabama Regional Seismographic Network have been published in the Southeastern United States Seismic Networks Bulletin. The principal areas for contribution are Alabama, Georgia and southeastern Tennessee. Supplemental data for events in South Carolina, North Carolina and the remainder of Tennessee were reported for special and large events. The seismicity reported by this project are plotted on figure 3.

Continuation of network studies

During the unfunded extension from August, 1989, to October 31, 1990, the contract provided only communication costs for the network. Most importantly, the extension has provided time to complete some of the topical studies initiated during the final year. Also, the extension has provided time to phase down the size of the network. Repair and maintenance will be absorbed by Georgia Tech to the extent possible. Following completion of the contract on October 31, 1990, the seismic data will continue to be recorded. As station fail, they will be taken off line. Georgia Tech will continue to maintain a teaching and research seismic net in Georgia for which alternate communication facilities are available.

Many of the topical studies were these topics under investigation by master's and Ph.D. students. Such students often need more time to develop background materials and capabilities and they do not feel constrained by contract deadlines. The unfunded continuation allowed students theses that are nearing completion to be recognized as contributing to the project. Topics of these theses are as follows:

(1) The inversion of short period surface waves in Alabama is a Master's thesis topic for Argun Kocaoglu. The study used the Rg phase which is well recorded from the many mining related events in central Alabama. The group velocity for each path was computed from spectral amplitude versus group velocity plots generated by using a maximum entropy spectral estimator. These group velocities were used in a tomographic determination of the group velocity in selected blocks. After solving for the group velocity in each block, the structure for the block was obtained by inversion of the computed group velocity. The method resolved structures to a depth of 2.5 km.

(2) The frequency dependence of amplitude decay in the shear or Lg waves in Alabama was the Master's thesis topic of David Chen. Approximately 25 events recorded at a minimum of 3 stations were chosen for spectral analyses of the shear or Lg arrival. The distance range of the recordings in Alabama are 25 to 150 km, with some events recorded at 250 km in southeastern Tennessee. Estimates of spectral amplitude from 0.5 Hz to 32 Hz in 6 dB increments were obtained from blasts digitized since system calibration in June 1989. A least squares reduction for attenuation rates included station corrections and equivalent source amplitude as a function of frequency.

(3) The modeling of seismic coda was the Ph.D. topic of Mitch Craig and the results of this study are presented in Appendix A. The model is essential for developing an inverse technique for computing the spatial distribution of scattering intensity and attenuation.

Abstracts of Presentations

Abstracts of talks which were made possible by data and research related to the Georgia/Alabama Regional Seismographic Network are presented below. These abstracts cover the time period of August 1985 to completion of the contract.

ATTENUATION OF THE LG WAVE IN NORTHERN ALABAMA

DEMERE, Judy and LONG, L.T., School of Geophysical Sciences, Georgia Institute of Technology, Atlanta, GA 30332

ABSTRACT: The maximum sustained amplitudes of the Lg phase were measured on 76 seismograms from 16 Alabama mining related events recorded on seven stations of the Georgia/Alabama Seismographic Network. Distances ranged from 30 to 300 km in the area covering the terminus of the Southern Appalachians in northern Alabama. Station corrections, S_c , were incorporated in the least squares reduction for event magnitudes using a magnitude equation in the form ($m_b = B + C \text{ Log}(\text{Dist.}) + S_c$). Stations MLA, in the thick Coastal Plane, and OCA, in the Appalachian Plateau, were consistently lower in amplitude and required positive corrections. The constant C for Alabama was 1.2, which suggests greater attenuation than implied by the 0.9 value for C in Nuttli's magnitude equation for the Central United States. By assuming an Airy phase decay rate proportional to $D^{-1/3}(\text{Sin}(D))^{-1/2}$ the rate of decay suggests an average value of $Q=800$.

A Talk presented at the Eastern Section, Seismological Society of America Meeting, October 1989.

DETERMINISTIC MODELING AND INVERSION OF THE P-WAVE CODA

CRAIG, M.S., LONG, C.F., and TIE, A. School of Geophysical Sciences, Georgia Institute of Technology, Atlanta, GA 30332

ABSTRACT: The P- and S-wave coda from earthquakes in southeastern Tennessee exhibit different degrees of scattering. In order to model zones of anomalous scattering and to model the frequency dependence of the scatterers, we assume that each scatterer is a sphere and compute the effects of propagation on each scattered wavelet. Thus, the seismic coda is modeled as a superposition of wavelets scattered from spherical heterogeneities embedded in a three-dimensional elastic medium. The scattered waves for an incident P-wave are determined for wavelengths as short as 1/3 the radius of the sphere using Bessel functions up to order 15. This provides P and SV responses as a function of scattering angle and wavelength for the material contrasts used to calculate the effects of scattering. Absorptive attenuation and scatterer response are combined in the frequency domain and minimum phase is determined by

spectral factorization. These spectral responses are calculated for each raypath, corrected for geometric spreading and free-surface effects, time-shifted according to the length of the travel path and superimposed to obtain the complete coda. The inverse method combines coda information from a group of seismograms recorded by a regional network. Since each arrival in a coda corresponds to a raypath from source to scatterer to receiver, the arrival time constrains the scatterer to lie on a shell which encloses the source and receiver. Areas intercepted by the shell are assigned weights depending on the energy density of the coda at the corresponding time and the properties of the propagation path. By stacking data from several earthquakes and stations, the principal scatterers can be resolved as points where many of the heavily weighted shells intersect.

A Talk presented at the Eastern Section, Seismological Society of America Meeting, October 1989.

THE SEISMIC CODA AS A RESULT OF SCATTERED BODY WAVES: MODELING AND INVERSE METHODS

CRAIG, M., and L.T. LONG, School of Geophysical Sciences, Georgia Institute of Technology, Atlanta GA 30332

ABSTRACT: The seismic coda is modeled as a series of wavelets scattered from spherical heterogeneities embedded in a three-dimensional elastic medium. Using this scattering model, synthetic seismograms are prepared for source and receiver locations which correspond to those of several digitally-recorded events. Both earthquakes and explosions are modeled, using oriented double-couple and spherically symmetric sources, respectively. Geometric spreading, absorptive and scattering attenuation, the free-surface effect, and instrument response are taken into account. Singly-scattered arrivals are obtained individually by calculating response and lapse time corresponding to each scatterer in the medium. This is done independently for P- and S-waves. The individual contributions are then superimposed to obtain the complete coda. The agreement between synthetic and observed seismograms is quite good in several cases.

The locations and relative contributions of the principal scatterers in a region can be determined by an inverse method which utilizes the scattering model of the seismic coda. The method combines coda information from a group of seismograms recorded by a regional network. Since each arrival in a coda corresponds to a raypath from source to scatterer to receiver, the arrival time constrains the scatterer to lie on a shell which encloses the source and receiver. In the case of a constant-velocity medium this shell is ellipsoidal with foci at the source and receiver. Areas intercepted by the shell are assigned appropriate weights depending on the energy density of the coda and a propagation

factor which includes geometrical and absorptive attenuation and normalized source amplitude. Energy density is preferred over instantaneous amplitude as a measure of coda strength because of the lesser time precision needed. By stacking data from several earthquakes and stations, the principal scatterers can be resolved as the points where many of the heavily weighted shells intersect. The resulting scatterer distribution is tested by using it as a model to generate synthetic seismograms for several combinations of source and receiver locations. This technique makes no assumption of horizontal layering and may prove more appropriate than conventional reflection or direct-raypath tomographic methods in regions where there is strong and heterogeneous scattering.

Presented at the IASPEI meeting, September 1, 1989, Turkey

A LOCAL SHALLOWING OF THE BRITTLE-DUCTILE TRANSITION CAN EXPLAIN SOME INTRAPLATE SEISMIC ZONES

LONG, L. T. and K.-H. ZELT, School of Geophysical Sciences, Georgia Institute of Technology, Atlanta GA 30332

ABSTRACT: A local decrease in the strength of the crust, which would accompany a shallowing of the brittle-ductile transition, could concentrate crustal deformation through viscous or dislocation creep in response to existing regional plate stress. Two-dimensional finite element models, which include a regional plate stress and various shapes of a local decrease in crustal strength, show concentrations of stress at the brittle-ductile transition surrounding the local decrease in strength. The deformation and stress of the model suggest that strike slip faulting should dominate in the central local area of decrease in crustal strength. Outside the central area, the deformation of the crust in the vicinity of the brittle-ductile transition predicts that the dominant strike slip faulting should exhibit components of normal and reverse faulting, and that these components should be more pronounced above the brittle-ductile transition. In southeastern Tennessee the seismicity is diffused over a narrow elliptical zone trending northeast with the greatest concentration of activity near the center. Focal mechanism solutions (43 in total) agree with the predictions of the finite element model within the confidence levels of the solutions. The central zone is characterized by deep strike slip focal mechanisms and events surrounding the central zone exhibit higher proportions of reverse or normal fault movements.

A poster paper displayed at the Symposium on Intraplate Deformation, Neotectonics, Seismicity and the State of Stress in Eastern North America, Montreal, Quebec, Canada, May 17, 1989.

RAYLEIGH-WAVE DISPERSION IN NORTHERN ALABAMA

KOCAOGLU, A. H. and L. T. Long, School of Geophysical Sciences, Georgia Institute of Technology, Atlanta, GA 30332.

ABSTRACT: Surface-wave dispersion analysis in general requires a method by which the spectrum of the non-stationary time sequence (dispersed seismic trace) can be estimated within a window along the trace. When short data segments are used, the spectral resolution of the Fourier transform is quite poor compared to the resolution of maximum entropy spectra. In this study a dispersion analysis of Rayleigh waves in Northern Alabama is carried out by using the maximum entropy spectral estimation method. The dispersion curves are obtained for a number of different raypaths defined by each source-receiver pair used in the analysis. Since the dispersion curve associated with a particular path represents an average along the path, the study area can be divided into regions where individual dispersion characteristics are assumed to be uniform. By employing a linear inversion technique, individual dispersion curves of regions can be calculated to determine the lateral variations of sediment thickness.

A talk presented at the Spring Meeting, American Geophysical Union, Baltimore, Maryland, May 8-12, 1989.

SCATTERER DISTRIBUTION DETERMINED FROM THE SEISMIC CODA

CRAIG, M. S. and L. T. Long, School of Geophysical Sciences, Georgia Institute of Technology, Atlanta GA 30332.

ABSTRACT: An inverse method is presented based on the model in which the seismic coda is composed of a series of wavelets scattered from heterogeneities embedded in an elastic medium. By applying the method to digital earthquake seismograms from a regional network, the relative contributions and locations of the principal scatterers can be determined. Each arrival in a coda corresponds to a raypath from source to scatterer to receiver. The arrival time constrains the scatterer to lie on a shell, which in the case of a constant-velocity medium is ellipsoidal with foci at the source and receiver. Areas intercepted by the shell are assigned appropriate weights depending on the energy density of the coda and a propagation factor which includes geometrical and absorptive attenuation and normalized source amplitude. Energy density is preferred over instantaneous amplitude as a measure of coda strength because of the lesser time precision needed. By stacking data from several earthquakes and stations, the principal scatterers can be resolved as the points where many of the heavily weighted shells intersect. This process is equivalent to a diffraction stack. The scatterer distribution thus determined is tested by using it as a model to generate synthetic seismograms for several combinations of source and receiver locations. This

technique makes no assumption of horizontal layering and appears to be more appropriate than conventional exploration methods in regions where there is strong and heterogeneous scattering.

A talk presented to the Spring Meeting, American Geophysical Union, Baltimore, Maryland, May 8-12, 1989.

A COMPARISON OF TWO TYPES OF SEISMICITY IN THE STABLE CONTINENTAL INTERIOR

LONG, L. T., School of Geophysical Sciences, Georgia Institute of Technology, Atlanta, GA 30332.

ABSTRACT: Earthquakes with hypocenters near the brittle-ductile transition in the stable continental interior occur only in a few active seismic areas, such as southeastern Tennessee (SET). In contrast, earthquakes such as those in central Georgia (CG), occur typically within the top few kilometers of the crystalline crust and are more widely distributed. In addition to depth, these two earthquake source types are different in most of their other properties. The focal mechanisms from SET are dominantly strike slip with systematic variations about a central zone of active seismicity. Focal mechanisms of CG have scattered orientations which may correlate only with local joint sets. Seismic velocity and attenuation in the crust of SET are anomalously low near the central zone. Changes in these properties unrelated to geologic structure have not been noted in CG. The high-frequency spectral decay is steeper for CG source displacements than for SET. The different properties of these two source types suggest distinct and different causative mechanisms. The CG seismicity is often associated with reservoir impoundment and occurs in response to fluid penetration and weakening of near-surface joint and fracture surfaces. The SET seismicity may be the seismic response to viscous deformation of the lower crust in a local zone of decreased strength at the depths of the brittle-ductile transition. Large events of the CG source type would be limited by the size of the shallow fracture planes, whereas, major intraplate earthquakes could be initiated by the viscous deformation mechanism.

A talk presented to the Annual Meeting, Seismological Society of America, Victoria, British Columbia, April 19-21, 1989.

CRUSTAL STRESS AND FAULTING FROM MAJOR INTRAPLATE CONTINENTAL EARTHQUAKES

LONG, Leland Timothy, School of Geophysical Sciences, Georgia Tech, Atlanta, GA. 30332

ABSTRACT: A new model for major intraplate continental earthquakes is based on a transient perturbation in crustal strength. Regional

plate stress provides the driving energy, but the faulting is controlled by crustal weakening in the vicinity of the major event. The weakening is triggered by a disturbance in the hydraulic or thermal properties of the crust. The weak central zone in the lower crust deforms in response to regional plate stress and transfers the stress load to the surrounding competent crust or to the thinned stronger crust above the disturbed zone. Finite element models of the stress field caused by a weak central zone predicts that normal and reverse faulting at the edge of the central weak zone. The central weak zone would exhibit strike slip faulting. At least two distinct patterns of faulting are possible for the major earthquake. One pattern would consist of two near-vertical faults striking parallel to the direction of maximum shear stress of the regional field and extending away from diagonally opposite edges of the central zone. These faults could be connected in the central weak zone by a series of faults. This pattern is exhibited by the New Madrid seismicity. The other pattern would develop when deformation is resisted by a thinned crust above the disturbed zone. The major earthquake would occur on a reverse fault with dimensions comparable to the size of the central weak zone.

A talk presented to the Southeastern Section, Geological Society of America, Annual Meeting, Atlanta, Georgia, April 6-7, 1989.

FOCAL MECHANISMS AND CRUSTAL STRESS IN SOUTHEASTERN TENNESSEE

LONG, L. T., and K.-H. ZELT, School of Geophysical Sciences, Georgia Institute of Technology, Atlanta, Georgia 30332

ABSTRACT: The seismicity of southeastern Tennessee is diffused over a narrow elliptical zone trending northeast with the greatest concentration of activity near the center. We have obtained 43 focal mechanism solutions with confidence levels covering this activity. The central active zone is dominated by strike-slip focal mechanisms. Events surrounding the central zone exhibit higher proportions of reverse or normal fault movements. The inhomogeneous pattern of stress can be modeled by a zone of weak crust at depths of 10 to 30 km. Deformation of this zone by regional plate stress predicts the strike-slip focal mechanisms in the center. Normal and reverse components in the focal mechanisms in the surrounding area corresponding to zones of relative compression or expansion of the crust. The stress models and consistent focal mechanisms support the hypothesis (Long, 1988) that major continental earthquakes are caused by a temporary perturbation of the fluid regime and, hence, strength of the lower crust.

Presented at the Western American Geophysical Union Meeting, San Francisco, California, Wednesday morning December 7, 1988.

THE MODELING AND INVERSION OF SEISMIC CODA, WITH APPLICATIONS TO SCATTERING IN SOUTHEASTERN TENNESSEE

OGILVIE, J.S., and L. T. Long, School of Geophysical Sciences, Georgia Institute of Technology, Atlanta, GA 30332.

ABSTRACT: Compressional and shear wave coda were modeled by accumulating individual wavelets scattered by many inhomogeneities in the crust. The source wavelet was created by finding the minimum phase wavelet for a typical displacement spectra and adjusting the amplitude for the take-off angle to the scatterer from a double-couple source function. Causal constant Q attenuation and geometrical attenuation were applied for the paths to the scatterer and from the scatterer to the recorder. The spectral response of a sphere was used to create the scattered wavelet from the incident wavelet. At the receiver, the effects of a free surface and instrument response were added. Seismograms generated by this technique were remarkably similar to observed records of earthquakes from southeastern Tennessee, except for events near a suspected anomalous zone. The inversion for scattering coefficients was accomplished by a three-dimensional diffraction stack, in which energy wavelets from each coda were distributed as reflection coefficients among appropriate scatterers. Highly reflecting structures would generate high-energy arrivals in all codas and these structures should appear as large reflection coefficients. The scattering coefficients are strongly dependent on absorptive Q . They suggest that Q is a function of depth (125 at the surface to 400 at 25 km depths for the shear wave) and that anomalous zones exist in southeastern Tennessee.

A talk presented to the Eastern Section, Seismological Society of America, State College, Pennsylvania, October, 12, 1988.

INDUCED SEISMICITY AT THE RICHARD B. RUSSELL RESERVOIR

LONG, L.T., School of Geophysical Sciences, Georgia Institute of Technology, Atlanta GA 31332.

ABSTRACT: On December 12, 1987, at 03:53 UTC (10:53 P.M., EST, December 11, 1987), an earthquake of magnitude 2.3 was felt in Elbert and Hart Counties, Georgia. This and subsequent events marked the first significant reservoir-induced seismicity at the Richard B. Russell Lake. The swarm of earthquakes lasted from December, 1987, to February, 1988. Three of the 33 events were felt. Before impoundment in December, 1983, no natural seismic activity had been observed. Between December, 1983, and December, 1987, 21 earthquakes of magnitude less than one were identified. The epicenters for the three felt events were near the Middleton-Lowndesville fault zone. No significant water level changes were observed before the swarm of seismicity.

A talk presented to the Eastern Section, Seismological Society of America, State College, Pennsylvania, October, 12, 1988.

A STUDY OF THE DISTRIBUTION OF FOCAL MECHANISM SOLUTIONS OF EARTHQUAKES IN SOUTHEASTERN TENNESSEE.

ZELT, K.-H. and LONG, L. T., School of Geophysical Sciences, Georgia Institute of Technology, Atlanta, Georgia 30332-0340.

The infrequent occurrence of earthquakes in the southeastern United States and sparse seismic station coverage limits the number and distribution of first motions and SV/P amplitude ratios available for the determination of focal mechanism solutions. Subsequently, only solutions from large $M_0 > 3.0$ earthquakes are well constrained. For most of the smaller events, the sparse coverage of the focal sphere introduces ambiguity to the focal mechanism. Consequently, the certainty of determining a local stress field or a deviation from the regional stress field is limited. In southeastern Tennessee, the pattern of seismicity is diffused and cannot be associated with a distinct single fault. The majority of large events ($M_0 > 3.0$) occur near the center of southeastern Tennessee activity and have a strike-slip mechanism with predominantly north-south striking nodal planes. Outside the central zone, smaller events which may be recorded on only a few stations show a spatial distribution of normal or reverse components in the predominant strike-slip component. A statistical treatment of the distribution of first motions on the focal sphere is used to establish a measure of confidence for the focal mechanism solution of the smaller events in southeastern Tennessee and to establish the validity of the special distribution of normal and reverse components.

Presented at the American Geophysical Union, Spring Meeting, Baltimore, Maryland, May 16, 1988.

A MECHANISM FOR MAJOR INTRAPLATE EARTHQUAKES

LONG, L.T., School of Geophysical Sciences, Georgia Institute of Technology, Atlanta, GA 30332.

The seismicity associated with a major intraplate earthquake is proposed to be a transient phenomenon triggered by a perturbation in the fluid and thermal regime of the lower crust. A major intraplate earthquake has a magnitude greater than 6, and a fault rupture of crustal dimensions; 20 km or greater. Regional plate stress provides the energy, and a perturbation in the fluid content, which decreases crustal strength, determines the location. The timing of a major earthquake and the characteristics of associated seismicity may be described by a sequence of five phases in the perturbation of crustal strength. The five phases are: (1)

initiation, (2) strength corrosion, (3) stress concentration, (4) failure, and (5) crustal healing. (1) A major intraplate earthquake is initiated by the underplating at Moho depths of a portion of the continental crust. (2) A corrosion in crustal strength follows the upward migration of fluids from the area of recent underplating. (3) As a weakened central zone deforms in response to tectonic plate stress, stresses are concentrated in the surrounding rigid crust. (4) A major earthquake occurs when the stress surrounding the weakened core exceeds the crustal strength, either because the concentrated stresses are anomalously high or because the dispersing fluids have spread beyond the core. (5) The final phase in the occurrence of a major intraplate earthquake is extended aftershock activity concentrated on the fault plane of the main event. The occurrence of a major intraplate earthquake as described above releases the strain energy in a perturbed area. Additional major events would not occur there again until the strength has recovered sufficiently for a repeat of the cycle.

Presented at the American Geophysical Union, Spring Meeting, Baltimore, Maryland, May 16, 1988.

PARADIGM FOR MAJOR INTRAPLATE EARTHQUAKES

LONG, L. T., Georgia Institute of Technology, School of Geophysical Sciences, Atlanta, Georgia, 30332.

Let us discard the traditional paradigms of continental seismicity. Let us assume, instead, that the seismicity associated with a major (magnitude 6 or larger) intraplate earthquake is a transient phenomenon triggered by a perturbation in the fluid and thermal regime of the lower crust. Regional plate stress may still provide the energy, but instead of high stress triggering an event, let us assume a decrease in crustal strength in the vicinity of the major earthquake. The timing of a major earthquake and the characteristics of the associated seismicity may be described by a sequence of five phases: (1) initiation, (2) strength corrosion, (3) stress concentration, (4) failure, and (5) crustal healing. (1) A major intraplate earthquake is initiated by the under-plating at Moho depths of a portion of the continental crust. (2) A corrosion in crustal strength follows the upward migration of fluids from the area of recent underplating. (3) As a weakened central zone deforms in response to tectonic plate stress, stresses are concentrated in the surrounding rigid crust. (4) A major earthquake occurs when the stress surrounding the weakened core exceeds the crustal strength, either because the concentrated stresses are anomalously high or because the dispersing fluids have spread beyond the core. (5) The final phase in the occurrence of a major intraplate earthquake is extended aftershock activity which is concentrated on the fault plane of the main event. The occurrence of a major intraplate earthquake as described above releases the strain energy in a perturbed area. Additional major events would

not occur there again until the strength has recovered sufficiently for a repeat of the cycle.

Presented at the National Workshop on Seismogenesis in the Eastern United States, University of Illinois at Urbana-Champaign, Urbana, Illinois, April 12, 1988.

ZONES OF INDUCED SEISMICITY DEFINED BY ROCK QUALITY

SORLIEN, C. C., LONG, L. T., Georgia Institute of Technology, Atlanta, Georgia, 30332, and SCHMITT, T. J., Georgia Geologic Survey, 19 Dr. Martin Luther Dr., Atlanta, Georgia 30334.

Preliminary measurements of fracture density and rock quality have shown a relation with reservoir induced seismicity. Fracture density maps have been made at Clarks Hill Reservoir. The results show that areas of higher joint spacing correspond to zones of induced seismicity. Also, in other reservoirs, the rock type typically described as granite gneiss has shown a spatial correlation with reservoir induced seismicity. In reservoir induced seismicity, earthquakes occur by failure on pre-existing joints. Hypocentral depths of these earthquakes are typically less than 1 km, and it has been demonstrated that fracture density is not strongly dependent on depth in the first km. Therefore quantitative surface measurements of rock quality (which includes fracture density) can be extrapolated to the zone of induced earthquake nucleation. In contrast, stress may be released through creep on (foliated) schists and altered mafic rocks, explaining the lack of seismicity in those rock types. A complementary measurement of slickenside data can usually be collected on the same outcrops. Very fine scratches, and fresh slickensides in saprolite are both assumed to be related to the recent stress field. The striation data is then inverted for the local and regional stress field at time of movement. In this manner, rock quality measurements can be used to predict susceptibility to induced or natural shallow seismicity, so that important facilities can be properly sited and engineered.

Presented at the Association of Engineering Geologists, 30th Annual Meeting, Atlanta, Georgia, October 8-13, 1987.

FOCAL MECHANISM SOLUTIONS FOR NORTH GEORGIA AND SOUTHEASTERN TENNESSEE EARTHQUAKES (1982-1987).

ZELT, K.-H., and LONG, L. T., School of Geophysical Sciences, Georgia Institute of Technology, Atlanta, GA 30332-0340.

Seventy-one earthquakes recorded on the Georgia Tech Seismic Network and adjacent stations operated by the Tennessee Valley Authority and the Tennessee Earthquake Information Center were

investigated to determine focal mechanism solutions. These events occurred during the period between January 1982 and December 1986 and have epicenters in North Georgia and southeastern Tennessee. First motion data and SV/P amplitude ratios were used to determine 36 single event and two composite focal mechanism solutions. The composite solutions were determined using data of two earthquakes. The solutions include four previously published focal mechanism solutions (Teague et al., 1984). The duration magnitude ranged from 0.7 to 3.8. Focal mechanism solutions of nine events could not be restricted to a unique domain. Including both unique and multiple domain solutions the results are divided into three categories of focal mechanism solutions: Twenty-two strike-slip, nine reverse and 18 normal. Twenty of the 38 earthquakes have data coverage over all four quadrants, 17 over three quadrants and one focal mechanism solution was determined from data coverage over two quadrants. The average depth of earthquakes investigated equals 17.68 kilometers. The percent of the nodal planes that strike north-south is 59, 44.5, 27.7 and for those that strike northwest 41, 55.5, 61 for strike-slip, reverse and normal focal mechanism solutions respectively, The strike-slip, reverse and normal focal mechanism solutions have average depths of 18.4, 15.3 and 17.9 kilometers respectively.

Published as [(abs.) Seism. Res. Lettrs., Vol. 58, No. 4, 1987, p. 106]

Presented at the 59th Annual Meeting Eastern Section, Seismological Society of America, St. Louis University, St. Louis, Missouri, October 7-9, 1987.

A FINITE DIFFERENCE STUDY OF THE EFFECT OF AN OVERTHRUST ON THE PROPAGATION OF SEISMIC WAVES.

LIOW, J.-S. and LONG, L.T., School of Geophysical Sciences, Georgia Institute of Technology, Atlanta, GA 30332

A two-dimensional finite difference technique was developed to study the effect of an overthrust on the propagation of seismic waves. The structural model consists of a 3.5 km thick sedimentary layer over a crystalline basement. The P-wave velocity of the sedimentary layer and the basement are 4.5 km/s and 6.15 km/s respectively. A wedge-shaped overthrust zone with P-wave velocity of 6.05 km/s replaces part of the sedimentary layer on one side of the model. Synthetic seismograms are generated for a compression-al line source at depths of 0.5 km and 7.0 km. The amplitude variation with distance of different phases are compared for waves traveling from the opposite direction. For a source at shallow depth, the existence of the high-velocity overthrust zone causes a more rapid decay of the amplitude of the direct wave. However, the overthrust zone does not affect the P and S reflections from the bottom of the sediments and the Rayleigh waves as strongly as it

affects the direct wave. The amplitude of the secondary phases increase on traveling from the overthrust zone into the sediments. For the deeper source, the existence of the overthrust zone does not significantly affect the amplitude decay of either the direct wave or the other phases. For the deep source underneath the overthrust zone, the amplitude of the direct wave observed in the sediments within a short distance from the edge of the overthrust zone is enlarged by a factor of three. Also, more scattered phases are observed in the sediments.

Published as [(abs.) Seism. Res. Lettrs., Vol, 58, No. 4, 1987, p. 100]

Presented at the 59th Annual Meeting, Eastern Section, Seismological Society of America, St. Louis University, St. Louis, Missouri, October 7-9, 1987.

A TECHNIQUE FOR THE INVERSION OF CODA Q

LONG, L. T., LIOW, J.-S., School of Geophysical Sciences, Georgia Institute of Technology, Atlanta, Georgia 30332 and JONES, F. B., Georgia Southwestern, Department of Physics, Americus, Georgia 31709

Digital data from station CBT in southeastern Tennessee provide estimates of coda Q with variations which depend on the direction to the earthquake. We interpreted this azimuthal variation to indicate a spatial variation of the properties of the crust that determine coda Q. Coda Q is a phenomenological parameter characterizing coda decay and it is determined by the integrated effects of crustal parameters in the ellipsoidal volume of crust with the recording station and hypocenter as foci. Zones of anomalous crust will influence the computation of coda Q differently for different station and hypocenter pairs. Through a sequence of approximations, we have linearized the relation between the measured apparent coda Q and an assumed constant coda Q for discrete zones of crust. Inversion of coda Q data from regional stations in the southeastern United States suggests a reduction in coda Q as one nears the coastal plane, consistent with the results of Singh and Herrmann (1983). Inversion of coda Q data near station CBT suggests an anomalously low coda Q region ($Q=38$) in a 300 square kilometer region northeast of station CBT.

Published as [(abs.) Seis. Res. Lettrs., Vol. 58, No. 4, 1987, p. 101]

Presented at the 59th Annual Meeting, Eastern Section, Seismological Society of America, St. Louis University, St. Louis, Missouri, October 7-9, 1987.

SPECULATION CONCERNING THE EFFECTS OF ATTENUATION AND SCATTERING ON THE SPECTRAL SIGNATURE OF WAVELETS COMPRISING THE P-WAVE CODA

LONG, L. T. and ALEXANDER, C. S., School of Geophysical Sciences, Georgia Institute of Technology, Atlanta, Georgia 30332-0340

The P-wave coda is generally interpreted as P wavelets scattered from heterogeneities in the lithosphere. The spectral signature of an individual P wavelet can depend on absorptive attenuation and scattering along its propagation path. In particle velocity records, the Brune source model generates a wavelet with a spectral peak near the corner frequency. With increased time, absorptive attenuation systematically shifts the corner frequency toward lower frequencies. The spectra of wavelets scattered from heterogeneities can be complex and depends on the size of the heterogeneity. For corner frequencies below the fundamental resonance of the heterogeneity, the corner frequency is systematically shifted to higher frequencies. In moving window high-resolution spectral analysis of P-wave coda, systematic increases and decreases in spectral peaks are observed that may be explained by shifts in the corner frequency caused by absorptive attenuation and scattering.

THE SCATTERING OF A SEISMIC WAVE BY A SPHERICAL INCLUSION

AN, TIE and LONG, L. T., School of Geophysical Science, Georgia Institute of Technology, Atlanta, GA 30332-0340

We have investigated two models in which a plane P-wave is incident on a spherical inclusion. The first model is an elastic spherical obstacle in a fluid medium. The second model is a fluid sphere in an elastic medium. The computational procedure used is the resonance scattering theory developed by Uberall and his co-workers (1978-1985). For the first case, only a scattered P wave can exist, but the properties of the elastic scatterer affect the scattering coefficient, i.e. the quality factor due to the scattering. In the second case, the spectral response of the scatterer is much more complicated because of resonances in the fluid-filled obstacle. Resonance of the scatterer plays an important role in the calculations of the scattering coefficients, especially for wavelength shorter than the diameter of the scatterer. The viscosity of the solid material affects the scattering coefficients; it smoothes its shape and it shifts the resonant eigenfrequency. The background scattering coefficients, which are computed by subtraction of the portion due to the resonance from the scattering cross section, can be strong frequency dependent.

A STUDY OF CRUSTAL HETEROGENEITY IN THE SOUTHEASTERN TENNESSEE AREA BY FINITE DIFFERENCE WAVE SIMULATION

JEIH-SAN LIOW and Leland Timothy Long (Both at: School of Geophysical Sciences, Georgia Institute of Technology, Atlanta, GA 30332)

The character of seismograms recorded at station CBT depend on azimuth. Events located to the east and southeast show clean impulsive arrivals. Events located to the west exhibit greater scattering. In order to evaluate the influence of local crustal structures on scattering, a two dimensional finite difference method was used to simulate the elastic wave propagation in a crustal model for southeastern Tennessee. The model consists of a lower-velocity sedimentary basin embedded in the continental crust with both overlaid by the Paleozoic sediments of the Valley and Ridge Geologic Province. A compressional line source was placed at depths of 7 to 15 km and at different locations relative to the structure. The waves from sources that are closer to or behind the subsurface sedimentary basin show more scattering than those from sources that are located away from the sedimentary basin. The synthetic seismograms suggest that the azimuthal variations observed at station CBT may be attributed to the existence of a southwest trending sedimentary basin located to the northwest of station CBT.

A DISCUSSION OF PRECISION IN HYPOCENTER DETERMINATION

LONG, L. T., School of Geophysical Sciences, Georgia Institute of Technology, Atlanta, GA.

The weighting matrix used in location programs contains important information concerning the uncertainty in earthquake hypocenters. The off-diagonal elements which are usually ignored have significant values for P- and S-wave arrivals at the same station and at stations close together. For these arrivals the ray paths are similar and the travel time errors will be strongly correlated. The larger off-diagonal elements increase the weights that should be applied to their respective arrivals. In the special case of S- and P-wave arrivals at the same station and small reading errors, the weighting matrix is nearly singular and the resulting weights make the origin time computation virtually independent of the location. Where data are inadequate to estimate the elements of the covariance matrix, the elements may be estimated from an autocorrelation function of travel time residuals along refraction lines or from gravity data. Use of the properly formulated weighting matrix yields consistent estimates of location errors which are independent of the precision implied by station residuals. The near-singularity of the weighting matrix for P- and S-wave arrivals at the same station suggests an alternate computation method whereby the location equations containing S and P waves at each station can be transformed to isolate the origin time computation from the epicenter computations.

SCATTERING BY A SPHERICAL OBSTACLE AND IMPLICATIONS FOR P-WAVE SCATTERING AND ATTENUATION

AN TIE and L. T. Long, School of Geophysical Sciences, Georgia Institute of Technology, Atlanta, GA 30332

The scattering of a plane longitudinal wave incident on a spherical obstacle for elastic and viscoelastic host and scattering media was investigated. The spherical obstacles considered included a rigid sphere, a spherical cavity, a liquid filled cavity and an elastic sphere. The computational technique utilized an orthogonal function expansion. Numerical results were obtained for wave number-radius products of 0 to 10, extending well beyond the region of validity of the Rayleigh scattering approximation. The analysis of the scattering cross sections and back and forward scattering coefficients have shown that (1) there exists a significant contribution to scattering at the shorter wavelengths which is not consistent with the Born approximation, (2) the variation in the shear modulus is the most important factor in determining the scattering amplitudes, (3) the velocity models predict the greatest influence of scattering to be in the shallow crust, (4) negative contrasts give a stronger scattering response than positive contrasts at the same percent deviation, (5) scattering functions can be separated into continuous scattering coefficients for the background and discrete scattering frequencies for resonances (6) in viscoelastic media the scattering coefficients are a function of Q in both media and they can be separated into background scattering, resonances, the interference due to the viscosity and their contrasts of the host media and scatterer, and (7) the total Q is not a simple linear combination of absorptive and scattering Q .

THE INFLUENCE OF A VELOCITY GRADIENT ON EARTHQUAKE LOCATIONS

Long, L. T., School of Geophysical Sciences, Georgia Institute of Technology, Atlanta, Georgia 30332

Recent seismic refraction data indicate that one gradient velocity model will satisfy most travel times observed in the granitic crust of the southeastern United States. The model simultaneously explains the 6.05 km/s P-wave velocity of the Georgia Piedmont, the 6.14 km/s velocity of central Alabama, and a 6.2 km/s velocity observed for the 10 km deep north Georgia earthquake. A lower crustal velocity of 6.7 km/s is not observed except in remnants of rift zones. In the Piedmont, use of the gradient in locating earthquakes tends to decrease their depths by an average of 10 percent, relative to depths computed from a constant velocity model. Unless a station is within a distance equivalent to the depth, multiple solutions for depth may exist. For earthquakes with hypocenters from 5 to 15 km deep, the velocity gradient predicts an unstable solution for depth because the gradient of travel time with depth changes sign and is near zero for a wide

range of distances. Inclusion of a velocity gradient in the location program, and the use of distance dependent weights in the depth computation can improve the accuracy and stability of earthquake locations.

Presented at Eastern Section, Seismological Society of America, meeting October, 1985, Knoxville, Tennessee.

EARTHQUAKE LOCATIONS; A CONSIDERATION OF INDEPENDENT COMPUTATION OF ORIGIN TIME, EPICENTER AND DEPTH

Liow, J.-S., An Tie, and L. T. Long, School of Geophysical Sciences, Georgia Institute of Technology, Atlanta, GA 30332

When using Geiger's method to locate earthquakes which are re'corded by a small number and an poor distribution of stations, uncertainty in the origin time, depth and epicenter interact. We have developed a location method that isolates the origin time computation by using S-P times and the assumption of a constant Poisson's ratio. Then the origin time is fixed and the epicenter is found by the traditional iterative least-squares method. When a satisfactory epicenter is found, the epicenter is held constant and the depth is found also by the iterative least-squares method. The epicenter and depth are obtained alternately until convergence is complete;. The method has two advantages over Geiger's method. First, computation of the origin time, epicenter, and depth are uncoupled. Second, separate weights can be used for epicenter and depth computations. A gradient velocity crustal model is used instead of a constant velocity model in order to compute the theoretical travel times. A weighting scheme which combines the reading accuracy and the scattering for the P- and S-wave arrivals in the southern Appalachian area is taken into consideration while finding the epicenter. An additional distance weight is incorporated into the weights for the depth computation.

Presented at Eastern Section, Seismological Society of America, meeting October, 1985, Knoxville, Tennessee.

SEISMICITY AND CRUSTAL STRUCTURE IN SOUTHEASTERN TENNESSEE

Long, L. T., J.-S. Liow, An Tie, and K.-H. Zelt (All at: School of Geophysical Sciences, Georgia Institute of Technology, Atlanta, GA 30332

Three major features define the crustal structure of southeastern Tennessee. First, the New York-Alabama Lineament (NYAL) probably represents the trace of an ancient strike-slip fault which separates crust of different thickness and seismic velocity. Second, a negative Bouguer anomaly which follows the trace of the NYAL in southeastern Tennessee can be interpreted as an area of

sediment thickening in the shallow crust. Third, a north-northeast striking positive gravity anomaly in northern Tennessee represents a Precambrian rift. This relic rift is truncated at the negative gravity anomaly and the NYAL. The area of the negative Bouguer anomaly and the intersection of the Precambrian rift with the NYAL correspond to the area of active seismicity in southeastern Tennessee. In this active zone, all events from 1981 through 1985 have been relocated by first using S-P times to obtain origin time and by, second, using a velocity gradient in the velocity model to obtain the epicentral parameters. The velocity model is based on an interpretation of refraction data from earthquakes and explosions. The travel time residuals at individual stations agree with the structural model and confirm a zone of low-velocity sediments. The relocated distribution of events suggests that both northwest and north trending zones of seismicity exist in response to crustal stresses resulting from structural inhomogeneities and topographic loading. The features responsible for these stresses in southeastern Tennessee are the Great Smoky Mountains and the truncation of the Precambrian rift at the NYAL.

Presented at American Geophysical Union spring meeting, May, 1986, Baltimore, Maryland.

STRESSES INDUCED BY THE TOPOGRAPHY AND LATERAL DENSITY VARIATIONS IN THE SOUTHEASTERN UNITED STATES

KUANG, Jian, School of Geophysical Sciences, Georgia Institute of Technology, Atlanta, GA 30332; MARESCHAL, J-C. Dept. des Sciences de la Terra, Unibersite du Quebec a Montreal, Montreal, PQ, H3C 3P8, Canada; LONG, L. T., School of Geophysical Sciences, Georgia Institute of Technology, Atlanta, GA 30332.

The stresses induced by the topography and by lateral changes in crustal structure are computed for a three-dimensional model of the lithosphere consisting of a horizontally layered slab over an inviscid fluid. The stresses are induced by surface (i.e., topography or bathymetry) or internal (changes in crustal thickness) loads. The density models of the lithosphere that are used as loading functions are based on constraints of the gravity data. Alternately, the gravity data are downward continued to determine directly the load of an equivalent layer. In both cases, the stresses induced in the crust are large (i.e., >100 MPa) and could perhaps account for the seismicity. Even larger stresses could be generated by the flexure of the lithosphere following the deposition of sediments.

Presented at the Seismological Society of America annual meeting, April, 1986, Charleston, South Carolina.

Results of Recent topical studies

Many topical studies achieved notable conclusions or were completed during the contract period of 1 August 1985 to July 1989. The principal conclusions of the recent topical studies are summarized below. Earlier studies have been reported in papers, talks, and interum reports. Many of the topical studies are still in progress and will be continued. The current status of these studies is given below. Significant conclusions that develop later will be reported in the open literature.

The Mechanism of Major Intraplate Earthquakes

Perhaps the most significant development, which was made possible by the Georgia/Alabama Regional Seismographic Network, is the discovery and development of a theory to explain major intraplate earthquakes. The new model for major intraplate earthquakes shows how tectonic plate stress can be concentrated for release in major intraplate earthquakes. The transient process starts by a weakening of the crustal stress channel, perhaps by a perturbation of the fluid regime of the lower crust. The crustal stress channel is the mid-crustal zone of high strength subject to forces at plate boundaries. The weakened core can then be deformed by plate stress and stress can be concentrated on the boundary of this core. Further weakening at the edge of the core can lead to a major earthquake. Following a major earthquake, the area remains active in an extended aftershock sequence. More details of the mechanism are presented in Appendix B (Long, 1988).

The relation between major earthquakes and a weakening of the brittle-ductile transition (see Appendix C) was derived largely from data obtained in southeastern Tennessee. The principle investigation responsible for developing an understanding of the relation between focal mechanism of small earthquakes and the mechanism of major intraplate earthquakes was a Ph.D. dissertation by Karl-Heinz Zelt. A critical factor in quantifying the results of this study was the development of statistical parameters to quantify the quality of a focal mechanism solution. The southeastern Tennessee data were used to show that the spatial variation of focal mechanism solutions in a seismic zone can be used to infer variations in the orientation of the stress field. In particular, in southeastern Tennessee, the observed variations in stress directions fit a model for a weak zone in a crustal plate.

There is a strong implication in the analyses and data from the focal mechanism study that a major earthquake has occurred (or could occur) in the southeastern Tennessee seismic zone. Many other observations of seismological and geological data in southeastern Tennessee are also in agreement with this solution.

The observations that support this statement include:

1) Correlation of focal mechanism of small earthquakes with a pattern of stress consistent with a weak zone in a compressed plate.

2) A pattern of epicenters extending in a northeast-southwest direction very similar in shape and size to the New Madrid seismic zone.

3) A suggestion of anomalously low velocity in a zone southwest of Knoxville.

4) A suggestion of anomalously low Q in a zone southwest of Knoxville.

5) The seismicity underlies a sedimentary basin which penetrates to depths of seven kilometers into the crust.

6) The earthquakes occur at depths of 8 to 20 km, and can not be explained by surface phenomena.

7) The gravity and magnetic data suggest that the crust responsible for the seismicity is a Precambrian rift, analogous to structures in the New Madrid seismic zone.

The model and evidence for the model have developed through a sequence of studies and presented in talks. Each has treated a different aspect of the model and its consequences. Papers on the description of the model (Appendix B) and the relation of the model to spatial variations in focal mechanisms (Appendix C) are presented below. Others will be developed into papers at a later date.

The objective of the paper "Crustal Stress and Faulting by Major Earthquakes" by L.T. Long which was presented at the Southeastern Section, Geological Society of America, was to show how the model for major intraplate earthquakes can explain some faults observed in the continents. The essential elements of the model are the crustal stress channel, intraplate compressive stress, and a perturbation in the strength of the stress channel caused by thermal or fluid mechanisms. The five-phase process of a major event proceeds as described in Appendix B and the stress field for the model is described in Appendix C.

The development of faults in response to the weakening of the crust depends on the extent of penetration of the fluids into the crust. Two characteristic responses can be recognized. The first occurs in the early stages of development of an intraplate seismic zone, when stress is concentrated in the thinned stress channel above the zone of perturbation. Earthquakes would be of thrust type and could range from magnitude 5.5 to 6.8. In this stage the

deformation and weakening have not extended to the shallow crust (5 to 10 km) the thinned stress channel fails because it is left supporting the regional stress. The length of the fault would correspond to the size of the zone of lower crustal weakening. An example of this type of response is the Bellair (GA) fault which is a 20 km long curved trace with the up block on the concave side of the arc. The second type is a failure of the entire plate starting at a weakened core. The New Madrid events characterize this response, which develops after the weakness has penetrated the crust. The major zones of failure extend beyond the core and involve the entire crust. The largest magnitude intraplate events would be of this type.

The observation that earthquakes in the southeastern United States can be classified as either shallow events on existing fractures or mid-crustal events associated with potentially major seismic zones was presented in a talk titled "A Comparison of Two Types of Earthquakes". The mechanisms for the generation and release of stress in these two types of earthquakes are different and an understanding of their distinct mechanisms carries significant implications for seismic risk. The shallow events are typical of earthquakes that occur in the Piedmont, including reservoir induced events, and are referred to as Piedmont type earthquakes. They occur principally on existing fractures and are triggered by fluid penetration from the free surface. The fluids, either through chemical erosion or changes in hydrostatic pressure, decrease the shear strength on fractures and release existing stress in the form of earthquakes. The mid-crustal events occur because plate driving forces are released by developing zones of weakness in the crust. These earthquakes generate new faults in response to the principal direction of plate stress and developing zones of weakness.

The implication of the mechanism for Piedmont type earthquakes is that the stress is limited to residual stress and the size of the fault plane is limited to the upper four to seven kilometers of the crystalline crust. This constrains the maximum magnitude to 5.5 to 5.7 and the exposure to earthquake damage from such events would be moderate, even near the epicenter. The implied seismic risk for the deeper focus crustal earthquakes is much greater. These events gain their energy from a combination of plate driving stress and the development of weak zones by fluids. They occur in response to viscous relaxation of the applied stress and the concentration of stress surrounding the zone of weakness. Their magnitudes are virtually unlimited, but the background activity should allow a prediction of their occurrence.

The concept that "A local weakening of the brittle-ductile transition can explain some intraplate seismic zones" was presented at the symposium on intraplate seismicity in Montreal and is given in detail in Appendix C.

The relation of focal mechanisms to stress in the crust was prepared for the western AGU. Details of this study are presented in Appendix C.

Finite Difference Applications

In his Ph.D. dissertation titled "Finite difference propagation of waves in elastic inhomogeneous media" Jehn-Son Liow used the finite difference computation method to model synthetic seismograms for southeastern Tennessee crustal structure. The synthetic data were compared with observed arrivals on the Georgia/Alabama Regional Seismographic Network seismic stations in Tennessee. The high-frequency limit on the synthetic finite difference seismograms was about 2 Hz and the size of the finite difference grid was too small to develop a realistic comparison with observed data without filtering the short-period seismograms for frequencies less than 1.0 Hz. The finite difference computation will be repeated later when a larger computer is available on an economic basis. The larger run will be designed to place the source at 15 km depth and extend for 40 km with a resolution of 4.0 Hz wavelets.

Reservoir Induced Seismicity

The locations of induced events in the Richard B. Russell reservoir area lie on (or close) to the Middleton-Lowndesville Fault and its splays. The association of induced seismicity with a mapped fault zone is distinct from the dispersed pattern of the seismicity observed in the Jocassee and Monticello reservoir areas in South Carolina and the seismicity observed to the south in the Clarks Hill Reservoir. However, the limited seismicity associated with the Oconee Reservoir was also concentrated on the Middleton-Lowndesville Fault.

In another possible type of induced seismicity, a swarm of events has been identified as natural near the station DCT in southeastern Tennessee. The swarm started soon after the underground copper mine was abandoned. At this time, we suspect that these events are triggered by the filling of the mine with ground water.

Coda Syntheses and Inversion

The understanding of the cause of the coda of local earthquakes can be important in understanding local variations in the physical properties of the crust, as well as understanding the amplitude decay of waves from an earthquake. In particular, variations in coda Q were observed in southeastern Tennessee from earthquakes at a variety of depths. A model was developed

(Appendix A) that can explain the coda observed in southeastern Tennessee as well as the coda from shallow explosions in central Alabama. These results show that a three dimensional distribution of scatterers is sufficient to explain the variations in seismic coda. The success of the model to generate synthetic coda make this model an appropriate basis for an inversion for local variations in scatterers and attenuation.

Mining Events

During March the paper "The Alabama, U.S.A. seismic event and strata collapse of May 7, 1986, by L.T. Long and C. W. Copeland, was accepted for publication in PAGEOPH. Subsequent monitoring in 1989 with a portable digital event recorder identified a swarm of events at the same time as the passage of the longwall past a critical position in the Alabama coal mine. The combination of a critical weak zone and the stresses generated by the longwall mining technique are critical to the triggering of larger seismic events. The data presented in this paper show that events in central Alabama with magnitudes as high as 3.5 can be triggered by mining activity.

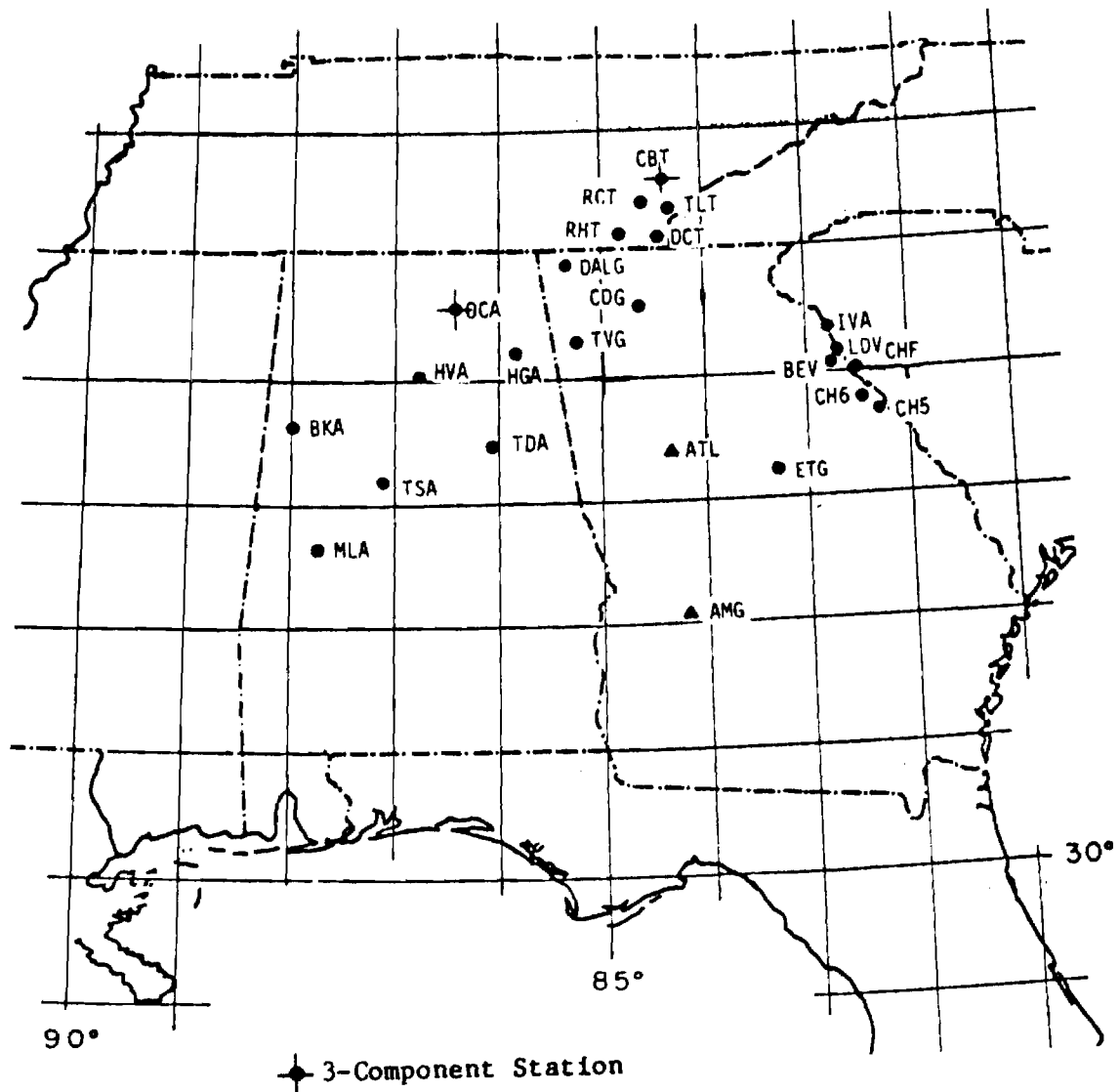


Figure 1. Locations of stations in the Georgia/Alabama Regional Seismographic Network maintained during the period of June 1, 1985, to July 31, 1989.

NETWORK COVERAGE FOR 1985-1986

Sta.	JUL-SEP	OCT-DEC	JAN-MAR	APR-JUN
OCAZ	XXX-----	-----	-----	-----X-XXX
OCAN	XXXXXXXXXX----	-----	-----XXXXXXXX	XXXX--X-XXX
OCAE	XXXXXXXXXX----	-----	-----XXXXXXXX	XXXX-XX-XXX
HGA	XXXXXX-----	-----	-----XXX	XXXXXX-----
HVA	XX----XXXXXXXX	XXX-----	-----	-----XXXXX
TDA	XXXX-----	-----	--XX-----X	XXXXX--XXX
TSA	-XXXXXX-----	-----	-----	-X-----
BKA	---X-----XXXX	XXXX-----	--XX-----	-----XXXX
MLAZ	XX-----XXX	XXXXXXXXXXXXXXXX	XXXX-----	-----XXXX
MLAN	XXXXXXXX-XXXXX	XXXXXXXXXXXXXXXX	XXXXXXXXXXXXXXXX	XXXXX--XXXX
MLAE	XXXXXXXX-----	XXXXXXXXXXXXXXXX	XXXXXXXXXXXXXXXX	----XX--XXX
SOUTHEASTERN TENNESSEE				
CBTZ	-----	-----X	XX--XXX-----	-----
CBTN	-----XX-	-----	----XXXXX-XXX	XX----X--
CBTE	-----XX-	-----	----XXXXXXXXXX	XXXXXXXXXX--
RCT	-----	-----	-----X-	-----
RHT	-X-----	-----	-----	-----XX--
TLT	-----	X-----	XXX--XXXXXXXXXX	XXXX-----
DCT	-----	-----	-----	-----
GEORGIA				
TVG	-----	-----	-----	--X-----
DALG	XX-----	----XXXXXXXXXX	XXXXXXXXXXXXXXXX	XXXX--XXXX
CDG	-----XX	XXXXXXXXXX--XX	XXXX-----	-----
ATL	XXXXXXXXXXXXXXXX	XXXXXXXXXXXXXXXX	XX--XXXXXX--	XXXXX-XXXXX
ETG	XXXXXXXXXXXXXXXX	--XXXXXXXXXX	XXXX-----	-----
CH6	-----	-----XX	X-----	-----XXXXXX
CHF	XXXXXXXXXXXXXXXX	-----XXXXXX	XXXXXX--XXX	X--XXX--
LDV	-----XX--X--	----XXX--XX--	-----	--XXXX--
BEV	-----XX-----	-----XX--	-----	--XXXX--
IVA	-----XX-----	----XXX--XX--	-----	--XXXX--X

"-" = Station Operating

X = Station Down

Figure 2a. Graphical representation of the operational status of the Georgia/Alabama Seismographic Network during the 1985-1986 project year.

NETWORK COVERAGE 1986-1987

Sta.	JUL-SEP	OCT-DEC	JAN-MAR	APR-JUN
ALABAMA				
OCAZ	XXXXXX--XXXXX	XXX-----	-----	-----
OCAN	XXXXXXXX-----	-----	-----	-----
OCAE	XXXXXXXX-----	-XXX-XXX-----	-----	-----
HGA	-----XXX---	-----X-----	-----	-----X-----
HVA	XXXXXX---XXXX	XXXX--XXXXXX	---XXXX-----	---XXXX-----
TDA	-----X---	-----XXXXX-----	-XX-----	-----X
TSA	XXXXXX---XXXX	XXXX-----	-XX-----	-----
BKA	-----X---XXX-	-----X-XXX	-XX-----XX-	-XX-----
MLAZ	XXXX-X--XXX-	-XX-XXXXXXXXXX	XXX-----	-----
MLAN	-----XXX-	--XX-XXXXXXXX	-----	-----
MLAE	XXXXX--XXXXXX	-----X-----	-----	-----
SOUTHEASTERN TENNESSEE				
CBTZ	XXXX--XXXXXXXX	XXX-XXXXXXXXXX	XX-----	-----
CBTN	-----XXX	XXXX-----	XX-----	-----
CBTE	XXXXXXXXXXXXXXXX	XXXXXXXXXXXXXXXX	XX-----	-----
RCT	-----	XXX-----	-----	-----X
RHT	---XXXXXXXXXXXX	-----	XXXX-----	-----
TLT	XXXXXXXXXX-XXX	XXX-----	XXXX-----	-----
DCT	-----X---	XX-----XXXX	-----	-----X
GEORGIA				
TVG	-XXX-----	-----	-----XXX-----	--XXXXXXXXXX
DALG	X-----X	-----	-X-----	XXXXXXXXXX-X
CDG	-----XXXX	-----	-----	-----
ATL	-X--XXXX-----	----XXXX---X	XXXXX-----	X-----XX---
ETG	XX--X---XXXX-	--XXXX-----	-----	-----
CH6	-XXXXXXXXXXXXXX	XXXXXX---XX	XXXXXXXXXXXXXX	XXXXXXXXXXXXXX
CHF	XXXXXXXXXXXXXX	XX-----XXX	XX-XXXXXXXXXXXX	-XXXXXXXXXXXX
LDV	X-X-XXXXXXXXXX	XXX-XX-----	-----	-X---XXXXX
BEV	XXXXX-----	-----	--XXX-----	-----XXXXX

"-" = Station Operating
 X = Station Down

Figure 2b. Graphical representation of the operational status of the Georgia/Alabama Seismographic Network for the period of July 1986 to June 1987.

Network Coverage for 1987-1988

Sta.	JUL-SEP	OCT-DEC	JAN-MAR	APR-JUN
ALABAMA				
OCAZ	XXXXXXXX-----	-----	-----	-----
OCAN	XXXXXXXX-----	-----	-----	-----
OCAE	XXXXXXXX-----	-----	-----	-----
HGA	-----XXX---	---X-----	-----	-----X----
HVA	XXXXXXXX--X-X	XXXXX--XXXXX	XXXXXXXXXXXX--	--XXXX-----
TDA	-----X---	-----	-----	-----X
TSA	XXX-XX---XX-	XXXX-----	-----	-X-----
BKA	-----X---XXX	-----	-----	-XXXX-----
MLAZ	-----XXX	-----	---X-----	-----
MLAN	-----XXX	-----	---X-----	-----
MLAE	-----XXX	-----	---X-----	-----
SOUTHEASTERN TENNESSEE				
CBTZ	-----XX-	-----	-----	-----
CBTN	-----XX-	-----	-----	-----
CBTE	-----XX-	-----	-----	-----
RCT	-----	XX-----	-----	-----X
RHT	-----XXXX	XX-----	-----	-----
TLT	XXXXXXXXXX-XXX	-----XXX	XXX-X-----	-----
DCT	-----XX-	-----	-----	-----X
GEORGIA				
TVG	-XX-----	-----	-----XXX----	--XXXXXXXXXX
DALG	X-----X	-----	-X-----	XXXXXXXXXX-X
CDG	-----XXXX	-----	-----	-----
ATL	-X--XXXX-----	-----	---XX-----	X----XX---
ETG	XX-XX---XXXX	-X-XXXX-----	-----	-----
CH6	-XXXXXXXXXXXXXX	XXXXXX----XX	XXXXXXXXXXXXXX	XXXXXXXXXXXXXX
CHF	XXXXXXXXXXXXXX	XX-----XXX	XX-XXXXXXXXXX	-XXXXXXXXXXXXXX
LDV	X-X-XXXXXXXXXX	XXX-XX-----	-----	-X----XXXXX
BEV	XXXXX-----	-----	--XXX-----	-----XXXXX

"-" = Station Operating
 X = Station Down

Figure 2c. Graphical representation of the operational status of the Georgia/Alabama Seismographic Network for 1987-1988.

Network Coverage for 1988-1989

Sta.	JUL-SEP	OCT-DEC	JAN-MAR	APR-JUN
	ALABAMA			*
OCAZ	-----XXXX-----	--XXXX-XXXX--	-----XXX	XXXXXXXX-----
OCAN	-----XXXX-----	-----X-XXXXX-	-----XXX	XXXXXXXXXX-----
OCAE	-----XXXX-----	-----X-XXXXX-	-----XXX	XXXXXXXX-XXXXX
HGA	----XXX-XXXXX	XXXXXXXXXXXXXXXX	XXXXXXXXXXXXXXXX	XXXXXXXX-XXXXX
HVA	----X-----	-----	---XXXX---XXX	XXXXXXXX-XXXXX
TDA	XX--XXXXXXXX-X	XXXXXX-----	-----	XX---XX-XXXXX
TSA	-X--X-----X-	----XX-----	-----	-----XX-----
BKA	----X-----	-----	-----	-XXXXXXXX-XXXXX
MLAZ	----X-----XXX	X-----XXXX	XXXXXXXXXXXX--	-----XXXX
MLAN	----X-----	-----XXXX	XXXXXXXXXXXX--	-----XXXX
MLAE	----X-----	-----XXXX	XXXXXXXXXXXX--	-----XXXX
	SOUTHEASTERN TENNESSEE			
CBTZ	-----XXX---	-----X---	-----	-XXXXXXXXXXXXXX
CBTN	-----XXX---	-----X---	-----	-XXXXXXXXXXXXXX
CBTE	-----XXX---	-----X---	-----	-XXXXXXXXXXXXXX
RCT	XXXXXXXXXX---	-----XXXXX	XXXXXXXXXXXXXX	XXXXX-----XX
RHT	---XXX-----	-----	-----	-----
TLT	----XXXXXX-XX	XXXXXXXXXX--XXX	-----XX	XXXXXXXXXXXXXX
DCT	X-----	-----	-----	-----
	GEORGIA			
TVG	XXXXXXXXXXXXXX	XXXXXXXXXXXXXX		
DALG	XXXXXXXXXXXXXX	XXXXXXXXXXXXXX	XXXXXXXXXXXXXX	XXXXXXXXXXXXXX
CDG	-----XXX---	XXXXXXXXXXXXXX	XXXX-----	-XXXXX-----XX
ATL	-----X-----	-----	-----	-XX-----
ETG	-----	-----XX-XX-	XXXXXXXXXXXXXX	---XX-----
CH6	XXXXXXXXXXXXXX	XXXXXXXXXXXXXX-	-----XXXXX-	XXXXXXXXXXXXXX
CHF	XXXXXXXXXXXXXX	XXXXXXXXXXXXXX	XXXXXXXXXXXXXX-	--XXXXXXXXXXXXXX
LDV	XXXXXXXXXXXXXX	XXXXXXXXXXXXXX	XXXXXXXXXXXXXX	XXXXXXXXXXXXXX
BEV	XXXXXXXXXXXXXX	XXXXXXXXXXXXXX	XXXXXXXXXXXXXX-	-----

"-" = Station Operating
 X = Station Down

Figure 2d. Graphical representation of the operational status of the Georgia/Alabama Seismographic Network for 1988-1989

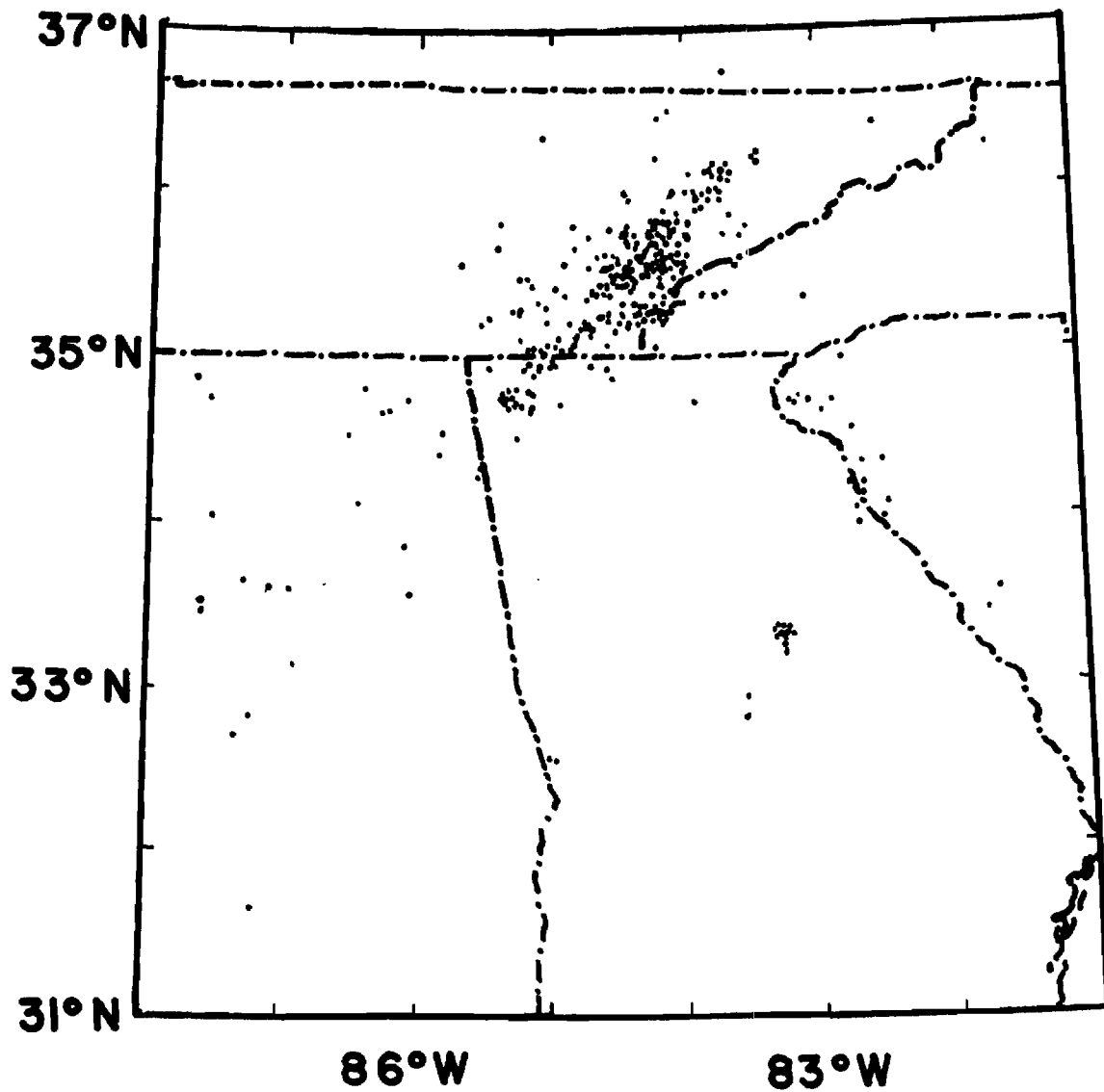


Figure 3. Seismicity reported by the Georgia/Alabama Regional Seismographic Network from August 1985 to July 1989.

APPENDIX A

Modeling the Seismic P Coda as the Response of a Discrete-Scatterer
Medium

by: M. S. Craig, L. T. Long, and An Tie,
School of Earth and Atmospheric Sciences
Georgia Institute of Technology
Atlanta, GA 30332 USA

In preparation for Proceedings of IASPEI Symposium "Scattering and
Attenuation of Seismic Waves" to be published as a special issue of
Physics of the Earth and Planetary Interiors.

Abstract

The seismic coda can be modeled as a composite of wavelets scattered from spherical heterogeneities embedded in an elastic medium. The exact scattering response of a spherical heterogeneity is calculated for elastic waves using Mie theory. To generate synthetic codas, a P source wavelet is defined for propagation along the ray paths from the hypocenter to the receiver via each scatterer in the model. Only singly-scattered waves are computed. Along the path, the wavelet is adjusted for geometric spreading, intrinsic attenuation, scattering response, the free-surface effect, and instrument response. The source-scatterer-receiver path length is used to determine the appropriate time-shift for the scattered wavelet. Scattered wavelets are obtained individually by calculating the response and lapse time corresponding to each scatterer in the medium. This is done independently for scattered $P - P$ and $P - S$ waves. The individual wavelets are then time-shifted and superimposed to obtain the complete coda. Synthetic codas were able to match the emergent P -wave codas from surface explosions in Alabama and the impulsive P -wave arrivals from earthquakes in southeastern Tennessee.

1 Introduction

The seismic coda, namely the portion of the seismogram that immediately follows the direct arrival, consists of numerous arrivals that cannot be explained completely by a layered-earth. Most workers attribute the unexplained coda energy to the scattering of elastic waves by heterogeneities (Aki, 1969; Sato, 1977a,b; Herraiz and Espinosa, 1987). The complexity of solutions to the wave equation propagation in heterogeneous elastic media has impeded the development of analytical solutions for the seismic coda. Statistical methods have been useful for describing the general shape of the envelope (Aki and Chouet, 1975). Sato (1977b, 1982, 1984) treated the scatterers as a continuous distribution to be integrated over a volume. The model presented in this work represents the seismic coda by the superposition of singly-scattered wavelets. The model differs from Sato's in that responses in that responses are calculated individually for each scatterer and then summed to form the complete coda. The principal advantage of our model is that the parameters can be varied as a function of position in the host medium.

The scattering of elastic waves has been studied by several workers, but relatively few studies have attempted to account for the angle dependence, or anisotropy, of seismic scattering. Sato (1984) and Snieder (1988) used the Born

approximation for a first-order approximation of the scattered wavefield. The exact solution is given by Mie theory (Ying and Truell, 1956) as an infinite series. Tie (1987) used the Mie method to calculate scattered wavefield potentials as a function of non-dimensional wavenumber ka for a wide range of geologic materials ($k = 2\pi/\lambda$, $a =$ scatterer radius). His work was extended in this thesis by explicitly evaluating the displacement fields and examining their variations as a function of scattering angle, and by implementing the asymptotic forms of the Hankel functions in the solution of the scattered field. The resulting scattering responses were incorporated in our coda modeling scheme, proceeding from the synthesis of an individual scattered wavelet to the generation of a complete coda.

A geologic model is specified by defining host and scatterer materials, and scatterer size and distribution. Path-dependent corrections include geometric spreading, intrinsic attenuation, and the free surface effect. The Mie method is used to determine scatterer responses. All of the above components are combined to produce the scattered wavelet and, finally, many scattered wavelets are superimposed to produce the complete coda. The effects of scatterer properties and source-receiver geometry on the seismic coda were investigated by generating synthetic seismograms for a range of parameters.

2 The Model

2.1 Overview

Scatterers in this study were approximated by elastic spheres embedded in an elastic crust. The elements of the response due to one scatterer are summarized as follows: A compressional wavelet is propagated from the source to the scatterer, where its energy is scattered in all directions. Part of the energy is scattered towards the receiver in the form of $P - P$ and converted P -to- S wavelets. Source-scatterer and scatterer-receiver pathlengths are calculated and used to correct the wavelet for geometric spreading and intrinsic attenuation. The scattering angle θ (see Figure 1) is required to calculate the amplitudes of the scattered P and S wavelets. The orientation of the plane that contains source, scatterer, and receiver is used to determine the component of scattered S wave polarized in the vertical plane. The emergent angle γ is used to correct P and S_V amplitudes at the free-surface. The path length $r_1 + r_2$ is used to time-shift the scattered P and S wavelets, which are then added together to obtain the complete response for a particular scatterer. In multi-scatterer models, this procedure is repeated for all scatterers within the region of influence associated with the desired coda duration. Each scattered response was added to accumulate the complete coda. The instrument response was applied to the final trace, thus synthetic seismograms may be prepared for a variety of seismometers without having to recalculate the scattered responses.

A more general geologic model containing many scatterers may be specified in terms of scatterer radius and spacing, intrinsic attenuation, and P and S -wave velocity structure. The host material was assumed to have constant P and S -wave velocity and horizontal layers with constant intrinsic Q . Scatterer radius and spacing were independently specified. The spatial extent, or region of influence, of the model was determined by specifying the duration of coda to be examined. The responses of all scatterers, including the associated path corrections, were calculated and summed to generate the theoretical coda.

2.2 Attenuation and Geometric Spreading

Attenuation of waves along the path from the source to the scatterer and from the scatterer to the receiver was attributed to the combined effects of intrinsic at-

tenuation, Q_i^{-1} , of the host medium and attenuation due to forward scattering, Q_s^{-1} , by the intervening scatterers (Dainty and Toksöz, 1980). Although attenuation was assumed to vary only as a function of depth in the geologic models used to prepare the synthetic seismograms in this paper, depth-dependent attenuation is not a restriction of the coda modeling scheme. Attenuation was calculated for each wavelet according to its travel time T by using

$$A(\omega) = A_0(\omega) \exp\left(-\frac{\omega T}{2Q}\right), \quad (1)$$

where $A_0(\omega)$ is the amplitude at the source, ω is the angular frequency, and Q is the combined effect of Q_s and Q_i . For seismograms of this study, travel-times were calculated for P and S waves, along the path from source to scatterer to receiver, by assuming a constant-velocity medium. The travel times for the scattered P wave, T_P , and the scattered S -wave, T_S , are given by

$$T_P = \frac{(r_1 + r_2)}{\alpha}$$

and

$$T_S = \frac{r_1}{\alpha} + \frac{r_2}{\beta},$$

where r_1 and r_2 (see Fig. 1) are the lengths of the first and second path segments, and α and β are the P - and S -wave velocities, respectively.

Scattering attenuation Q_s and intrinsic attenuation Q_i are difficult to distinguish because they are coupled:

$$\left(\frac{1}{Q_s} + \frac{1}{Q_i}\right)^{-1}.$$

Q is often observed to be constant in a given frequency band. However, waves traveling through a strongly scattering medium may suffer greater depletion of high frequencies (Rayleigh, 1896, §296). In the case of a medium with strong scattering and high Q , the high frequencies are shifted to later time in the coda. This effect is manifested as an enrichment of high frequencies in the later portions of seismic codas recorded in southeastern Tennessee and may cause the frequency dependence of $Q = Q_0 f^n$ often observed in spectral studies of L_g wave codas.

Wavelets were corrected for spherical spreading both from the source and the scatterer. The amplitude decay depends on path length and therefore scatterer position but is assumed to be independent of frequency. The correction for geometric spreading along the source to scatterer to receiver path ($\mathbf{r}_1\mathbf{r}_2$ in Fig. 1), must account separately for the source to scatterer distance, r_1 , and the scatterer to receiver distance, r_2 . The total attenuation of a wavelet due to geometric

spreading along the source-scatterer-receiver path is given, for a constant-velocity approximation, by

$$A(r_1, r_2) = A_0 \frac{a_{\text{src}} a_{\text{scat}}}{r_1 r_2}. \quad (2)$$

A_0 is the initial amplitude (at the source), A is the amplitude at the receiver, and a_{src} and a_{scat} are the radii of source and scatterer. We assumed the medium to have a constant Poisson ratio, thus the P and S waves share the same ray path and have the same geometric spreading correction.

2.3 Source, Free Surface, and Instrument Response

2.4 P -Wave Source

The response of a spherical cavity to a pressure step function (Blake, 1952) was used to model an explosive (P -wave) source. Far-field displacement is given by

$$\begin{aligned} s(\tau) &= \frac{C_1 P_0}{r} e^{-C_2 \tau} \sin(\omega_0 \tau) && \text{if } \tau \geq 0, \\ s(\tau) &= 0, && \text{if } \tau < 0, \end{aligned}$$

where $\tau = (t - r/c)$, t = time, r is the distance from the center of the cavity to the observer, c is the velocity of the medium, P_0 = pressure amplitude, and ω_0 is the cavity resonant frequency. C_1 and C_2 are constants that depend on the density and Poisson's ratio of the medium. We initially calculated source amplitude at the surface of the source cavity and later applied geometric spreading corrections according to path length.

The amplitude of a plane wave incident on a free surface depends on the angle of emergence γ (see Fig. 1). The ratio of emergent P and S_V amplitudes to vertical displacement amplitudes (Ben-Menahem and Singh, 1981, pp. 89-98) were used to convert confined amplitudes to vertical free-surface amplitudes.

The response of a 1.0 Hz seismometer was used as the instrument response of the model. Figure 2 shows the amplitude spectrum, $|R(\omega)|$, of the response to be linear for 1-50 Hz.

3 Scattering Response

3.1 Background

The response of the individual scatterer to an incident plane wave is a unique component of our model. Scatterers were modeled as spherical elastic heterogeneities embedded in an elastic host material. The assumption of sphericity is a first-order approximation that should yield reasonable results for media that contain many scatterers of arbitrary shape and orientation and for non-dimensional wave number $ka \leq 1$. k is wave number, $2\pi/\lambda$, and a is scatterer radius, thus, when $ka = 1$, wavelength λ equals scatterer circumference. Responses for values of ka greater than one are more strongly influenced by higher-order terms, which are required for an accurate solution, but which also lead to resonance effects that are not expected to be sustained by the shapes of scatterers more typically found in the crust.

The range of scatterer radii used in this study was 0.1-1.0 km. The lower bound was based on the resolution of the system, *i.e.* the wavelength of 25 Hz waves that travel with a velocity of 6 km/s. The maximum reliable ka and effective passband of the system determine the upper bound on scatterer size.

Energy scattered from the sphere varies as a function of non-dimensional wavenumber ka , scattering angle θ , and the material contrast between host and scatterer. The problem of determining the scattered wavefield was addressed first by Rayleigh (1896), for scalar (acoustic) waves. He demonstrated that for $ka \ll 1$, *i.e.* wavelengths which are much greater than the size of the scatterer, scattered amplitudes are inversely proportional to the fourth power of wavelength. Mie (1908) extended Rayleigh's work to obtain the general solution which expresses the scattered vector wave field for all frequencies and the complete range of contrasts between host and scatterer materials. Mie theory has been applied extensively in many of the physical sciences, such as chemistry, meteorology, and astronomy (van de Hulst, 1956). Researchers have only recently considered its applications in elastic materials. Ying and Truell (1956) determined the scattered P and S wave fields that are generated when a P wave impinges upon an elastic sphere embedded in an elastic host medium. Their approach is followed in this work.

3.2 Separation of the Wave Equation

The wave field that is scattered when a wave impinges upon a spherical obstacle is determined by solving the elastic wave equation in spherical coordinates with appropriate boundary conditions. In a homogeneous, isotropic, elastic medium, wave motion is described by

$$\rho \frac{\partial^2 \mathbf{u}}{\partial t^2} = (\lambda + 2\mu) \nabla(\nabla \cdot \mathbf{u}) - \mu \nabla \times (\nabla \times \mathbf{u}), \quad (3)$$

where \mathbf{u} is displacement, ρ is density, and λ and μ are Lamé's elastic constants (see, *e.g.*, Aki and Richards, 1980, p. 68, or Elmore and Heald, 1969, pp. 225-229).

Following Ben-Menahem and Singh (1981, pp. 54-63), \mathbf{u} is found by solving for the radial (P) and transverse (S) components of displacement separately and then combining them for the complete solution. The radial component is represented as the gradient of a potential Φ and the transverse component is represented as the curl of a potential Ψ . By taking the incident wave to be purely P from the negative z direction (Fig. 3), the particle motion of the scattered S -waves is confined to the plane that contains the the source, scatterer and receiver. The corresponding solution to eq. 3 is

$$\mathbf{u} = \frac{1}{k_\alpha} \nabla \Phi - \frac{1}{k_\beta} \nabla \times \nabla \times (\mathbf{r} \Psi). \quad (4)$$

The two terms represent the radial and transverse (P and S) components, respectively:

$$\mathbf{u} = (\mathbf{u}_r + \mathbf{u}_\theta).$$

3.3 Polarization of the Scattered S Wave

Amplitudes of scattered S waves are calculated in the plane of the source, scatterer, and receiver. In order to synthesize vertical-component seismograms, we need to determine the S_V amplitude, *i.e.* the component of S -wave amplitude that lies in the vertical plane which passes through the scatterer and receiver. This vertical plane and the plane that contains source, scatterer, and receiver intersect along the line that joins scatterer and receiver. The angle between these planes is used to determine the S_V component of the scattered S -wave. In the coordinate system shown in Figure 4, source, scatterer, and receiver are denoted by A , B , and C . Coordinates for longitude, latitude, and depth are given by x , y , and z . The source-scatterer path is represented by

$$\mathbf{r}_1 = (x_b - x_a) \mathbf{i} + (y_b - y_a) \mathbf{j} + (z_b - z_a) \mathbf{k}$$

and the scatterer-receiver path by

$$\mathbf{r}_2 = (x_c - x_b)\mathbf{i} + (y_c - y_b)\mathbf{j} + (z_c - z_b)\mathbf{k}$$

(see Figure 1). The normal to the plane which contains source, scatterer, and receiver is obtained from the cross product of the two path segment vectors,

$\mathbf{r}_3 = \mathbf{r}_1 \times \mathbf{r}_2$. Direction angles of \mathbf{r}_3 are

$$\alpha_3 = \cos^{-1} \left(\frac{r_{3x}}{|\mathbf{r}_3|} \right), \quad \beta_3 = \cos^{-1} \left(\frac{r_{3y}}{|\mathbf{r}_3|} \right), \quad \text{and} \quad \gamma_3 = \cos^{-1} \left(\frac{r_{3z}}{|\mathbf{r}_3|} \right)$$

The normal to the vertical plane which passes through the scatterer and receiver is designated \mathbf{r}_4 . Its direction angles are

$$\beta_4 = \tan^{-1} \left(\frac{x_c - x_b}{y_c - y_b} \right), \quad \alpha_4 = 90^\circ - \beta_4, \quad \text{and} \quad \gamma_4 = 90^\circ.$$

The angle between the plane ABC (see Figure 4), which contains the source, scatterer, and receiver, and the vertical plane BCO , which passes through the scatterer and the receiver, is the same as the angle between their normals. The particle motion of the scattered S -wave is confined to the plane ABC and is perpendicular to the raypath \overline{BC} between scatterer and receiver, which is also the line of intersection of the two planes discussed above. Since the amplitude of particle motion is known in the plane ABC , its projection or component in plane BCO can be determined, given the angle between the two planes.

3.4 Scattered Wave Potentials

The potentials Φ and Ψ are needed to evaluate eq. 4. Ying and Truell (1956) and van de Hulst (1957) used the Mie approach to obtain solutions for scattered wavefield potentials. The frequency-domain solution is obtained by writing the potentials Φ and Ψ as spherical basis functions multiplied by undetermined Mie coefficients:

Incident P -wave;

$$\Phi^{\text{inc}} = \sum_{n=0}^{\infty} (-i)^n (2n+1) j_n(k_1 r) P_n(\cos \theta) \quad (5)$$

$$\Psi^{\text{inc}} = 0, \quad (6)$$

Scattered waves:

$$\Phi^{\text{scat}} = \sum_{n=0}^{\infty} (-i)^n A_n h_n(k_1 r) P_n(\cos \theta) \quad (7)$$

$$\Psi^{\text{scat}} = \sum_{n=0}^{\infty} (-i)^n B_n h_n(k_2 r) P_n(\cos \theta), \quad (8)$$

Internal waves:

$$\Phi^{\text{intern}} = \sum_{n=0}^{\infty} (-i)^n C_n j_n(k_3 r) P_n(\cos \theta) \quad (9)$$

$$\Psi^{\text{intern}} = \sum_{n=0}^{\infty} (-i)^n D_n j_n(k_4 r) P_n(\cos \theta). \quad (10)$$

h_n denotes the Hankel functions of the second kind,

$$h_n^{(2)}(kr) = j_n(kr) - in_n(kr),$$

used in the expressions above for outgoing scattered waves. A_n , B_n , C_n and D_n are the Mie coefficients, which must be determined for each order n and each non-dimensional wave number kr . The Bessel functions j_n and h_n are functions of the product, kr , of wave number k and radial distance r . Wave numbers are defined as

$$k_1 = \frac{2\pi f}{\alpha_h}, \quad k_2 = \frac{2\pi f}{\beta_h}, \quad k_3 = \frac{2\pi f}{\alpha_s}, \quad \text{and} \quad k_4 = \frac{2\pi f}{\beta_s} \quad (11)$$

where α and β are the P and S wave velocities in the host material and scatterer, as indicated by subscripts h and s , respectively.

3.5 Boundary Conditions

The boundary conditions at the host-scatterer interface are used to construct a system of equations in terms of the undetermined Mie coefficients A_n and B_n . Since the scatterer is modeled as an elastic heterogeneity embedded in an elastic host material, displacements and stresses are required to be continuous across the host-scatterer interface. The set of equations may be written as

$$u_r^{\text{scat}} - u_r^{\text{intern}} = -u_r^{\text{inc}} \quad (12)$$

$$u_\theta^{\text{scat}} - u_\theta^{\text{intern}} = -u_\theta^{\text{inc}} \quad (13)$$

$$\sigma_{rr}^{\text{scat}} - \sigma_{rr}^{\text{intern}} = -\sigma_{rr}^{\text{inc}} \quad (14)$$

$$\sigma_{r\theta}^{\text{scat}} - \sigma_{r\theta}^{\text{intern}} = -\sigma_{r\theta}^{\text{inc}} \quad (15)$$

evaluated at $r = a$, on the host-scatterer interface (Ying and Truell, 1956). r is the distance from the origin, the center of a spherical scatterer having radius a . u_r and u_θ are the radial and tangential components of displacement; σ_{rr} and $\sigma_{r\theta}$ indicate normal and tangential tractions.

The displacements may be written in spherical polar coordinates as

$$u_r = \frac{1}{k_\alpha} \frac{\partial \Phi}{\partial r} - \frac{1}{k_\beta} \frac{1}{r^2 \sin \theta} \left[\frac{\partial}{\partial \theta} \left(\sin \theta \frac{\partial}{\partial \theta} (r \Psi) \right) \right] \quad (16)$$

$$u_\theta = -\frac{1}{k_\alpha r} \frac{\partial \Phi}{\partial \theta} + \frac{1}{k_\beta r} \frac{\partial}{\partial r} \left(r \frac{\partial \Psi}{\partial \theta} \right) \quad (17)$$

Assuming a linear relation between stress and strain,

$$\sigma_{rr} = (\lambda + 2\mu) \frac{\partial u_r}{\partial r} \quad (18)$$

$$\sigma_{r\theta} = \mu \left(\frac{1}{r} \frac{\partial u_r}{\partial \theta} + \frac{\partial u_\theta}{\partial r} \right). \quad (19)$$

3.6 Construction of the Scattering Matrix

In order to write the boundary conditions (equations 12 - 15) in terms of the undetermined Mie coefficients A_n , B_n , C_n , and D_n , the displacements u and stresses σ are expressed in terms of their corresponding potentials Φ and Ψ (equations 5-10). The resulting equations were evaluated by using the differentiation relations among Bessel functions, *e.g.*

$$\frac{d}{dr} f_n(kr) = \frac{1}{r} [n f_n(kr) - kr f_{n+1}(kr)]$$

(Boas, 1966, p. 564) and Legendre's equation expressed in terms of differentiation with respect to θ (Arfken, 1970, p. 542),

$$\frac{1}{\sin \theta} \frac{d}{d\theta} \left(\sin \theta \frac{dP_n(\cos \theta)}{d\theta} \right) + n(n+1)P_n(\cos \theta) = 0. \quad (20)$$

After performing the necessary algebra (see, *e.g.* Pilant, 1979), the system of equations that correspond to the boundary conditions (12 - 14) may be written as

$$\begin{pmatrix} g_{11} & g_{12} & g_{13} & g_{14} \\ g_{21} & g_{22} & g_{23} & g_{24} \\ g_{31} & g_{32} & g_{33} & g_{34} \\ g_{41} & g_{42} & g_{43} & g_{44} \end{pmatrix} \begin{pmatrix} A_n \\ B_n \\ C_n \\ D_n \end{pmatrix} = \begin{pmatrix} y_1 \\ y_2 \\ y_3 \\ y_4 \end{pmatrix} \quad (21)$$

The elements of the scattering matrix, \mathbf{G} , are listed in Pao and Mao (1963). In general, they are complex. The complex 4×4 system was converted to a real 8×8 before solving (Tie, 1987). In order to determine the scattered wavefield, only A_n and B_n need be calculated.

3.7 Scattered Displacements

With A_n and B_n in hand, the n^{th} -order components of the scattered wave field can be evaluated using

$$u_{r,n}^{\text{scat}}(k_1 r) = \frac{(-i)^n}{r} \left\{ \frac{A_n}{k_1} [n h_n(k_1 r) - k_1 r h_{n+1}(k_1 r)] - n(n+1) B_n h_n(k_2 r) \right\} \times P_n(\cos \theta) \quad (22)$$

$$u_{\theta,n}^{\text{scat}}(k_2 r) = \frac{(-i)^n}{r} \left\{ \frac{A_n}{k_1} h_n(k_1 r) - \frac{B_n}{k_2} [(n+1) h_n(k_2 r) - k_2 r h_{n+1}(k_2 r)] \right\} \times \frac{dP_n(\cos \theta)}{d\theta} \quad (23)$$

In the far field (for large r) equations 22 and 23 may be approximated by

$$u_{r,n}^{\text{scat}}(k_1 r) \cong -(-i)^n A_n h_{n+1}(k_1 r) P_n(\cos \theta) \quad (24)$$

$$u_{\theta,n}^{\text{scat}}(k_2 r) \cong (-i)^n B_n h_{n+1}(k_2 r) \frac{dP_n(\cos \theta)}{d\theta}. \quad (25)$$

Substitution of the asymptotic form for the Hankel functions,

$$h_n^{(2)}(kr) \sim \frac{i^{n+1}}{kr} e^{-ikr}, \quad (26)$$

produces

$$u_{r,n}^{\text{scat}}(k_1 r) \sim \frac{(-1)^n A_n}{k_1 r} \exp(-ik_1 r) P_n(\cos \theta) \quad (27)$$

$$u_{\theta,n}^{\text{scat}}(k_2 r) \sim \frac{(-1)^{n+1} B_n}{k_2 r} \exp(-ik_2 r) \frac{dP_n(\cos \theta)}{d\theta}. \quad (28)$$

The final scattered displacements are obtained by individually calculating and summing the components of each order n :

$$u_r^{\text{scat}} = \sum_{n=0}^N u_{r,n}^{\text{scat}} \quad \text{and} \quad u_{\theta}^{\text{scat}} = \sum_{n=0}^N u_{\theta,n}^{\text{scat}} \quad (29)$$

u_r and u_{θ} are the scattered P and S -wave displacements, as were to be determined. N is the maximum order of Bessel functions and Legendre polynomials included in the summation. Although the exact solution requires $N = \infty$, in practice, the series may be truncated at $N \approx ka$ without significantly affecting the results (Stenzel, 1938; van de Hulst, 1957).

4 Scattered Radiation Patterns

Scattering responses were calculated for contrasts which approximate granite or basalt scatterers embedded in a sandstone matrix. These combinations correspond to P -wave velocity contrasts of 14% and 28%, respectively. Elastic properties of the materials are specified in terms of P and S -wave velocities and density in Table 1. Figures 5 and 6 contain a series of radiation patterns, or scattering diagrams, which show the response of the inclusions to an incident plane wave. Each radiation pattern shows the angular variation in displacement amplitudes of scattered waves. An incident P -wave arrives from the left and impinges upon a scatterer indicated by the star, the plot origin. For each value of ka , a pair of radiation patterns are plotted; the top one corresponding to scattered P waves and the bottom to the scattered P -to- S . Since a P -wave source was used, scattered amplitudes are symmetric about the horizontal axis and the angular variation in amplitudes is described completely by the two-dimensional plots; note also that the S -wave response is always zero at $\theta = 0^\circ$ and 180° .

In reviewing the following results, it may be helpful to note that that nondimensional wave number ka is proportional to frequency; $k = 2\pi f/c$. Velocity c of the model is approximately 6 km/s, so $k \approx f$. For ka less than one, the response is relatively weak and the backscattered amplitudes are slightly stronger than those of the forward scattered waves. For ka of 0.4 – 1.0, the shape of the radiation patterns does not change significantly, but amplitudes grow rapidly as ka increases. At ka greater than one, there are major changes in character. Forward scattering becomes larger than backscattering in both the P and S wavefields as ka increases, but the effect becomes much stronger for the P waves at ka greater than two. Backscattered amplitudes reach their maxima fairly early, roughly between ka of one and two.

The response of the granite scatterer (Fig. 5) was used for most of the simulations that follow. The radiation patterns of the basalt scatterer (Fig. 6) are similar in shape to those of the granite scatterer, their main differences are in amplitude. The P -wave radiation patterns are similar to those prepared by Stenzel (1938), who also used Mie theory to calculate the acoustic wavefield scattered by a rigid sphere. Both the P and $P - S$ radiation patterns determined by us closely resemble those prepared by Wu and Aki (1985) who used the Born approximation to calculate the response of an elastic inclusion in an elastic host. The interested reader may compare our Fig. 6 with their Fig. 16.

Despite the strength of the forward-scattered P -wave at high ka , the backscat-

tered waves tend to dominate the typical seismic coda because they persist for a much greater time (Aki, 1969). For single scattering and a uniform density of scatterers, the dominance of backscattering is explained by comparing the number of scatterers between source and receiver that can be sampled by forward-scattered paths with that sampled by backscattered paths. There is a cutoff time after which there can be no more forward-scattered arrivals, but backscattered waves will be observed until either they become too attenuated to detect or until the limit of the scattering region is reached. Although the amount of forward-scattered S -waves is small compared to that of the P -waves at high ka , the backscattered S -waves have amplitudes on the same order as those of the P for all values of ka considered.

In order to minimize computation time, scattered displacement responses were calculated independently of the synthetic coda computation. Scattered displacements were computed for scattering angles of $\theta = 0 - 180^\circ$ at 15° increments for $0 < ka \leq 2.5$, $\Delta(ka) = 0.1$, including up to 4th-order spherical functions. During the synthetic coda computation, the response for a particular scatterer size, wave number, and scattering angle was obtained by interpolating between the previously tabulated values.

5 Scattered Response Spectra

The response spectra of waves scattered from a granite scatterer embedded in sandstone are shown for a series of scattering angles in Figure 7. These responses were calculated up to $ka = 6$ (scatterer circumference equals six times wavelength) and include up to eighth order terms. All of the curves show a very weak response for $ka \ll 1$, which is consistent with Rayleigh scattering and indicates that waves much longer than the size of an obstacle are not scattered. For increasing values of ka that approach one, scattered amplitudes increase rapidly, but reach a maximum at large ka . It is evident, upon comparison of the amplitudes of forward-scattered and backscattered amplitudes, that forward scattering is much stronger than backscattering for ka greater than two. The value of ka at which the maximum response is reached decreases as scattering angle increases. The response curves for backscattering ($\theta = 120^\circ$ and 180°) show that for $ka \gg 1$ the response is modulated and does not appear to converge to a constant value. This is a resonance effect caused by the generation of scattered pulses (see Varadan and Varadan, 1979; Gaunard and Uberall, 1976).

6 Synthesis of the Scattered Wavelet

Synthetic seismograms were generated by calculating the frequency-domain response associated with each scatterer, finding the associated minimum-phase wavelet, and time-shifting the wavelet to its correct position in the coda. The complete coda was obtained by superimposing all scattered wavelets. As an example of the computational method, a synthetic seismogram was calculated for a model which contains only one scatterer. The scattering response u is initially calculated as a function of non-dimensional wavenumber, ka . Velocity and scatterer radius a are used to convert ka to frequency ω so that the scattering response u can be combined with other elements of the model in the frequency domain.

The scattering response and the attenuation operator were combined in the frequency domain. The spectral response of the medium, corrected for geometric spreading and the free-surface effect, is given by

$$|X_{P,S}(\omega)| = \frac{a_{\text{src}} a_{\text{scat}}}{r_1 r_2} F_{P,S}(\gamma) |u_{P,S}(\theta, \omega)| \exp\left(-\frac{\omega T_{P,S}}{2Q}\right). \quad (30)$$

The first factor is the geometric spreading correction, F is the free surface correction, u is the scattering response, and the exponential factor corrects for intrinsic attenuation in the host medium. Vertical bars indicate the amplitude spectrum, or modulus, of a complex spectrum:

$$|X| = \left([\Re(X)]^2 + [\Im(X)]^2\right)^{0.5}$$

The scattering response and attenuation were modeled as having minimum phase. The Hilbert-transform algorithm (Oppenheim and Shafer 1989, pp. 782-789) was used to determine the minimum phase wavelet associated with $|X(\omega)|$, described as follows. First the discrete inverse Fourier transform of the logarithm of $|X[k]|$ is computed,

$$c[n] = \frac{1}{N} \sum_{k=0}^{N-1} \log |X[k]| \exp\left[\left(\frac{i2\pi}{N}\right) kn\right], \quad (31)$$

where k and n denote frequency and time samples, respectively. Then, the Fourier transform

$$C'[k] = c(0) + 2 \sum_{n=1}^{N-1} c[n] \exp\left[\left(\frac{-i2\pi}{N}\right) kn\right], \quad (32)$$

is exponentiated and inverse Fourier transformed,

$$x[n] = \frac{1}{N} \sum_{k=0}^{N-1} \exp[C'[k]] \exp\left[\left(\frac{+i2\pi}{N}\right) kn\right], \quad (33)$$

to yield the minimum phase wavelet, $x[n]$. Claerbout's (1976, p. 62) subroutine was used to execute this algorithm.

Figure 8 shows sample moduli $|X_P(\omega)|$ and $|X_S(\omega)|$ and the wavelets, $x_P(\tau)$ and $x_S(\tau)$, which were obtained by finding and inverse Fourier-transforming the minimum-phase spectra associated with $|X_P(\omega)|$ and $|X_S(\omega)|$.

7 Superposition of Scattered Wavelets

The travel-times for the direct P , scattered P -to- P and scattered P -to- S waves associated with a particular source, scatterer, and receiver are denoted by T_0 , T_P and T_S , respectively. These times are used to position the scattered wavelets in the synthetic coda. Time measured from the onset of the scattered wavelets is given by $\tau_{P,S} = t - T_{P,S}$, where t is the time after source initiation. In a simple one-scatterer model, scattered P and S wavelets are time-shifted and combined with the direct wave in a single time-trace as

$$y(t) = x_0(t - T_0) + x_P(t - T_P) + x_S(t - T_S). \quad (34)$$

where x_0 , x_P , and x_S are the direct, scattered P , and scattered S wavelets, respectively. In a medium containing many scatterers, they can be iteratively incorporated in a single time trace as

$$y(t) = x_0(t) + \sum_{n=1}^N x_{P,n}(t - T_{P,n}) + x_{S,n}(t - T_{S,n}), \quad (35)$$

where $x_{P,n}$ and $x_{S,n}$ are the P and S responses of the n^{th} of N scatterers in the medium. $T_{P,n}$ and $T_{S,n}$ are the travel times from source to receiver via the n^{th} scatterer.

8 Convolution of Source and Instrument Response with the Coda

The contributions of a spherically-symmetric explosive source and instrument response are the same for all scatterers. Their incorporation may be postponed until the end and applied in a single operation on the entire coda, rather than

individually for each scattered wavelet. The combined response of the source and instrument is convolved with the coda trace in the time domain. The convolution of the combined source and instrument response with the coda to generate the synthetic seismogram completes the computation. Figure 9 illustrates the synthetic seismogram generated for a one-scatterer case, it consists of a direct wave, scattered P , and scattered S wavelet.

9 Synthetic Codas

Synthetic codas were generated for models using several sets of parameters. Results are compared with observed seismograms of blasts in Alabama and earthquakes in Tennessee. Our models consisted of a 50 km thick crust with several hundred scatterers spaced 5 km apart (Figure 10). Scatterer radius was varied from 0.1 to 0.6 km, but held constant within a given model. Q was assigned to horizontal planar layers in the model. Typically a two-layer model was used, in which a low Q was assigned to the upper 5 km and a higher Q was used at greater depths.

The emergent onset typical of blasts recorded in Alabama at station BKA is best matched by synthetic codas generated with a model that has small scatterers (100 m radius) and a low- Q surface layer ($Q=150$). The low- Q layer corresponds to the 2.0 km thick Paleozoic sediments. Figure 11 compares synthetic codas with an observed event. Codas with more impulsive onsets are matched by using models with 400-600 m scatterers and a $Q = 1500$ surface layer (Figure 12). Synthetic codas were generated for a wider range of model parameters by Craig (1990).

When geological contacts are rough, with irregularities having sizes comparable with wavelength, conventional normal-moveout techniques cannot explain observed data. We used the discrete-scatterer method to investigate the response of a layer of scatterers at depth. Figure 13 schematically shows the geometry and a few raypaths. A model was considered that contained scatterers only in layers at depths of 5 km and 40, and 45 km. The near-surface zone was highly attenuative ($Q=150$). At greater depths $Q=3400$ was used. The scattering response was again taken as a 14% velocity contrast. The model and corresponding synthetic seismogram are shown in Figure 14. The seismogram has a sharp onset, followed by a fairly rapid decay (11.3 to 15s), which correspond to the direct wave and arrivals scattered in the near-surface zone. Arrivals from the deeper layers become noticeable shortly after 17 s and persist until the end of the trace. The character of the synthetic trace is unlike the expected response of a flat reflector, but very much like Moho reflections observed on COCORP lines.

The model of a 28 km deep earthquake is shown in Fig. 15. The computed response is quite different from those of models which have a surface source (Fig. 10) chiefly because the direct raypath from source to receiver is no longer confined to the near-surface zone. Q was specified as 1000 for the upper 20 km and 3000 for greater depths. A stronger velocity contrast (28% instead of the previous 14%) was used to calculate the scattering response in an effort to increase scattered

amplitudes relative to the amplitude of the direct arrival. Synthetic seismograms were prepared for a series of models in which scatterer radius was varied from 100 to 600 m (Fig. 16). Amplitudes increase with increased scatterer size, but in all cases they decay more rapidly with time after the direct wave than do observed data (Fig. 17).

In order to investigate the validity of the single-scattering assumption as used in the modeling process, we calculated the mean free time of seismic waves between scatterers. Provided that the synthetic coda length is kept shorter than the mean free time for the associated model, the single scattering assumption is valid. In a medium having scatterers of a constant size, the mean free path may be expressed as $\ell = (n\sigma)^{-1}$, where n is the number density of scatterers and σ is the effective cross-section of the scatterer. For a distribution of scatterers having a constant spacing Δx , we may write $\ell = (\Delta x)^3/\sigma$. Mean free time is given simply by $t = \ell/c$, the mean free path divided by velocity c .

Mean free time was determined for several models. The results show that mean free time is shortest for high- ka waves traveling through models with large scatterers which contrast sharply against the host material. Consider, for example, the basic model having scatterers spaced 5 km apart in a host medium which has a P -wave velocity of 6 km/s: Waves with $ka = 1.0$ that travel in the model with scatterers of radius 0.2 km and a velocity contrast of 14 % will have a mean free time $t = 2240$ s. A wave having $ka = 1.5$ traveling through the same model has $t = 1080$ s. Models with larger scatterers have much lower mean free times. Waves having ka equal to 1.0 and 1.5 in a medium populated with 0.6 km radius scatterers have mean free times of 623 and 301 s, respectively. A stronger contrast between scatterer and host material increases the cross-section σ of the scatterer and thus decreases the mean free time. By increasing the velocity contrast to 28%, the times for the previous example drop to 126 and 71 s, respectively. Mean free times for all of the models used in this work are greater than the typically 15-20 s lengths of the corresponding synthetic codas, thus single scattering is a reasonable assumption in these simulations.

10 Discussion and Conclusions

A model of heterogeneities in the earth's crust as a distribution of spherical scatterers was found to be effective in synthesizing the seismic P -wave coda. The model incorporates the complete frequency-dependent anisotropic scattering response for an elastic sphere embedded in an elastic host medium. Codas were synthesized by combining the scattered P and S waves from many scatterers distributed throughout the crust. The scattering model is particularly appropriate in regions where the geology cannot be accurately represented with smooth layers. Computations were limited to singly-scattered wavelets. The validity of the single-scattering assumption was justified by ensuring that the durations of the synthetic codas were less than mean free times in the models.

Mie theory provides the exact solution for the scattered wavefield for any combination of frequency and material contrast and can be efficiently applied to seismic scattering problems. Scattering responses were demonstrated to vary strongly as a function of scattering angle and frequency. Radiation patterns and response spectra were prepared, using a P -wave source, for both scattered P and scattered S waves. For an elastic scatterer embedded in an elastic medium, a significant portion of incident P energy is converted to S -waves. For non-dimensional wavenumber ka of the incident wave less than one, backscattering is stronger than forward scattering for both P and S waves. Within this range, as ka is increased, scattered amplitudes grow significantly but the shape of their radiation patterns changes very little. For larger ka , forward scattering becomes dominant.

Responses calculated using Mie theory were incorporated in the synthesis of P codas for geologic models containing several hundred scatterers. Simulations investigated the effects of scatterer size and spacing and source-receiver geometry on the onset and decay characteristics of seismograms. Synthetic codas were able to provide reasonable simulations of P -wave codas recorded from blasts and earthquakes in Alabama and Tennessee.

The marked difference in character between the synthetic seismograms prepared for the Alabama blasts and the Tennessee earthquakes appears to be largely due to differences in the path geometry of the direct wave. The direct wave and nearly direct scattered waves from the Alabama surface source are selectively attenuated in the near-surface zone, whereas the direct and nearly direct paths from the deeper Tennessee source to the surface traverse much the same material as do the paths of scattered waves that arrive later in the coda.

Some of the difference between observed seismograms and the synthetics may be due to $S - P$ conversions, which were not modeled. Our model employed an ideal explosive source that produced only P waves, and considered only singly-scattered waves. $S - P$ conversions were not modeled since they could arise only through multiply-scattered $P - S - P$ conversions. In practice, mine blasts (such as those displayed in Figs. 11 and 12) generate both P and S waves due to source asymmetry. Earthquakes are more likely to generate $S - P$ scattered waves. If such scattering occurs near enough to the source, the $S - P$ arrivals will be superimposed on the P -coda.

P -wave codas of relatively deep-focus earthquakes recorded under a station have strong direct arrivals, relative to scattered waves. However, the ratio of the direct-wave amplitude to amplitudes in the coda is less than predicted by the synthetic seismograms. A model with more densely-spaced scatterers would improve the match between synthetic and observed data. An alternative is a model with lateral variations in scatterer density. If a zone of anomalously high scatterer density were to exist between source and receiver, waves traveling nearly direct paths would be attenuated more than those traveling via the longer scattered paths that avoid the zone.

Computing resources may limit the precision and complexity of the model as dictated by scatterer spatial density, frequency bandwidth, and sampling rate. Timing precision will be affected by uncertainties in the location of source and by the assumption of minimum phase for the scattering response. Realistic synthetic codas were obtained in this study with constant velocity models and a uniform spacing of spheres of the same diameter. Improvement should be expected for more realistic crustal velocity models, although the commensurate demands of raytracing will add significantly to the computation time. Models could also be improved by using an appropriate random distribution of the location and size of scatterers.

Part of the motivation for this work lies in the hope that temporal variations in Q may prove to be detectable precursors to earthquakes. Accurate and regionally specific models of the coda are needed to detect and interpret temporal variations in Q . The model presented in this work provides a means for representing the seismic coda as a linear combination of scattered responses, and can assist in the development of inversion schemes that seek to determine scattering properties of a region from seismic codas.

Acknowledgements:

Support for the first and third authors was provided by the School of Earth and Atmospheric Sciences through Research and Teaching Assistantships. Seismic data and computing facilities were provided through the Georgia Tech Seismic Observatory and the support of the U. S. Nuclear Regulatory Commission, Office of Nuclear Regulatory Research, Earth Sciences Branch.

11 References

- Aki, K., 1969. Analysis of the seismic coda of local earthquakes as scattered waves, *J. Geophys. Res.* **74**: 615-663.
- Aki, K., and B. Chouet, 1975. Origin of coda waves: Source, attenuation, and scattering effects, *J. Geophys. Res.*, **80**, 3322- 3343.
- Aki, K., and P. Richards, 1980. *Quantitative Seismology, Theory and Methods*, Freeman.
- Arfken, G., 1970. *Mathematical Methods for Physicists*, 2nd ed. Academic Press, New York, 815 pp.
- Ben-Menahem, A. and Singh, S. J., 1981. *Seismic Waves and Sources*. Springer-Verlag, New York, 1108 pp.
- Blake, F. G., 1952. Spherical wave propagation in solid media, *J. Acoust. Soc. Amer.* **24**: 211-215.
- Boas, M., 1966. *Mathematical Methods in the Physical Sciences*. Wiley, New York, 778 pp.
- Claerbout, J., 1976, *Fundamentals of Geophysical Data Processing*. McGraw-Hill, 274 pp.
- Craig, M. S., 1990. *A Discrete-Scatterer Model of the Seismic P Coda*, Ph.D. Dissertation, Georgia Institute of Technology, Atlanta, 131 pp.
- Dainty, A. M. and Toksöz, M. N., 1980. Seismic codas on the earth and the moon: A comparison, *Phys. Earth Planet. Inter.* **26**: 250-260.

- Elmore, W. C. and M. A. Heald, 1969. *Physics of Waves*. McGraw-Hill; republished in 1985 by Dover, New York, 477 pp.
- Gaunard, G. C. and H. Überall, 1983. RST analysis of monostatic and bistatic acoustic echoes from an elastic sphere, *J. Acoust. Soc. Am* **73**: 1-12.
- Herraiz, M. and A. F. Espinosa, 1987. Coda waves: A review, *Pageoph* **125**: 499-577.
- Hulst, van de, 1957. *Light Scattering by Small Particles*. Wiley, New York. Republished in 1981 by Dover, New York, 470 pp.
- Marion, J. B., 1970. *Classical Dynamics of Particles and Systems*, Academic Press, New York, 573 pp.
- Mie, G., 1908. Beiträge zur Optik trüber Medien, speziell kolloidaler Metallösungen (Optics of turbid media), *Annalen der Physik*, **25**: 377-445.
- Oppenheim, A. V. and R. W. Shafer, 1989. *Discrete-Time Signal Processing*. Prentice-Hall, Englewood Cliffs, New Jersey, 879 pp.
- Pao, Y-H, and C. C. Mao, 1963. Scattering of plane compressional waves by a spherical obstacle, *J. Appl. Phys.* **34**, 493-499.
- Pilant, W. L., 1979. *Elastic Waves in the Earth*. Elsevier, Amsterdam, 493 pp.
- Rayleigh, J. W. S., 1896. *The Theory of Sound*, 2nd ed., Macmillan; Republished in 1945 by Dover, New York, v1: 480 pp, v2: 504pp.
- Sato, H., 1977a. Energy propagation including scattering effects: Single isotropic scattering approximation, *J. Phys. Earth* **25**: 27-41.
- Sato, H., 1977b. Single isotropic scattering model including wave conversions, simple theoretical model of the short period body wave propagation, *J. Phys. Earth* **25**: 163-176.
- Sato, H., 1982. Coda wave excitation due to nonisotropic scattering and nonspherical source radiation, *J. Geophys. Res.* **87**: 8665-8674.
- Sato, H., 1984. Attenuation and envelope formation of three-component seismograms of small local earthquakes in randomly inhomogeneous lithosphere, *J. Geophys. Res.* **89**: 1221-1241.

- Snieder, R., 1988. Large-scale waveform inversions of surface waves for lateral heterogeneity; 1. Theory and numerical examples, 2. Application to surface waves in Europe and the Mediterranean, *J. Geophys. Res.* **93**: 12055-12080.
- Stenzel, H., 1938. Über die von einer starren Kugel hervorgerufene Störung des Schallfeldes (On the disturbance of a sound field brought about by a rigid sphere), *Elektrische Nachrichten Technik* **15**: 71-78, radiation patterns reproduced in Clay and Medwin (1980), pp. 192-193.
- Tie, An, 1987. *On scattering of seismic waves by a spherical obstacle*, Ph.D. Dissertation, Georgia Inst. of Tech., Atlanta, 126 pp.
- Varadan, V. V. and V. K. Varadan, 1979. Scattering matrix for elastic waves. III. Application to spheroids *J. Acoust. Soc. Am.* **65**: 896-905.
- Wu, R. and K. Aki, 1985. Scattering characteristics of elastic waves by an elastic heterogeneity *Geophysics* **50**: 582-595.
- Ying, C. F. and R. Truell, 1956. Scattering of a plane longitudinal wave by a spherical obstacle in an isotropically elastic solid, *J. Appl. Phys.* **27**: 1086-1097.

Rock Type	α (km/s)	β (km/s)	ρ (g/cm) ³
Sandstone	5.0	2.7	2.5
Granite	5.7	2.9	2.67
Basalt	6.4	3.2	3.0

Table 1: Properties for typical geologic materials. $\alpha = P$ wave velocity, $\beta = S$ wave velocity, and $\rho =$ density (after Dobrin, 1976, pp. 456-458).

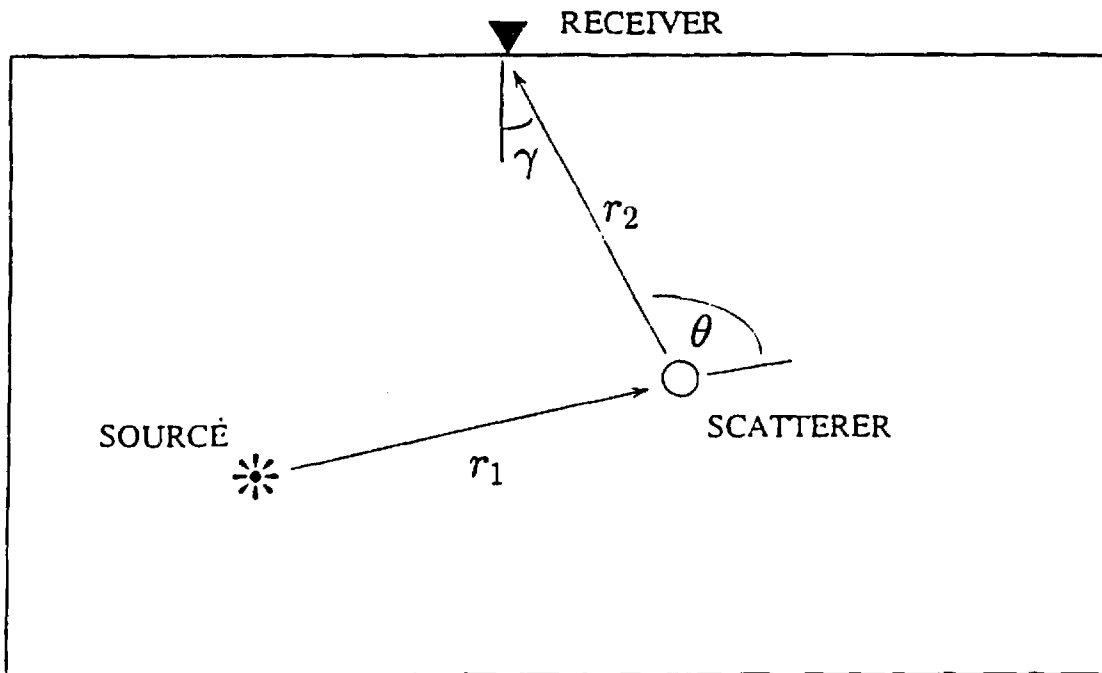


Figure 1: Scattering angle, θ , is measured in the plane of the source, scatterer, and receiver. Emergent angle is given by γ . The plane of source, scatterer, and receiver is vertical in this figure.

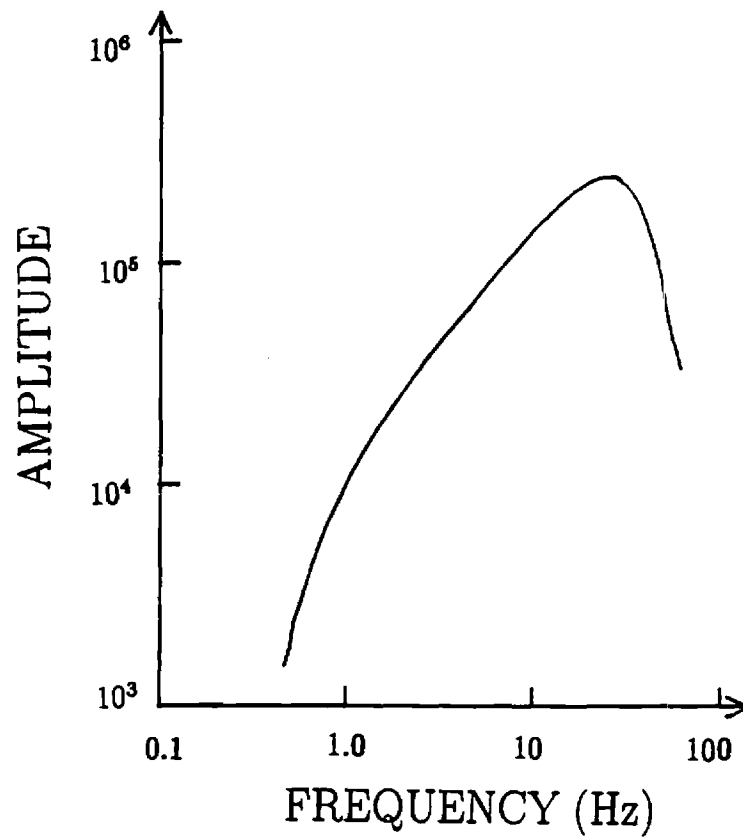


Figure 2: System response, Georgia Tech Seismic Network. Modulus, or amplitude spectrum.

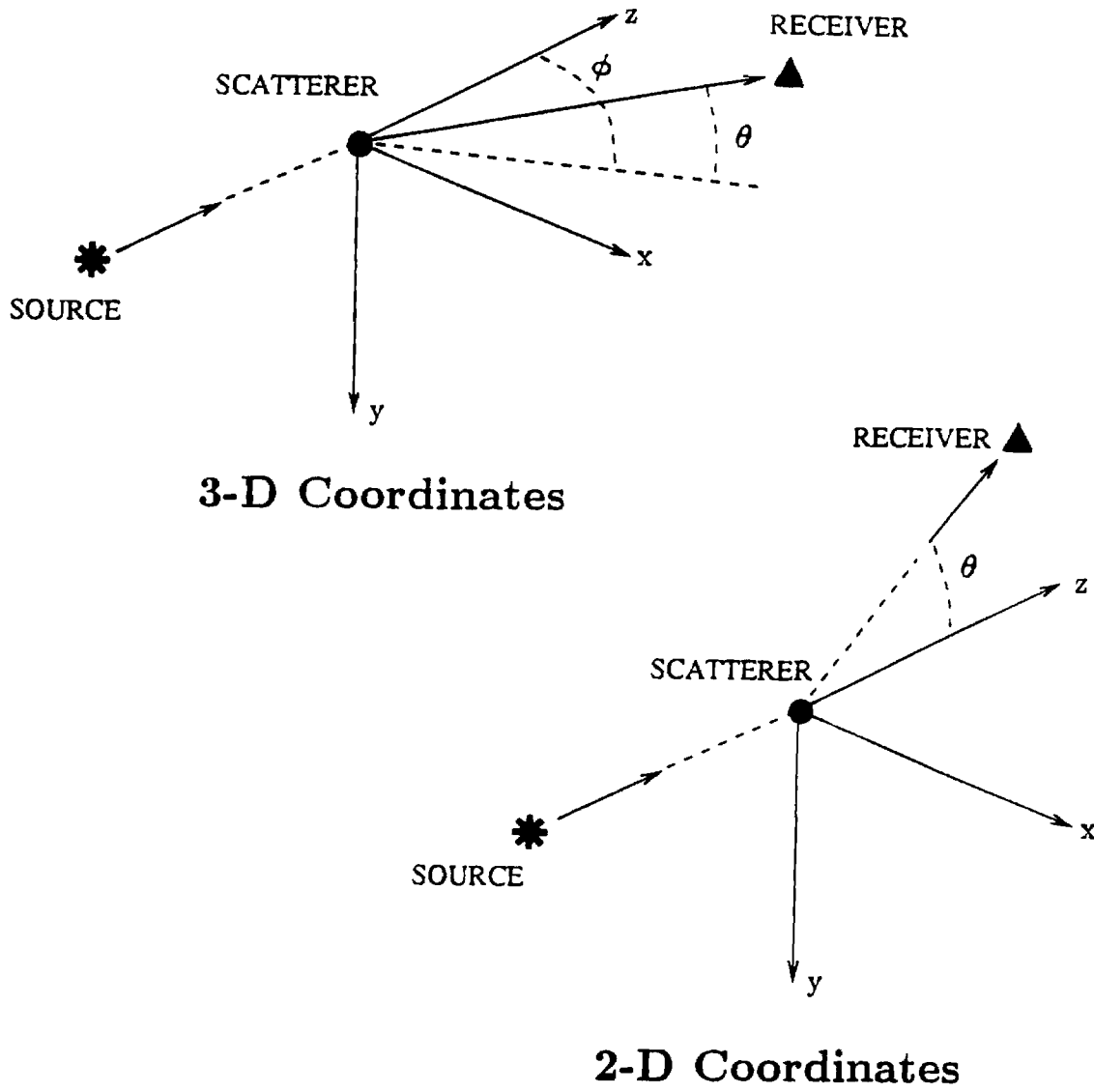


Figure 3: Scatterer-based polar coordinate systems. Scatterer is located at the origin. The source, indicated by a star, is located on the negative z axis and the receiver is indicated by a triangle. The deflection of the ray path from scatterer to receiver is given by azimuthal angle ϕ and polar angle θ .

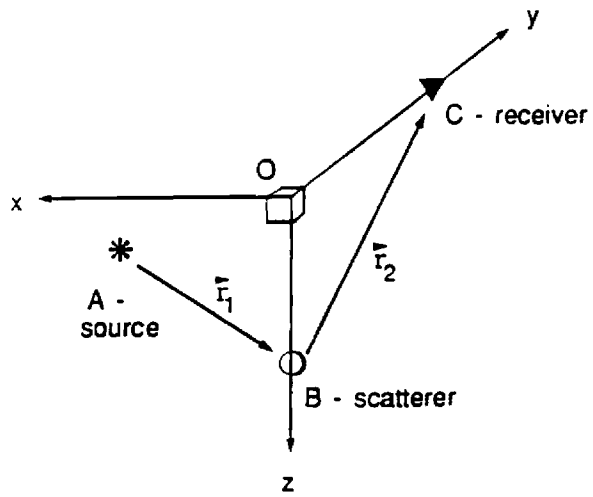


Figure 4: Coordinate system used to determine polarization of the scattered *S*-wave

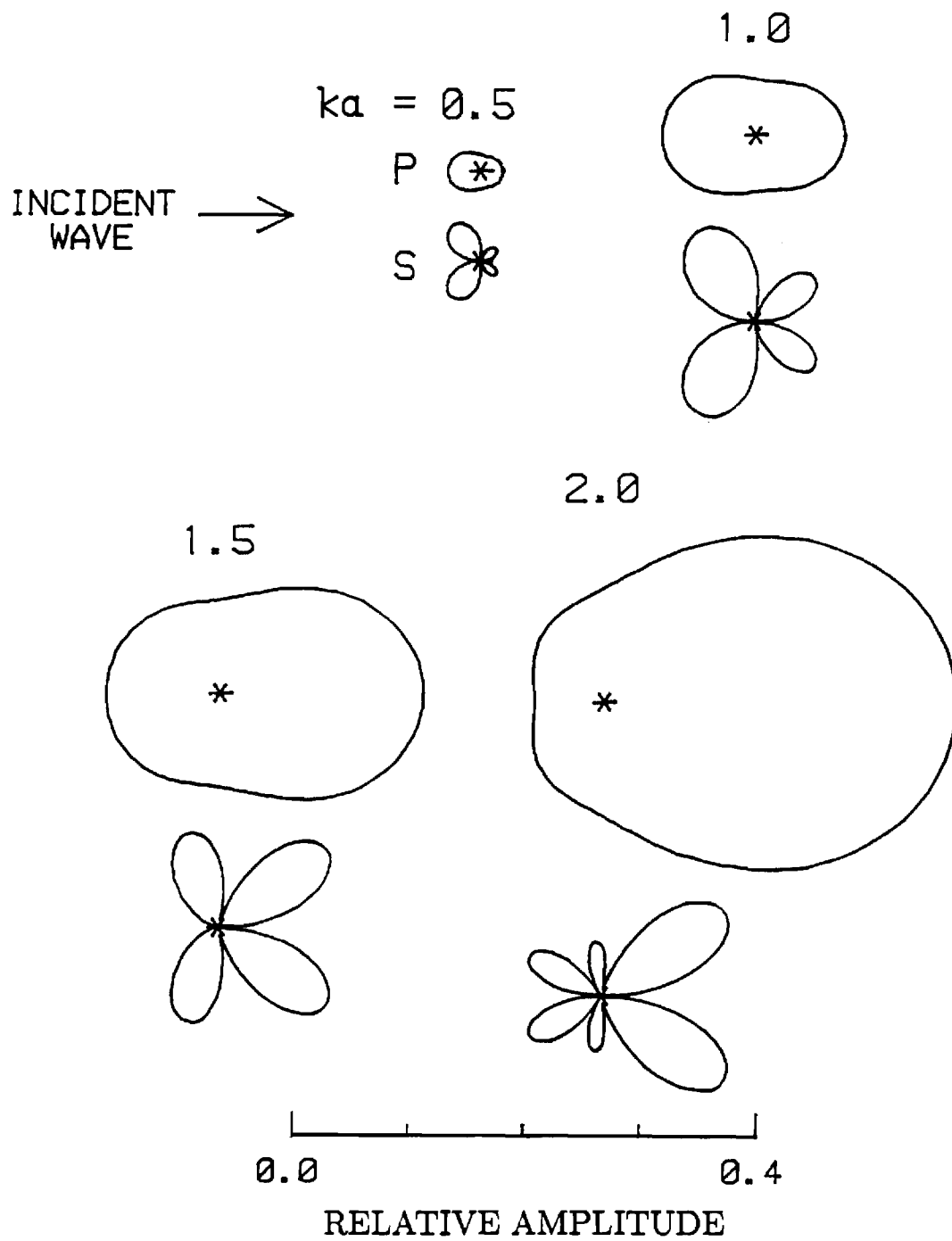


Figure 5: Radiation patterns, 14% P -wave velocity contrast. ka is non-dimensional wavenumber of P -waves in the host medium. Responses shown for $ka = 0.5, 1.0, 1.5,$ and 2.0 . The distance from the origin to the solid curve indicates the amplitude (modulus) of the scattered response.

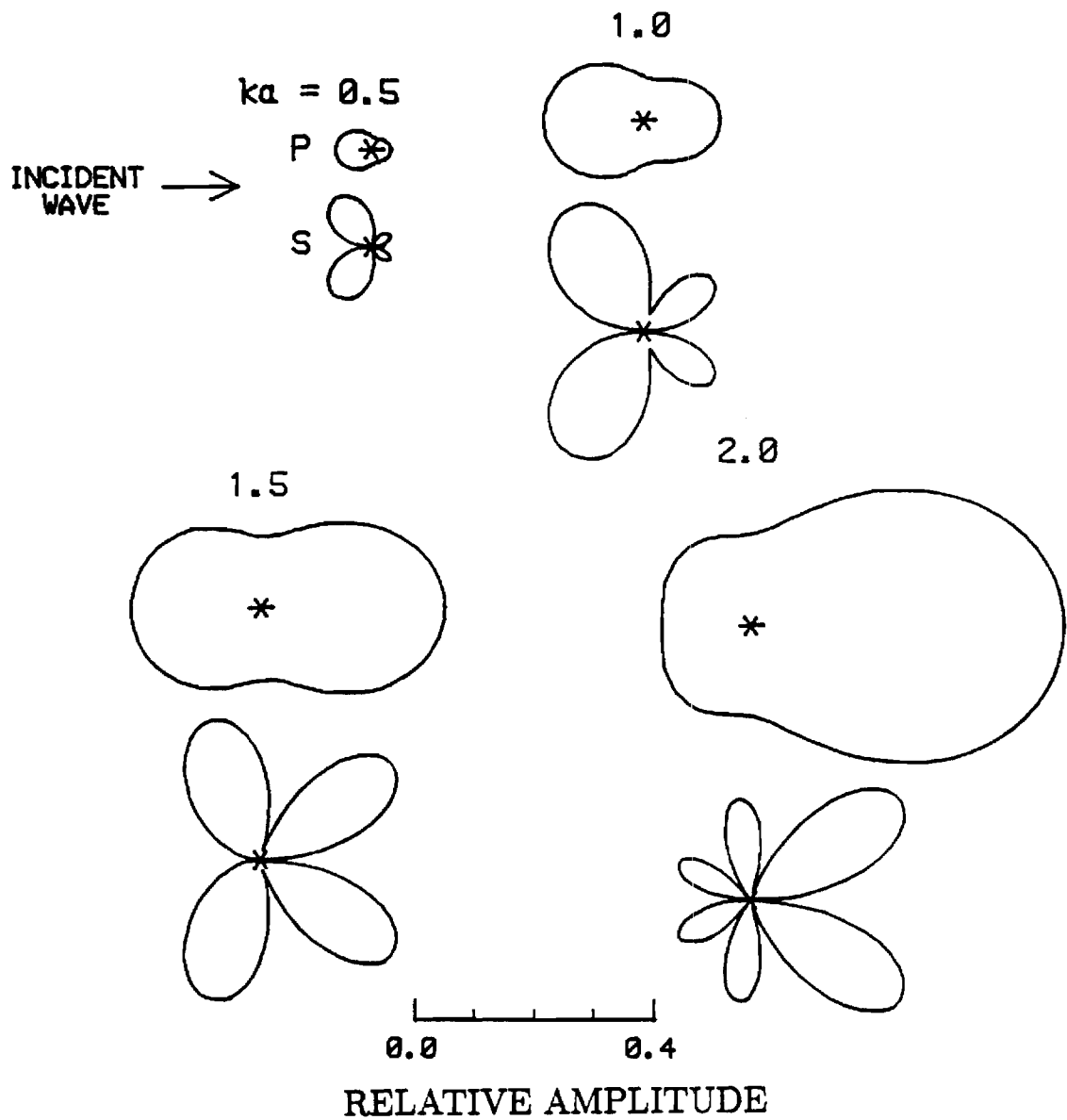


Figure 6: Radiation patterns, 28% P -wave velocity contrast. host. ka is non-dimensional wavenumber of P -waves in the host medium. Responses shown for $ka = 0.5, 1.0, 1.5,$ and 2.0 . The distance from the origin to the solid curve indicates the amplitude (modulus) of the scattered response.

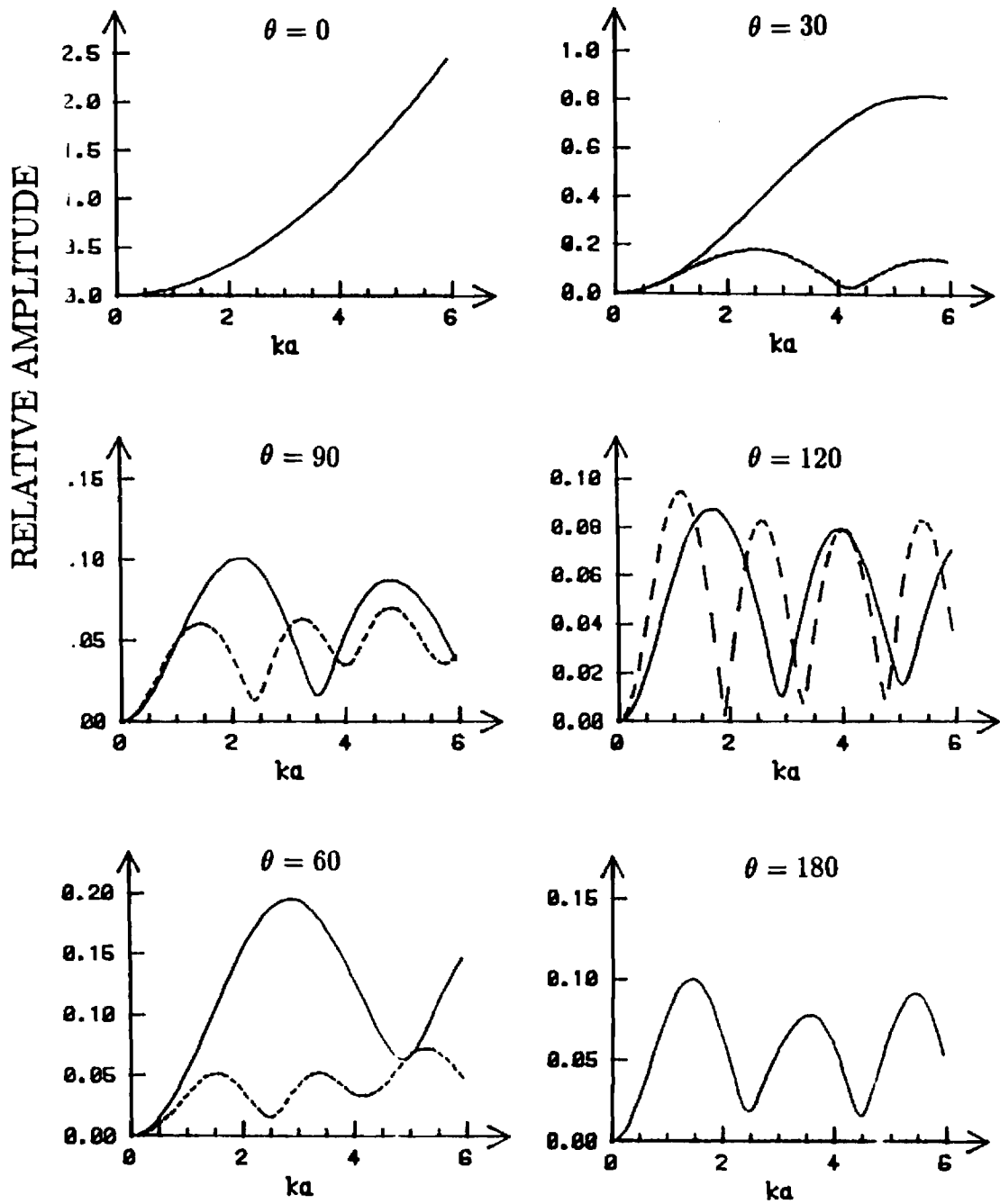


Figure 7: Scattered responses, 14% P -wave velocity contrast. P responses are indicated by solid curve, S responses are dashed. ka indicates non-dimensional wavenumber of P -waves in the host medium. Amplitudes are relative to an incident wave of amplitude one for all ka . Note that the vertical scale varies among the plots.

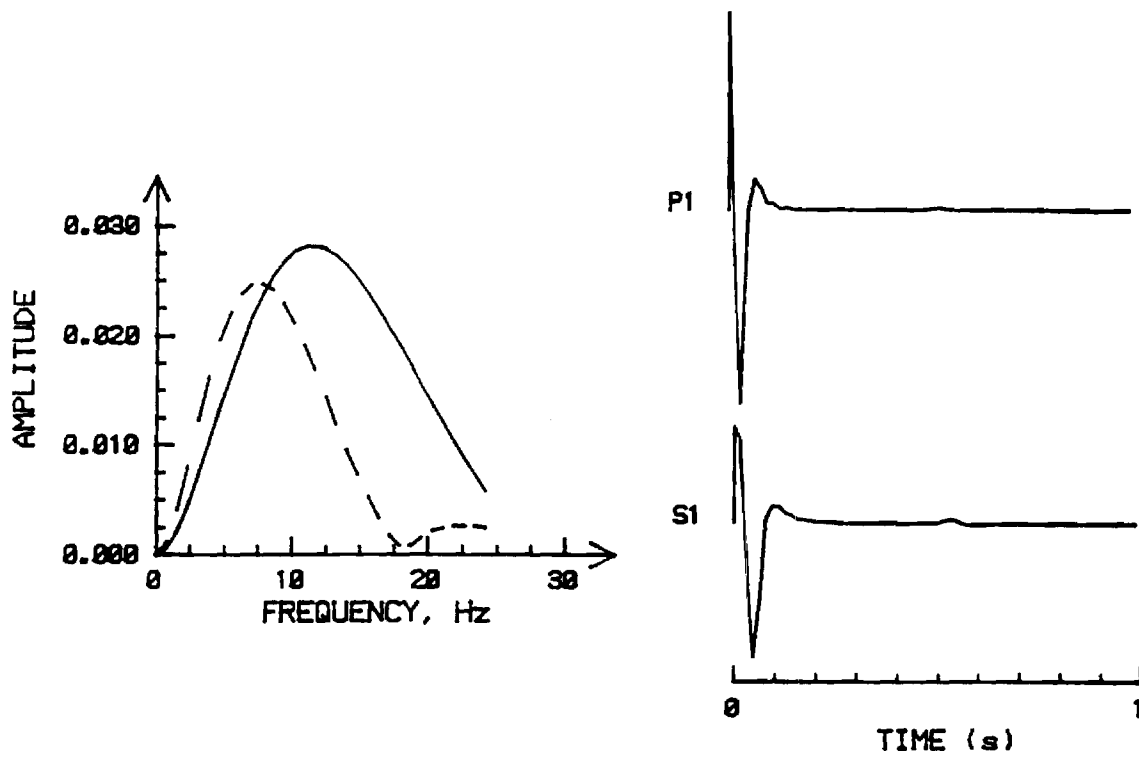


Figure 8: a. Products of attenuation operator and scattering response, P wave (solid) and S wave (dashed). b. Inverse Fourier transforms of their minimum-phase spectra.

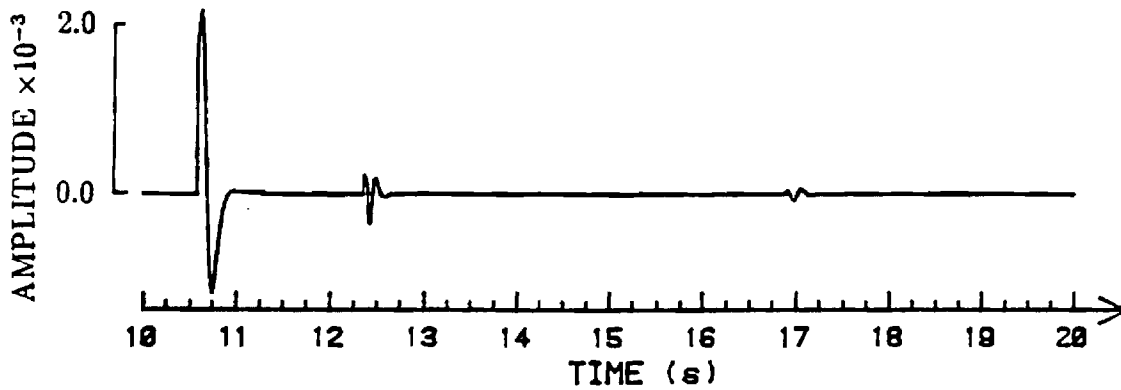
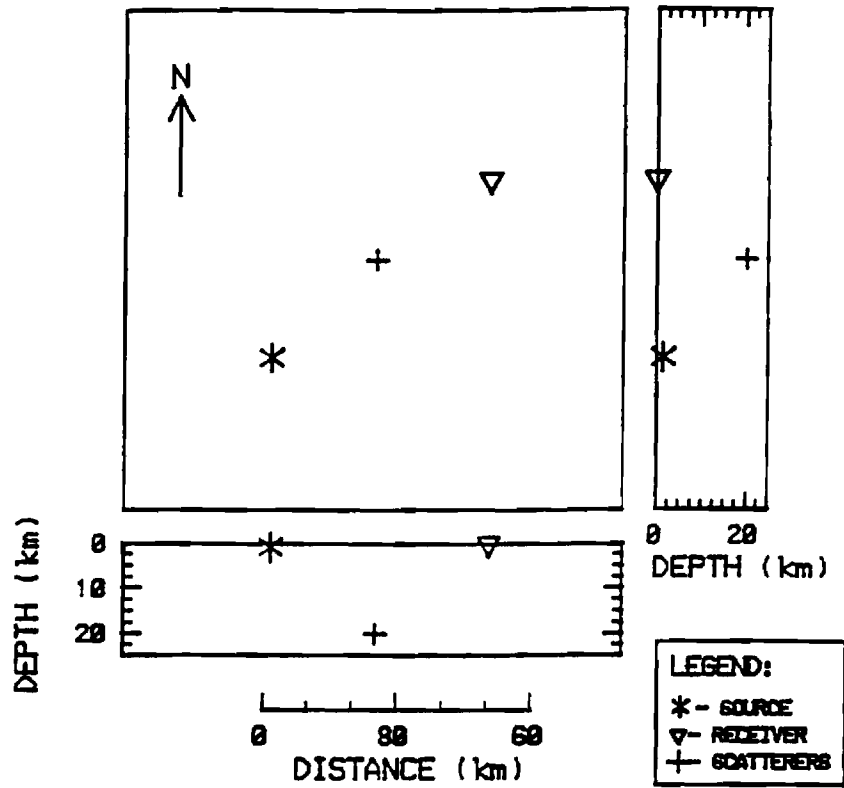


Figure 9: One-scatterer model and synthetic seismogram. The model is shown in plan view and two profiles. The direct wave, scattered P -, and scattered S -waves are shown in the seismogram.

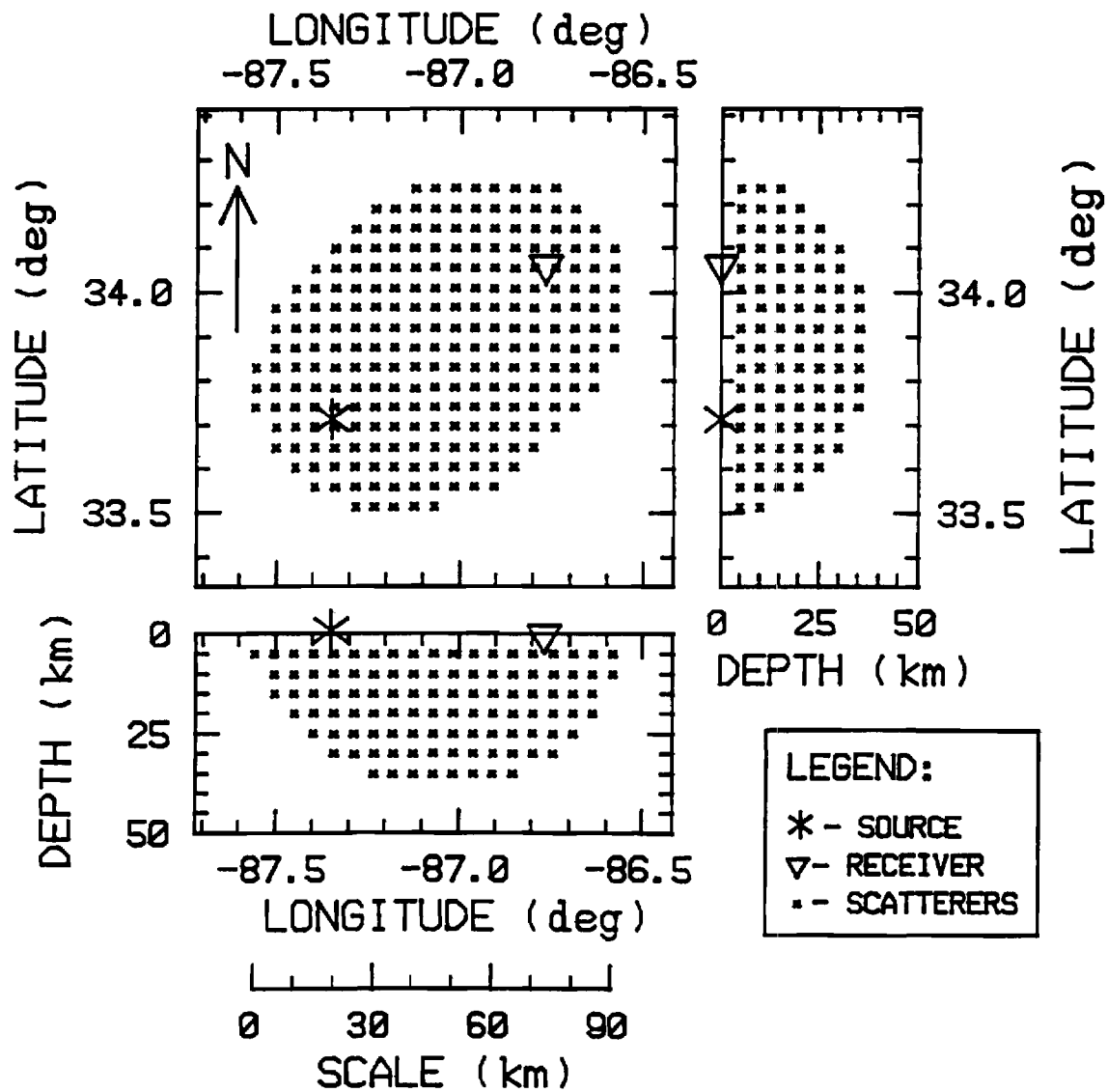


Figure 10: Alabama blast model, plan view and cross-sections. Source and receiver indicated with star and triangle. Scatterers to be considered in coda synthesis are indicated with plusses.

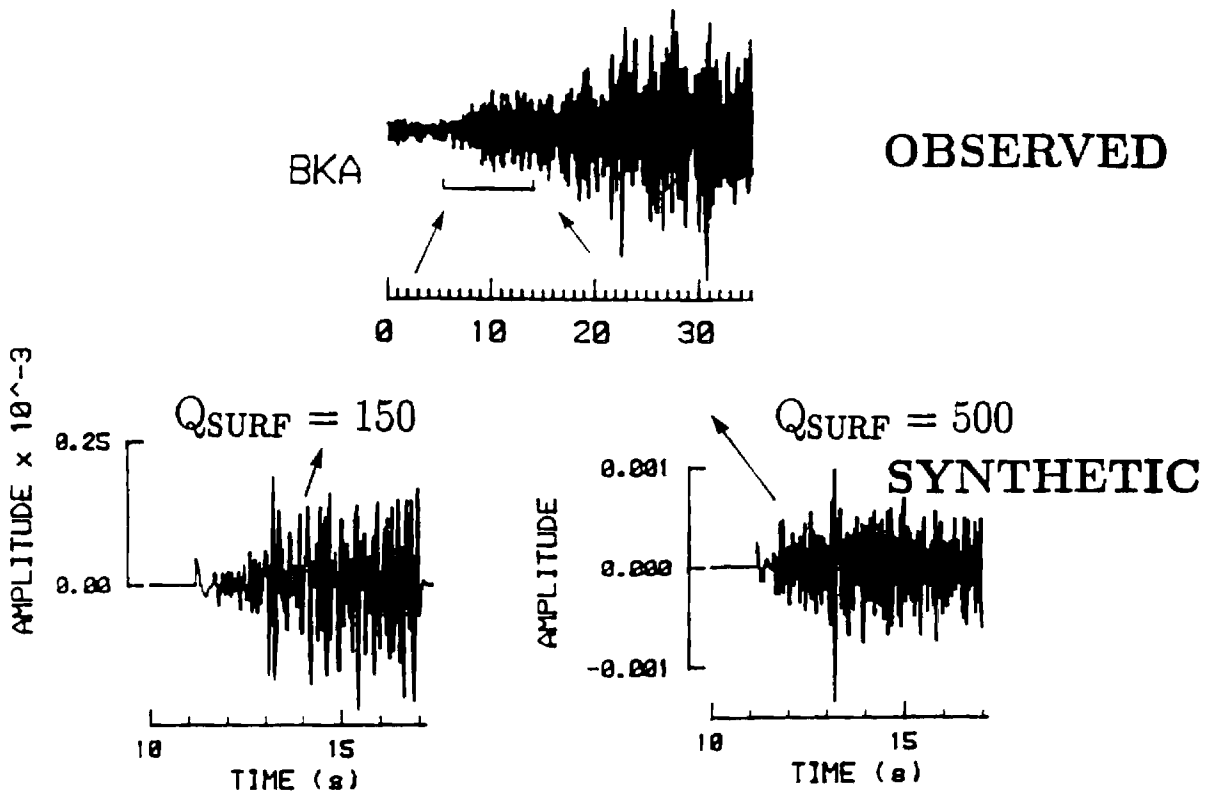


Figure 11: Comparison of observed blast (top), emergent onset, with synthetic seismograms (bottom). *P* coda in observed data is indicated by square bracket. Models for both synthetics used scatterers of radius $a = 0.1$ km.

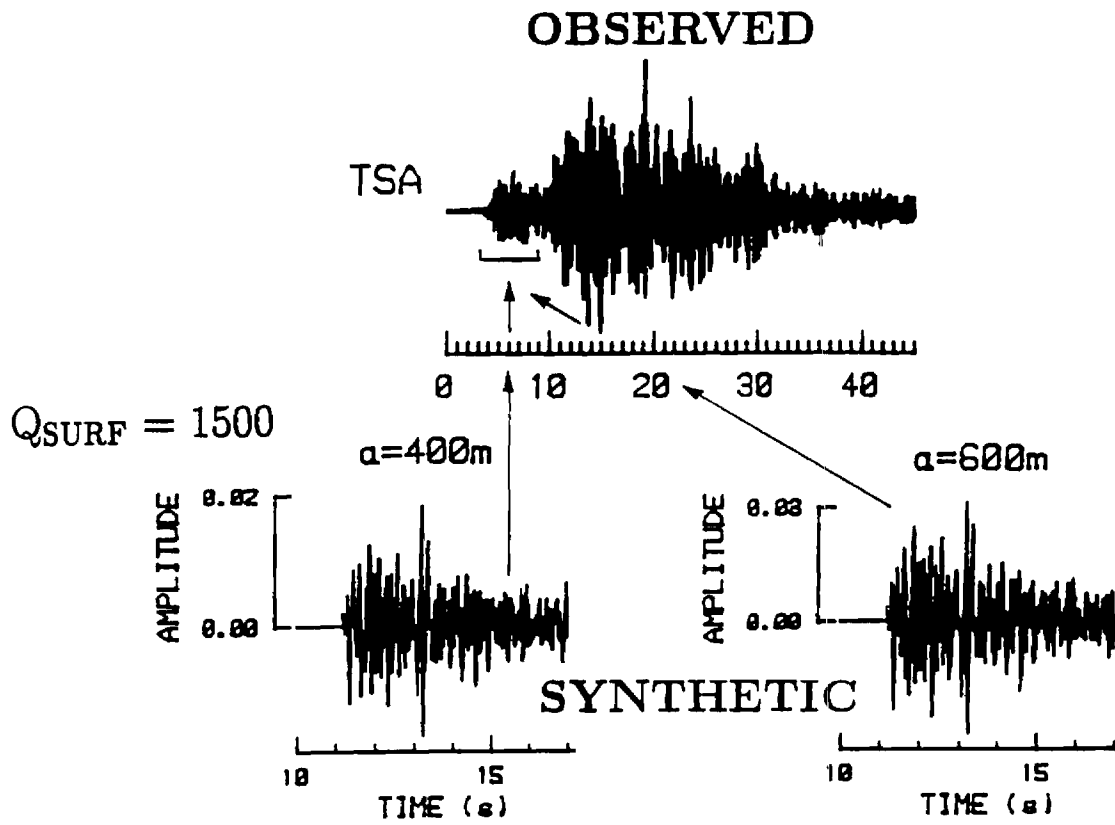


Figure 12: Comparison of observed blast (top), impulsive onset, with synthetic seismograms (bottom). *P* coda in observed data is indicated by square bracket.

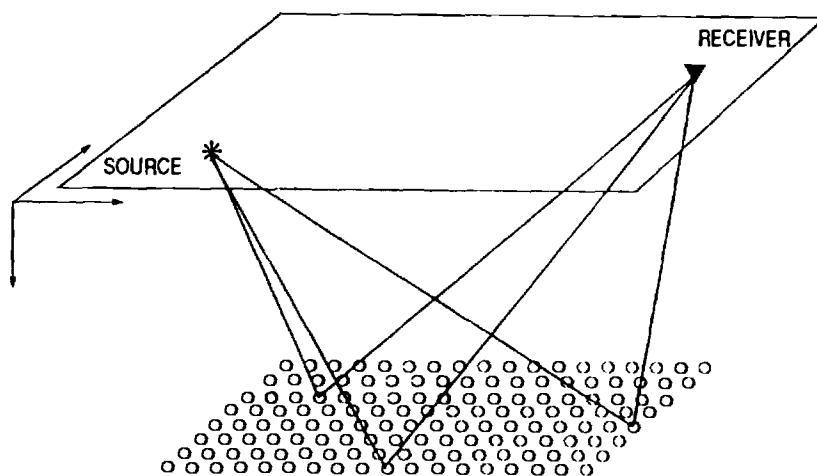


Figure 13: Schematic model for horizontal layer of scatterers. A few of the scattered raypaths are indicated.

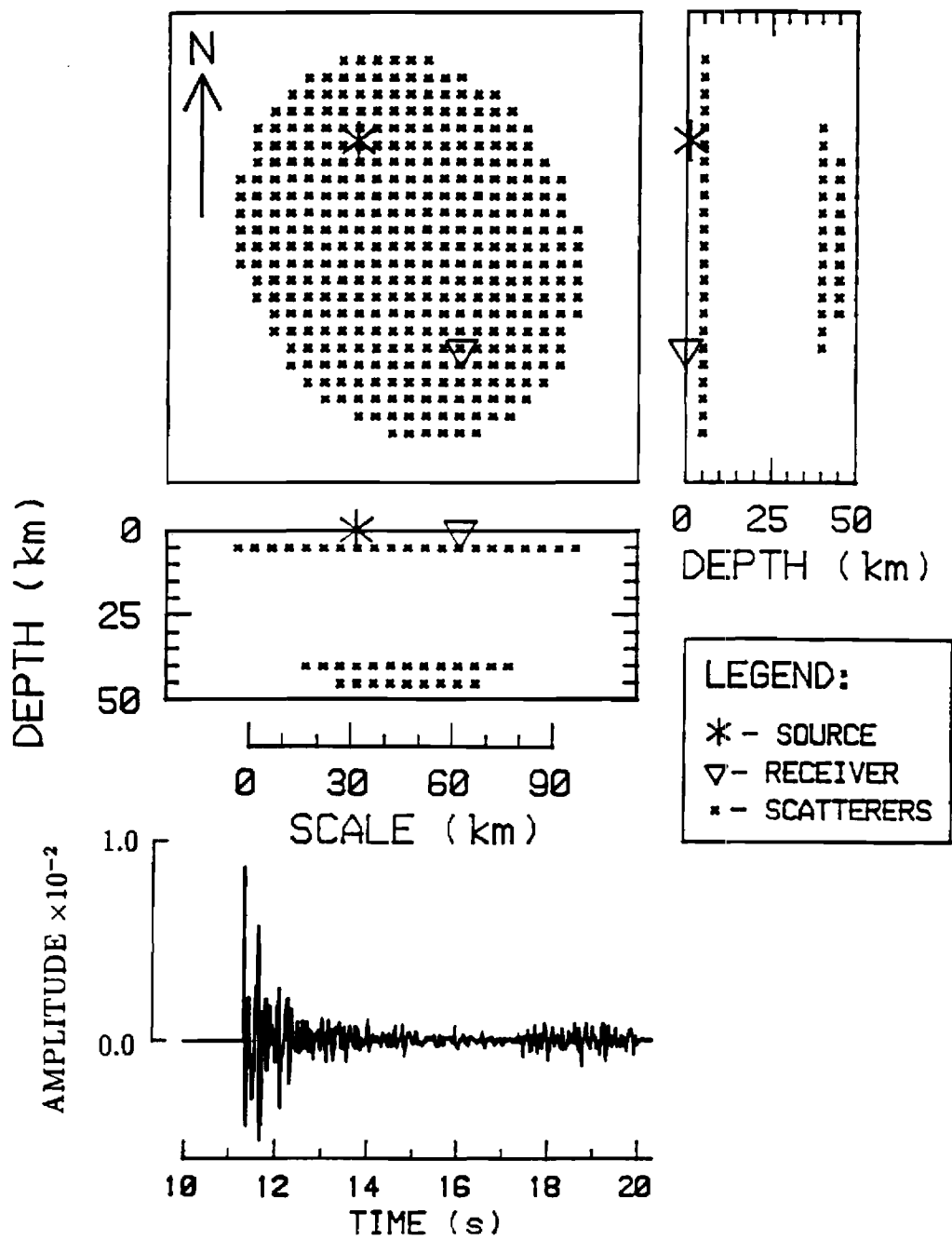


Figure 14: Model and synthetic seismogram for horizontal layer of scatterers.

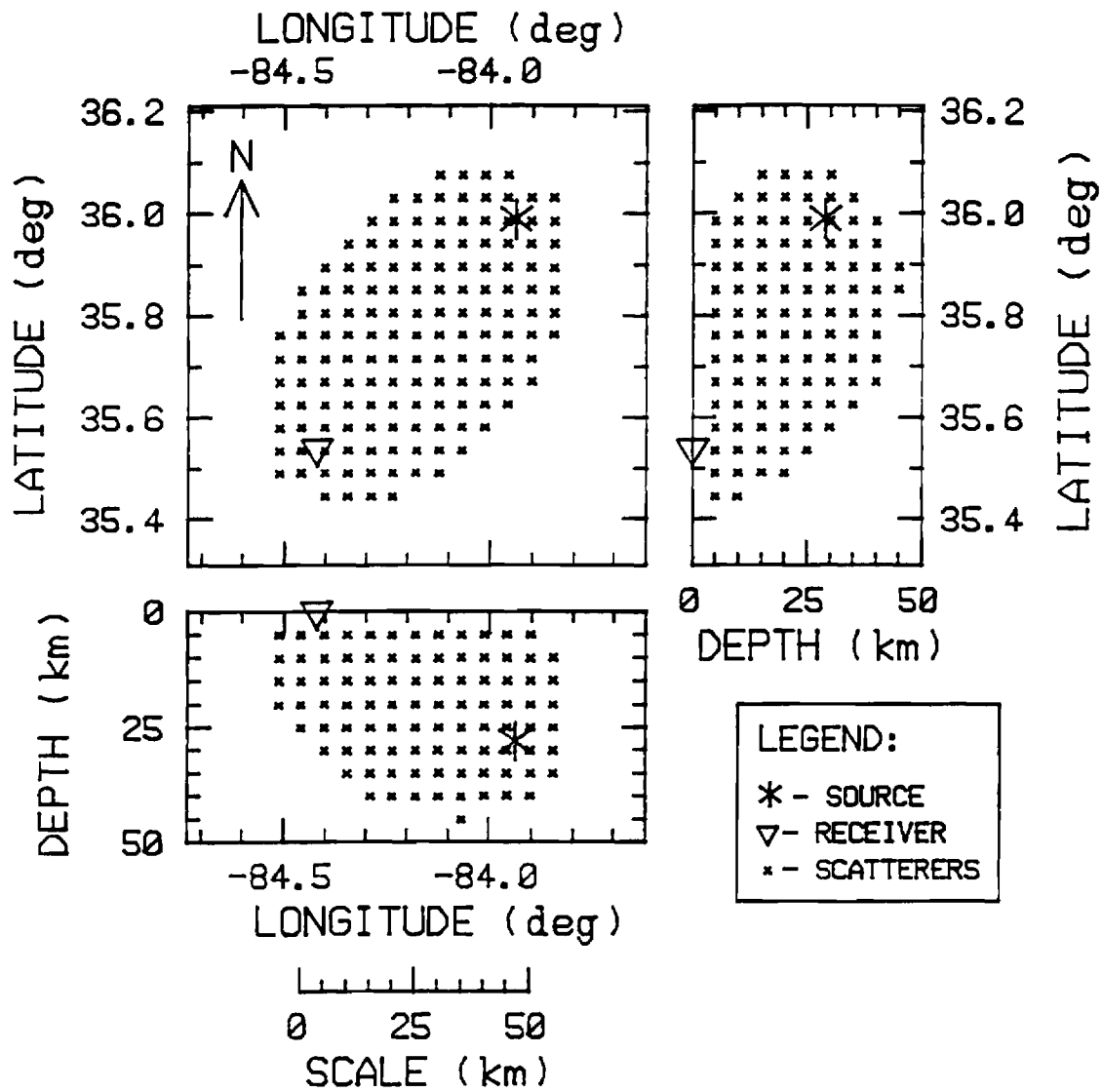


Figure 15: Earthquake model, plan view and cross-sections. Source and receiver indicated with star and triangle. Scatterers to be considered in coda synthesis are indicated with plusses.

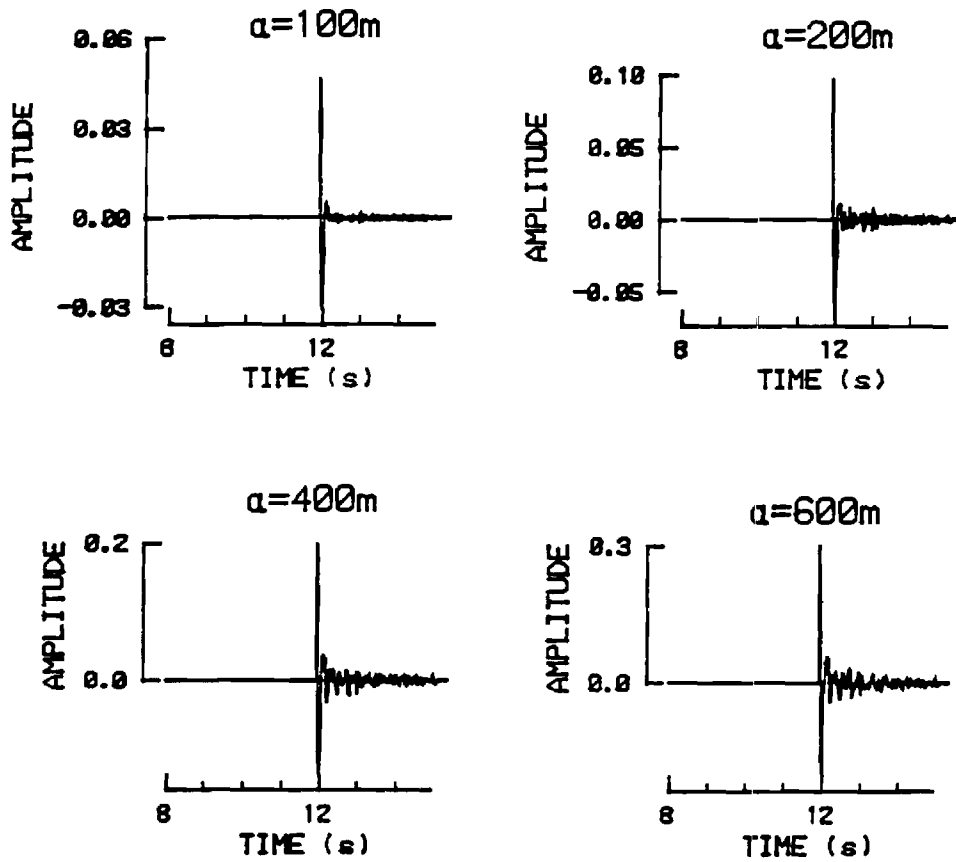


Figure 16: Synthetic seismograms generated using earthquake model, scatterer radius 100-600m.

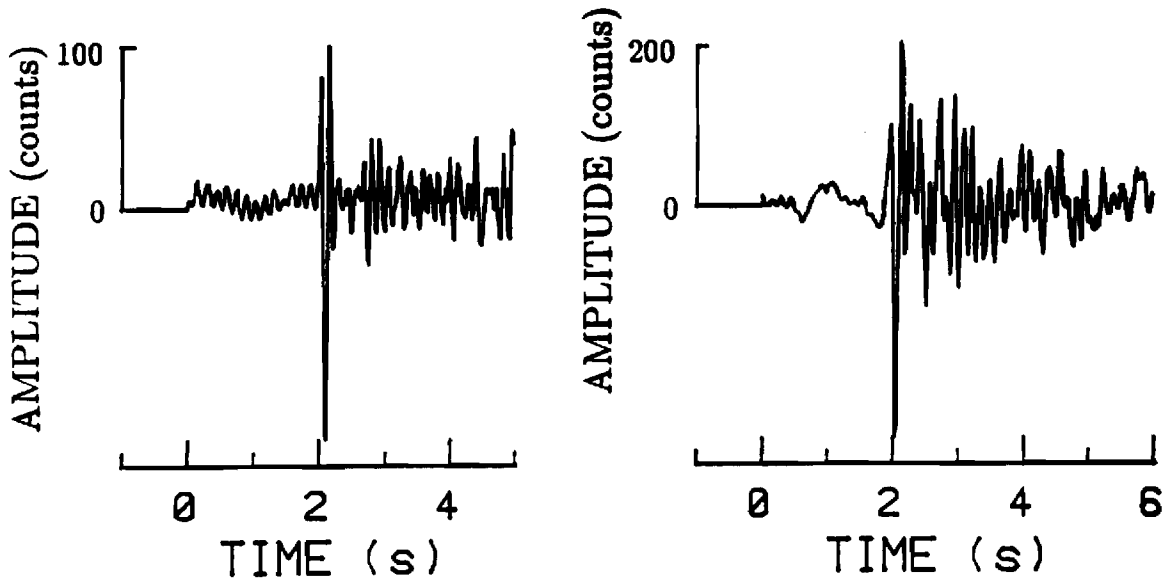


Figure 17: *P*-wave codas of earthquakes recorded in Tennessee

APPENDIX B

A Model for Major Intraplate Continental Earthquakes

Leland Timothy Long
School of Geophysical Sciences
Georgia Institute of Technology
Atlanta GA 30332

Published in: Seismological Research Letters, Volume 59, No. 4,
October-December, 1988.

APPENDIX B

A MODEL FOR MAJOR INTRAPLATE CONTINENTAL EARTHQUAKES

Leland Timothy Long

ABSTRACT: Traditional paradigms of continental seismicity assert the stationarity of the earthquake process and a causal association of earthquakes with active faults, increasing levels of stress, and crustal structures, in a framework of Plate Tectonics. I propose, instead, that the seismicity associated with a magnitude six or greater intraplate continental earthquake is a transient phenomenon responding to a perturbation in crustal strength independent of existing faults and crustal structures. Regional plate stress may still provide the driving energy, but the causative stress is released by a perturbation in crustal strength in the vicinity of a major earthquake. The timing of a major earthquake and the characteristics of the associated seismicity may then be described by a sequence of five phases which are as follows: (1) Initiation. A major intraplate continental earthquake is initiated with a disturbance in the hydraulic or thermal properties of the crust below the epicenter. Such disturbances could be induced by the intrusion of a sill or by partial melting. (2) Strength corrosion. A corrosion in crustal strength follows the upward migration of fluids or heat from the area of recent disturbance. (3) Stress concentration. As a weakened central zone deforms in response to tectonic plate stress, stresses are concentrated in the surrounding rigid crust. (4) Failure. A major earthquake occurs when the stress surrounding the weakened core exceeds the crustal strength, either because the concentrated stresses are anomalously high or because the dispersing fluids have spread beyond the core. (5) Crustal healing. The final phase in the occurrence of a major intraplate continental earthquake is an extended aftershock sequence which is concentrated along the rupture zone of the main event. The occurrence of a major intraplate earthquake as described above releases the strain energy in a perturbed area. Additional major events would be unlikely until the strength has recovered sufficiently to equalize intraplate stress and permit a repeat of the cycle.

INTRODUCTION

The advent of Plate Tectonics has for many achieved the status of a Paradigm in the sense of Kuhn (1970). Although this assessment of the Plate Tectonics hypothesis is not immune from controversy (Mareschal, 1987), Plate Tectonics has achieved virtually universal acceptance and has for the last 20 years provided the earth science community with a basis for modeling and understanding the dynamic lithosphere. Present studies of

the continental and oceanic lithosphere consist largely of verifying the Plate Tectonics model through data acquisition and perfecting this model through the construction of sets of auxiliary hypothesis. A notable exception to the success of Plate Tectonics has been the lack of agreement on a generally acceptable model for major intraplate continental earthquakes. Hypothesis of diverse character (for examples see Dewey, 1985; Long et al., 1986) are yet to be rejected. Although the Plate Tectonics model deserves recognition for some measure of success (Dewey, 1988), formidable problems for its application to major intraplate continental earthquakes still exist because many observations, such as the sparsity of continually active surface ruptures, have not been reconciled with Plate Tectonics and because the existing models do not predict or explain isolated large earthquakes. Although Dewey (1988) does not see anomalies sufficient to imply an imminent revolution in seismotectonics, one might question whether the existing confusion in the understanding of intraplate continental earthquakes could suggest that the current routine science phase may be heading for a crisis, albeit only in intraplate seismotectonics, and whether at this time an examination of the application of commonly accepted paradigms to intraplate earthquakes might be in order.

For discussion purposes in this paper, a major intraplate earthquake or closely timed earthquake sequence is one with magnitudes greater than six and minimum fault rupture lengths on the order of 20 km. The Charleston, South Carolina, 1886, earthquake is such an event and the 1811-12 New Madrid sequence of at least 4 events would represent another. These and other major earthquakes are assumed to cause a failure of the strongest portion of the crust, which is typically in the depth range of 10 to 25 km. At these depths the tractional resistance to fault slip increases to the maximum stress sustainable in a viscous lower crust subject to a given strain rate (Chen and Molnar, 1983).

Intraplate continental earthquakes may be divided into two classes. The class containing large damaging earthquakes is the subject of the new model to be presented in this paper. These large events pose the dominant risk from intraplate continental earthquakes, but are limited to locations and time periods associated with a perturbation in the properties of the lower crust. The second class of events is dominated by small shallow earthquakes with limited seismic risk. The second class includes most of the shallow (0-10 km) focus earthquakes which can be attributed to many sources of stress or strength perturbation on existing shallow fractures. This class would include induced seismicity. These smaller shallow events play a role in this model for major earthquakes, as well as being widely distributed outside potential sites of major events.

In this paper I present alternatives or, perhaps, opposites to five paradigms in the seismotectonics of intraplate continental earthquakes and suggest a mechanism which is consistent with these alternatives. These alternatives are implicit in the basis for the proposed new model and question the extent that interiors of continental plates mimic the plate geometry and strength distributions of the more homogeneous oceanic plate and the extent that plate tectonics boundary phenomena can be transferred to intraplate tectonics. The model, if acceptable, could support the possibility that the alternate paradigms may be more appropriate for plate interiors. Also, the acceptance of this model could pose the possibility that adherence to the plate tectonics model has inhibited recognition of some dynamic processes in the lower crust that could play a large role in intraplate continental seismotectonics. If such a model can resolve inconsistencies in observations, explain why the old model does not work and predict new observations, then, perhaps, a change in our perspective of midplate continental seismotectonics is indeed in order.

FIVE PARADIGMS

Five paradigms for intraplate continental earthquakes are outlined in Table I. All have been questioned before and their degree of acceptance varies; but, in this paper a model is presented that simultaneously satisfies alternatives that are not generally accepted.

Paradigm 1: Earthquakes occur on active faults. This paradigm predates Plate Tectonics and holds that earthquakes occur through the release of stress accumulated on locked portions of active faults.

Alternative: Faults and related zones of weakness are created by the earthquake process and are not necessarily sites of future events. Faults are simply a manifestation of the earthquake process.

Paradigm 2: Earthquakes are the result of increases in deviatoric stress, released along faults or concentrated by structures in the crust.

Alternative: Earthquakes are a release of stress triggered by a decrease in strength which may be attributed to changes in physical properties of the crust.

Paradigm 3: The seismicity of the continental crust is associated with blocks of crust, major geologic structures, and their associated faults. The study of these structures should lead to an explanation for major earthquakes.

Alternative: The earthquake mechanism is independent of tectonic events and major geologic structures which are evident from studies of near-surface geology. The strength of the crust would be more dependent on depth than rock type and, perhaps, crustal strength would be controlled more by properties such as fluid content in the lower crust and upper mantle than by the rock type.

Paradigm 4: Short-term changes in pore-fluid pressure influence seismicity only in the vicinities of reservoirs.

Alternative: In this case the alternative is an expanded role for fluids in triggering earthquakes, including those at depth in the crust. This is the Hydroseismicity hypothesis as proposed by Costain et al. (1988).

Paradigm 5: Seismicity is a stationary process, with past events strongly suggesting the locations and magnitude distribution of events in the future. Locations of earthquakes in the past will continue to be active at the same rate.

Alternative: A major mid-plate earthquake and its aftershock sequence is a transient phenomena. Contemporary seismicity consists only of aftershocks from major past earthquakes and, as such, is of minimal utility in predicting future major events.

TABLE I Conventional Paradigms and Alternates.

<u>Conventional Paradigm</u>	<u>Alternate</u>
Active faults cause earthquakes	Earthquakes create faults
Increases in stress causes failure on crust	Change in strength causes failure
Crustal blocks and geologic structures control plate dynamics	Plate strength independent of block composition or block boundary
Reservoir induced seismicity is shallow and only near reservoirs	Hydraulic mechanism may occur anywhere "hydroseismicity"
Stationary process	Transient process

THE ALTERNATE MODEL

On discarding the traditional paradigms of intraplate continental seismicity and considering seismicity with the perspective of selected alternatives (or opposites), a model can be devised that describes the creation of a major earthquake and the characteristics of its associated seismicity. In this new model a major earthquake may be described as a sequence of five phases in the transient perturbation of the strength of the crust. The five phases are: (1) initiation, (2) strength

corrosion, (3) stress redistribution, (4) failure, and (5) crustal healing (see also Figure 1). I tender this model as an improvement over traditional paradigms for a description of the principal characteristics of zones of seismicity associated with a single major intraplate earthquake.

Phase 1 Initiation: The sequence of events leading to a major intraplate earthquake may be initiated with a disturbance in the hydraulic or thermal properties at Moho depths in a small portion of the continental crust. Such a disturbance could be induced by the intrusion of a sill or by partial melting. At the time of the initial disturbance, the strongest portion of the crust at a depth of 10 to 25 km cannot be penetrated by fluids from below. A horizontal zone of partial melt is formed and becomes a source for fluid and thermal perturbation of the overlying crust.

Evidence: During phase 1, the fluids generated in crustal underplating by intrusion of sills or partial melting in viscous deformation could create or enhance reflections from horizontal sills and provide direct evidence for the initiation of a major earthquake sequence. The existence of viscous deformation or multiple sills in the lower crust is suggested by the prominence of thin reflectors observed in deep crustal seismic reflection data (Allmendinger et al., 1987). Also, sills of molten material are observed at mid-crustal depths in areas of active tectonics (Brown et al., 1979). At Moho depths, studies suggest that a sharp reflecting Moho is the signature of recent tectonic activity and may be explained with the formation of sills. A reflecting Moho often is observed to truncate crustal structures of the most recent tectonic events, such as the vertical movements of the crust in the Basin and Range province (Klemperer et al., 1986). A possible association between seismicity and a sharp Moho (and hence recent tectonic activity) is suggested in the zone of active seismicity in southeastern Tennessee, where the Moho is clearly defined by reflections (Long and Liow, 1986), although the surrounding area is characterized by a gradational Moho (Owens et al. 1984).

Phase 2, Strength Corrosion: A corrosion in the strength of the lower crust could be caused by an upward migration of fluids or heat from the recently implanted sill or partial melting of the lower crust. The fluids may be driven by the higher temperatures of the sill or they may follow vertical tension cracks related to regional plate stress. Fluid pressures could vary between hydrostatic and lithostatic in sealed compartments controlled by a complex feedback among fluid flow, temperature, chemistry and strength.

A spatial variation in the crustal strength-versus-depth relation for the crust is generally accepted as an explanation

for differences in the maximum depth-of-focus of intraplate earthquakes (Chen and Molnar, 1983; Meissner and Strenhlau, 1982). Continental crust with earthquakes at a maximum depth of 5 to 15 km is characterized by high heat flow and recent tectonic activity. Continental crust with earthquakes at a depth of 15 to 25 km are characterized by limited tectonic activity and low heat flow. At shallow depths, the maximum possible stress is controlled by the mineralogical and physical properties of existing fractures, and Byerlee's law governing frictional strength versus depth. At depths below approximately 15 km the viscosity of the lower crust controls the ability to sustain stress. Increases in fluid content or temperature decrease the strength of the crust and shallow the zone of maximum possible stress. The corrosion of strength in a localized volume of the lower crust of a stable tectonic area could initiate seismicity by releasing regional compressive stress. This central zone or core of weakness would be a continuing zone of anomalous seismicity through phase 3. The dominant focal mechanism would be strike slip because the distortion of the weakened central zone, which would be analogous to the distortion in a hole in a plate, will keep the vertical axis the neutral axis. The corrosion of strength would imply preference over existing fault planes for new fault planes defined by the directions of maximum shear stress .

Evidence: Coda Q , which can be estimated using a space-time function for coda energy density, varies with seismic activity. Zones of anomalous Q are observed under volcanic regions and the Q value is observed to vary with the progress of a volcanic eruption (Fehler, et al., 1988). In China areas of low coda Q are associated with the largest earthquakes (Jin and Aki, 1988). In southeastern Tennessee coda Q was computed by the technique of Jin and Aki (1986). A simple inversion for Q structure suggests that azimuthal variations of coda decay can be explained by a zone of anomalously low coda Q (less than 100) in the area of southeastern Tennessee (see figure 2) which contains the largest and most numerous events (Long et al., 1987). This area exhibits a uniform strikeslip focal mechanism (Teague et al., 1986). The low coda Q suggests a perturbation in the fluid or fracture properties of the crust and the strikeslip focal mechanisms are consistent with the reaction of a central zone of weakness to regional plate stress. The presence of fluids in cracks and microcracks at depth in the crust explains (Al-Shukri and Mitchell, 1988) the association of enhanced earthquake activity with low velocity in the crust near the New Madrid seismicity.

Phase 3, Stress Concentration: The development of a central zone or core of weakness through a disturbance in the fluid and thermal properties is not sufficient in itself to cause a large earthquake. The area of developing weakness must also be under stress if energy is to be available for a large event. A likely source of the stress would be horizontal plate stress, usually

attributed to ridge push mechanisms. As a weakened central zone relaxes, stress is transferred to the surrounding more rigid crust where it is concentrated the greatest at the boundary of the core of weakness. In this phase, earthquake activity is greatest in the central zone, but surrounding the central zone earthquakes may occur with fault planes too small to rupture the strongest portion of the crust. These could represent stress adjustments on shallow planes of weakness, where the source of stress could be a reaction of the shallow crust to flexure about the deforming core of weakness. These events could also be triggered by a changing hydraulic regime.

Evidence: Finite element and theoretical models (Campbell, 1978) of a plate with core of weakness show increased stress surrounding the core. Stress within the core would be less, but uniform in its response to the regional stress. In this theoretical model the pattern of stress directions outside the core depend on the concentration at the boundary of the core and can include principal axes directions and magnitudes that deviate significantly from those of plate stress.

In southeastern Tennessee, a concentration of stress is suggested by the distribution of focal mechanisms (see figure 2). Inside the low coda Q area, which may coincide with a core of weakness, the dominant focal mechanism is strikeslip. Focal mechanisms outside this area show significant thrust and normal components. The pattern of seismicity in southeastern Tennessee is one of a concentration of activity in the vicinity of the low-Q area and activity becoming more diffuse with distance away from the central zone. The shallower events outside the core may represent a response of crustal zones above the maximum strength depth zone to distortion of the stress channel around the core of weakness.

Phase 4, Major Failure: A major earthquake occurs when the stress surrounding the central disturbed zone exceeds the strength of the crust, perhaps, because the dispersing crustal fluids have spread beyond the central disturbed zone and weakened the crust or because the stress load has shifted to the outside of the core of weakness. The geometrical pattern of the central zone and the dispersion of the fluid may determine the location and existence of the major earthquake. If the major earthquake occurs, at least two distinct patterns of faulting are possible. One pattern would consist of two near-vertical faults striking parallel to the direction of maximum shear stress of the regional field and extending away from diagonally opposite edges of the central core. These faults could be connected in the central zone by a fault or a series of faults in the complimentary direction. The other pattern would develop when deformation is resisted by a thinned strong portion of the crust above the core. In this case the major earthquake will occur on a reverse fault

with dimensions comparable to the size of the core of weakness.

Evidence: In the New Madrid seismic zone the pattern of aftershocks define two sub-parallel faults trending north-northeast and a connecting west-northwest sequence of faults (see figure 2). Various segments of these faults are believed to have ruptured during the sequence of four large events in 1811 and 1812. Hence, for the New Madrid earthquake zone, the contemporary pattern of faulting was developed through a sequence of earthquakes. The other pattern was exhibited by the Marryat Creek, Australia, earthquake (McCue et al., 1987). The focal mechanism was strike slip with a thrust component which was more evident in the surface displacement.

Phase 5, Decay: The final phase in the occurrence of a major intraplate earthquake is an extended aftershock sequence. The fluids, no longer replenished by the hydraulic or thermal disturbance of the lower crust, dissipate from the core, subsequently increasing the strength of the crust and inhibiting additional earthquakes, except along the weakened fractures of the major event. Aftershock activity concentrates on the fault plane of the main event(s) and associated faults instead of in the core. Also, the amplified stress around the core is released, decreasing the overall level of stress and limiting the potential for additional significant activity.

Evidence: Most major earthquake areas in the eastern United States can be modeled as aftershock sequences. This is a controversial conclusion that is best illustrated by the Charleston seismicity. Seismologists generally accept the assumption that the immediate aftershock activity ended within a few years (Seaber and Armbruster, 1987); however, the felt events for the full 100 years are satisfied just as well by Omori's law for aftershocks (Long, 1982; Bollinger, 1983). Prior to 1886, the Charleston area showed little evidence of seismic activity.

DISCUSSION

Each phase of the proposed model suggests phenomena that could be observed with available geophysical techniques. Such observations could answer questions concerning the details of this mechanism. In phase 1 the strength and coherence of a reflecting Moho in an incipient seismic area could be an indication of recent underplating of the crust and evidence that new fluids or thermal perturbations are available to initiate the sequence of events leading up to a major intraplate earthquake. Variation in time of the Moho reflection amplitude, including the appearance of bright spots, could identify new locations of possible major events and answer questions concerning the rates

of fluid movement in the lower crust. In phase 2, the orientation of fractures with the direction of principal regional stress might be measured with shear-wave anisotropy. In phase 3 the depth distribution and focal mechanism of events surrounding the active central core should reflect the deformation and accumulation of stress. The dominant strike-slip focal mechanisms in the core of weakness suggests conditions that should continue to foster anisotropic behavior of the crust. Also, the central core should exhibit anomalously low Q. By identifying potential candidate seismic zones for phase 3, the areas of high risk may be restricted to a few areas where the pattern of seismicity suggests a potential for a major earthquake. In phase 4 the size and perhaps existence of the major event would be proportional to the magnitude of plate stress, as well as the size of the perturbed zone. In phase 5 the seismicity should exhibit a decay in activity typical of extended aftershock sequences.

The occurrence of a major intraplate continental earthquake as described in this model decreases the stress in the perturbed area. Additional major events would not be expected there again until the strength has recovered enough for a repeat of the cycle and until the regional plate stress has re-equilibrated. The rate of strength recovery is one unanswered question, but the time to recover half the strength must be on the order of an extended aftershock sequence. Incomplete recovery could provide paths for later intrusions, particularly if located over a recognized hotspot, and explain evidence for repeated major events in areas like New Madrid. Another unanswered question is the time required to progress through phase three. Evidence on the rate of movement of magma suggest this time could be on the order of years. Other unanswered questions concern the size of the lower crustal disturbance needed to trigger a major event and the certainty of the major event occurring in a seismic zone currently in phase three.

Many of the phenomena suggested above have not been observed, perhaps, in some cases because of a lack of data. However, many of the enigmas of major continental earthquakes, such as the pattern of epicenters in New Madrid, the lack of continuous seismic activity on the Meers fault, and the lack of continuous shear zones showing long-term deformation, are described by a model satisfying alternatives to traditional paradigms for continental seismicity. If such a model can resolve these and other inconsistencies in observations, explain why some aspects of the Plate Tectonics model do not work and predict new observations, then, perhaps, a change in our perspective of continental tectonics is indeed in order.

REFERENCES

- Allmendinger, R. W., K. D. Nelson, C. J. Potter, M. Barazangi, L. D. Brown, and J. E. Oliver (1987). Deep seismic reflection characteristics of the continental crust, Geology, 15, 304-310.
- Al-Shurri, H. J., and B. J. Mitchell (1988). Reduced seismic velocities in the source zone of New Madrid earthquakes, Bull. Seism. Soc. Am., 78, 1491-1509.
- Brown, L. D., P. A. Krumhansl, C. D. Chapin, A. R. Sanford, F. A. Cook, S. Kaufman, J. E. Oliver, and F. S. Schilt, (1979). COCORP seismic reflection studies of the Rio Grande rift, in Rieker, R. E., ed., Rio Grande rift: Tectonics and magmatism: Washington, D. C., American Geophysical Union, 169-184.
- Bollinger, G. A. (1983). Speculations on the nature of seismicity at Charleston, South Carolina, in Gohn, G. S., ed., Studies related to the Charleston, South Carolina, earthquake of 1886; Tectonics and Seismicity: U. S. Geological Survey Professional Paper 1313, T1-T11.
- Campbell, D. L. (1978). Investigation of the stress-concentration mechanism for intraplate earthquakes. Geophys. Res. Lett., 5, No. 6, 477-479.
- Chen, W. P., and P. Molnar (1983). Focal depth of intracontinental and intraplate earthquakes and their implications for the thermal and mechanical properties of the lithosphere, J. Geophys. Res., 88, 4183-4214.
- Costain, J.K., G.A. Bollinger, and J.A. Speer (1987). Hydroseismicity: a hypothesis for the role of water in the generation of intraplate seismicity, Seism. Res. Lett., 58, 41-64.
- Dewey, J.W. (1988). Hypocenter mapping and the extensibility of seismotectonic paradigms, Proceedings, Univ. California Seismographic Stations. Centennial Anniversary Symposium, Univ. California Press, Berkeley.
- Dewey, J.W. (1985). A Review of Recent Research on the Seismotectonics of the Southeastern Seaboard and an Evolution of Hypotheses on the Source of the 1886 Charleston, South Carolina, Earthquake, U.S. Geological Survey NUREG/CR-4439.
- Fehler, M., P. Roberts, and T. Fairbanks (1988). A Temporal Change in Coda Wave Attenuation Observed During an Eruption of Mount St. Helens, Geophys. Res., 93, 4367-4374.
- Jin, Anshu, and K. Aki (1986). Temporal Change in Coda Q before

the Tangshan earthquake of 1976 and the Haicheng earthquake of 1975, Journal of Geophysical Research, 91, No. B1, 665-673.

Jin, Anshu, and K. Aki (1988). Spatial and temporal correlation between coda Q and seismicity in China, Bull. Seism. Soc. Am., 78, 741-769.

Klemperer, S. L., T. A. Hauge, E. C. Hauser, J. E. Oliver, and C. J. Potter (1986). The Moho in the northern Basin and Range, Nevada, along the COCORP 40°N seismic reflection transect, Geological Soc. Am. Bull., 97, 603-618.

Kuhn, T.S. (1970). The Structure of Scientific Revolutions (2nd ed.), University of Chicago Press, Chicago, 210 pp.

Long, L. T. (1982). Seismicity of Georgia, in Proceedings, Second Symposium on the Petroleum Geology of the Southeastern Coastal Plain, Information Circular 53, Georgia Geological Survey, Atlanta, Georgia, 202-210.

Long, L. T., and J.-S. Liow (1986). Crustal thickness, velocity structure, and the isostatic response function in the southern Appalachians, in Reflection Seismology: The Continental Crust; Geodynamics Series Volume 14. American Geophysical Union, Washington D.C., p 215-222.

Long, L. T., R. E. White, and J. Dwyer (1986). The Charleston Earthquake Hypotheses - A Classification by Fundamental Tectonic Processes, Proceedings of the Third U. S. National Conference on Earthquake Engineering, August 24-25, 1986, Charleston, South Carolina, 25-32.

Long, L. T., J.-S. Liow, and F. B. Jones (1987). A technique for the inversion of coda Q, (abs.) Seismological Research Letters, 58, 101.

Mareschal, Jean-Claude (1987). Plate Tectonics: Scientific Revolution or Scientific Program, EOS Trans. Am. Geophys. Union 68, 532.

McCue, K., B.C. Barlow, D. Denham, T. Jones, G. Gibson and M. Michael-Leiba (1987). Another Chip Off the Old Australian Block, EOS, Trans., Am. Geophys. Union, 68, 609.

Meissner, R., and J. Strenhlau (1982). Limits of stress in continental crusts and their relation to the depth-frequency distribution of shallow earthquakes, Tectonics, 1, 73-89.

Owens, T. J., G. Zandt, and S. R. Taylor (1984). Seismic evidence for an ancient rift beneath the Cumberland Plateau, Tennessee: A detailed analysis of broadband teleseismic P

waveforms, J. Geophys. Res., 89, 7783-7795.

Seeber, L. and J. G. Armbruster (1987). The 1886-1889 aftershocks of the Charleston, south Carolina, earthquake: a widespread burst of seismicity, J. Geophys. Res. 92, 2663-2696.

Teague, A. G., G. A. Bollinger and A. C. Johnston (1986). Focal mechanisms analyses for eastern Tennessee earthquakes (1981-1983), Bull. Seism. Soc. Am., 76, 95-109.

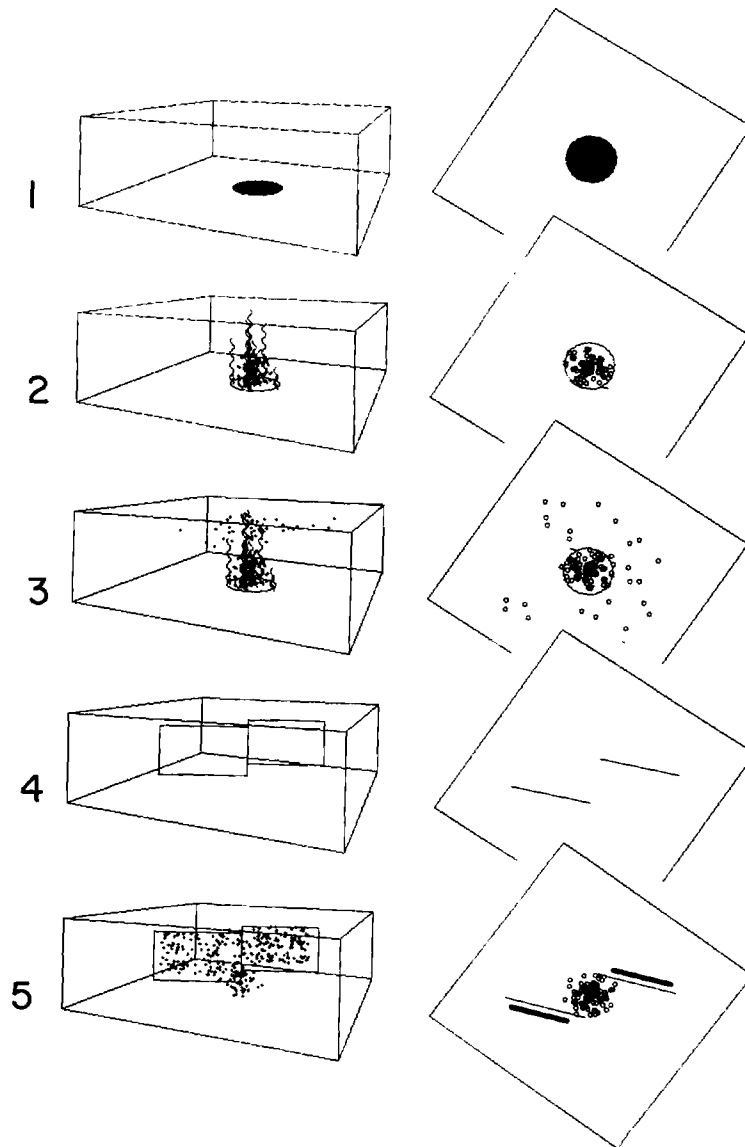


Figure 1. Illustration of the five phases of a major intraplate earthquake. 1) Initiation by underplating. 2) Strength corrosion by fluid and thermal diffusion. 3) Stress concentration as indicated by increased shallow seismicity (epicenters are small dots). 4) Failure along major faults (outlined by rectangles). 5) Crustal healing during an extended aftershock sequence.

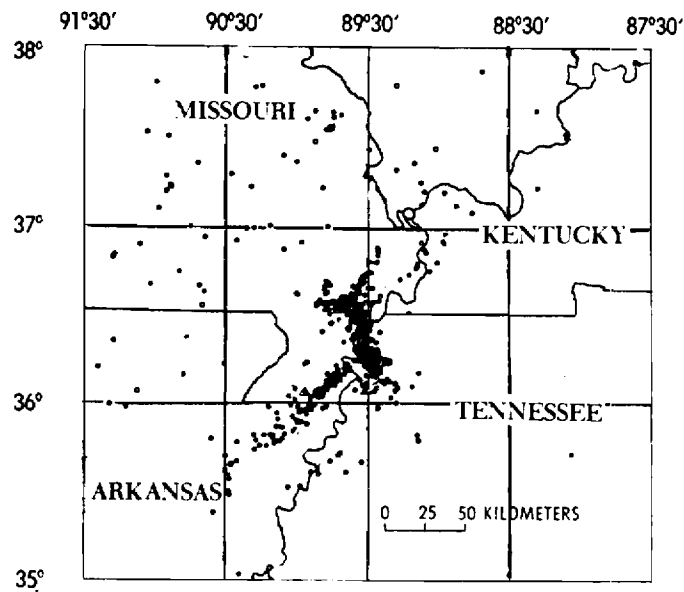
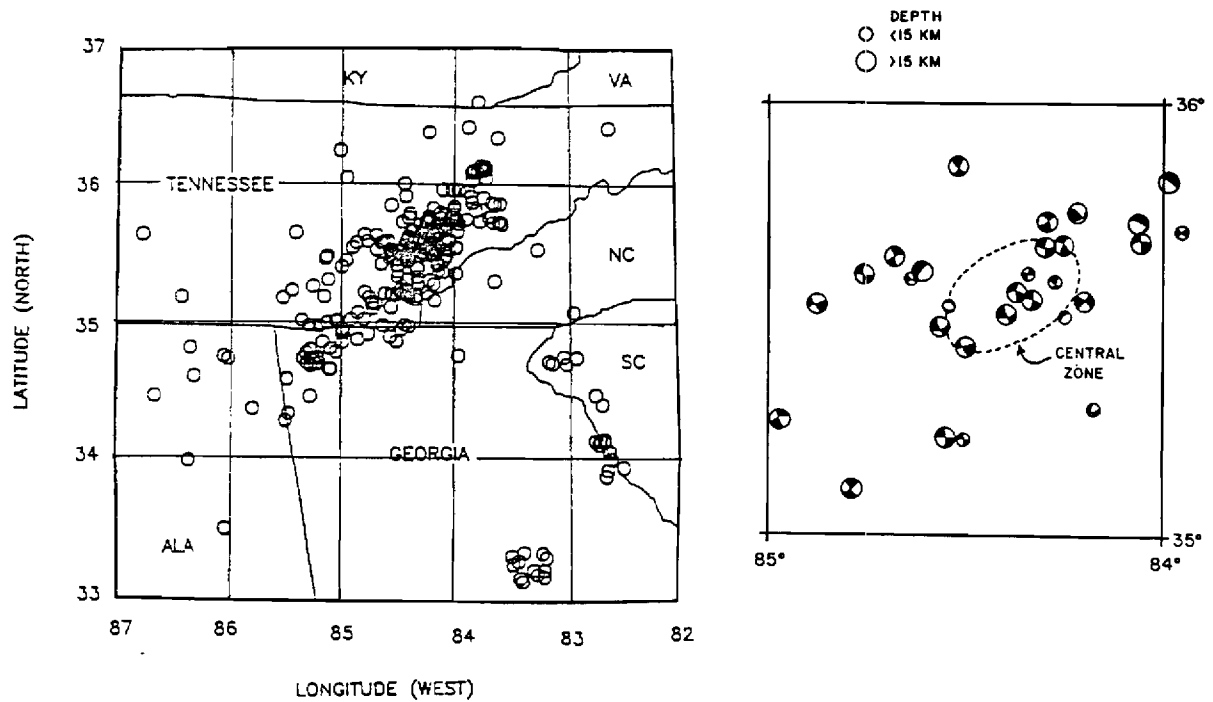


Figure 2. Pattern of seismicity and focal mechanisms for southeastern Tennessee; a possible example of phase 3. Pattern of seismicity for New Madrid; a possible example for phase 5.

APPENDIX C

A Local Weakening of the Brittle-Ductile Transition
can Explain Some Intraplate Seismic Zones

Leland Timothy Long and Karl-Heinz Zelt

Accepted for publication in Tectonophysics

APPENDIX C

A LOCAL WEAKENING OF THE BRITTLE-DUCTILE TRANSITION CAN EXPLAIN SOME INTRAPLATE SEISMIC ZONES

Leland Timothy Long and Karl-Heinz Zelt⁺

⁺ Now with Shell International, Den Haag, Netherlands

ABSTRACT: A decrease in the strength of a localized area of the lower crust would decrease the depth to the brittle-ductile transition and concentrate stress in the stronger elastic crust around and above the zone of decreased strength. Deformation within the zone of weakened lower crust would occur through viscous or dislocation creep in response to regional plate stress as well as by elastic failure in small earthquakes. Two-dimensional finite-element models of zones of weakness subjected to a regional plate stress predict stress amplification of 10 to 100 percent surrounding the local decrease in strength. A finite element model for an irregular zone of weakness in the lower crust can generate stress directions and relative magnitudes that satisfy the focal mechanisms and seismicity of southeastern Tennessee. An analysis of the displacements and stresses in the central area of decreased crustal strength suggests that strike slip faulting should dominate. Above this zone the strike slip faulting should exhibit a strong thrust component. The compression and extension of the crust surrounding the weakened zone at the level of the brittle-ductile transition predicts that the dominant strike slip faulting should exhibit components of normal faulting on the edges of the weak zone which are near a line through the weak zone parallel to the regional stress and reverse faulting on the edges which are near a line transverse to the regional stress.

The seismicity of southeastern Tennessee is diffused over a narrow elliptical zone trending northeast. The greatest concentration of activity is near the center. The central zone is characterized by deep-focus strike slip events with predominantly north or east striking nodal planes. These events are responding directly to compression in the direction of the regional compressive stress and extension perpendicular to the regional compressive stress within the weak zone. The uniformity of the focal mechanism solutions suggest that these earthquakes are not occurring on a random distribution of fractures and may be forming new faults. The area surrounding the central zone is characterized by focal mechanisms with larger components of reverse or normal fault movements. Events with normal components are dominant on the edges in line with the regional stress as predicted by the stress model for a weak central zone under stress. The agreement between observed earthquake focal mechanisms in southeastern Tennessee and models of crustal stress surrounding a zone of weakness suggests that these events may be

caused by a zone of weakness in the lower crust.

INTRODUCTION

Many hypotheses have been offered for major intraplate earthquakes and seismic zones (Dewey, 1985; Long, et al., 1986). Most efforts to identify hypotheses have concentrated on describing a causative structure common to active seismic zones; however, differences in the tectonic setting of seismic zones such as the southeastern Tennessee seismic zone and the aftershock zone of the 1886 Charleston, South Carolina, earthquake have made identification of common structures difficult. A pervading paradigm underlying most hypotheses is that the stresses generated by forces at plate boundaries and, possibly, by topographic or density loads reactivate preexisting faults or other weak structures. This study considers the response of weak zones in the lower crust to regional tectonic stress and compares crustal stress surrounding simulated weak zones with focal mechanism solutions for earthquakes in southeastern Tennessee.

The consistency of principal compressive stress directions in the interiors of crustal plates has long been recognized (McKenzie, 1969; Sbar and Sykes, 1973; Zoback and Zoback, 1980). Stresses in plate interiors exist in response to forces at mid-ocean ridges (Turcotte and Schubert, 1982, pg 287) and these forces can be transmitted over a large distance by the elastic lithosphere. Other forces associated with plate boundaries are those of slab-pull near subduction zones (Bott and Kusznir, 1984), forces associated with transform faults (Byerlee, 1978) and those related to viscous shear of asthenospheric convective flow (Richardson et al., 1979; Solomon et al., 1980; Fleitout and Froidevaux, 1982, 1983). Mareschal and Kuang (1987), and Kuang, et al. (1989) investigated the role of stresses from topographic and gravitational loading and concluded that variations in the stress field do to topography and density anomalies are comparable in magnitude to regional stresses generated by the forces of plate tectonics. They observed that zones of increased stress are consistent with the seismicity in southeastern Tennessee, but that the observed strike slip focal mechanisms could not be predicted with the same pattern of zones of higher stress. The maximum stresses associated with these forces are on the order of tens of MPa. In comparison, stresses required to cause brittle failure of the upper crust can range from 8 MPa at shallow depths to 9000 MPa in the lower crust (Meissner and Strehlau, 1982). Consequently, tectonic stresses alone cannot cause brittle failure unless the strength of the crust is low at the earthquake focus, usually assumed to be on an old fault.

The southeastern United States is situated within the North American Plate, where earthquakes of magnitude greater than 5.0

are rare and where the last major tectonic activity occurred in the Jurassic Period, during the opening of the Atlantic. In-situ stress measurements and earthquake focal mechanisms (Sbar and Sykes, 1973; Zoback and Zoback, 1980; Zoback, 1983) show that the greatest principal (compressive) stress in North America is horizontal and trends along the direction of plate motion, consistent with the regional stress originating from ridge push forces near the mid-Atlantic ridge. For southeastern Tennessee Zoback and Zoback (1980) predict northeast-southwest compression, consistent with 14 previously available focal mechanism solutions (Johnston et al., 1985; Teague et al., 1986).

Sykes (1978) proposed that intraplate earthquakes reactivate and follow preexisting zones of weakness, such as sutures developed in the Appalachian orogenic belt during the closing of the Proto Atlantic Ocean. Other cited zones of weakness which exhibit seismicity are the Ottawa-Bonnechere rift graben (Rankin, 1976) and the late Precambrian-early Paleozoic continental rift in the New Madrid area (Zoback, 1980). Talwani (1988) argued that major earthquakes prefer the intersection of zones of weakness. Other authors have stressed high-angle reverse motion on reactivated normal faults bordering Triassic basins along the eastern seaboard (Prowell and O'Connor, 1978; Reinhardt et al., 1984; Aggarwal and Sykes, 1978). Bollinger and Wheeler (1988) argued that the Giles county, Virginia, seismicity was best explained by reactivation of Iapetan normal faults.

These hypotheses do not explain the temporal and spatial clustering of earthquake epicenters in southeastern Tennessee and western North Carolina (Bollinger, 1973) or in the Charleston area. Estimates of recurrence rates from contemporary seismicity imply cumulative Quaternary displacements that are much larger than geological data can justify without invoking temporal clustering (Coppersmith, 1988). To explain the spatial clusters of seismicity in the eastern United States, attempts have been made to correlate earthquakes with mafic crustal units. These correlations are largely attempts to associate seismicity with concentrations of stress in the crust induced by inhomogeneous distributions of material properties. Fox (1970) was one of the first to speculate on the possible significance of the association of epicenters with mafic Paleozoic rocks in the Blue Ridge province. In studies of the Bowman and Charleston, South Carolina, seismicity, Long (1976) proposed a stress amplification mechanism that may explain seismicity near mafic intrusives and noted that the stress concentrations around or in an inclusion are a function of the ratio of the Young's modulus of the inclusion to that of the host, the shape of the inclusion and the applied stress. Kane (1977) extended the correlation of mafic intrusions with seismicity to other areas in the eastern United States. Long and Champion (1977) argued that earthquakes in the Charleston, South Carolina, area were better explained by stress amplification in or near a large mafic crustal intrusion

than by reactivation of the known faults. McKeown (1978) correlated the orientation of mafic intrusives with fault orientations and existing focal mechanism solutions for the New Madrid seismic zone and the southern Appalachian seismic zone. McKeown (1978) then used the stress calculations of Oudenhoven et al. (1972) to explain anomalous stress around solid inclusions. Whereas the above mentioned authors assumed intrusions stiffer than the surrounding plate, Campbell (1978) determined theoretical stress values associated with weakened intrusions. He suggested that mafic intrusions weakened possibly by serpentinization may concentrate stresses more than 200 percent above the regional values. The highest differential stress factor was found in the plate just outside the inclusion, implying that most or all brittle-failure earthquakes near a weak inclusion will occur in the plate nearby, not in the inclusion itself. The lack of a definitive association with seismicity has characterized all the mafic intrusion and stress concentration hypotheses. While they demonstrate the capability of variations in crustal rigidity to generate anomalous stress, many significant crustal units which should be anomalously rigid do not exhibit seismicity and the predicted stress distributions have not been confirmed with focal mechanisms

The discovery and improved understanding of the brittle-ductile transition at mid-crustal depths (Chen and Molnar, 1983; Meissner and Strehlau, 1982) has added a new dimension to discussions of stress distributions in the crust. They have shown that the depth to the brittle-ductile transition correlates with the maximum depth of earthquakes in continental interiors. A perturbation in the depth to the brittle-ductile transition due to the thermal effects of the cooling of a mid-crustal intrusion was investigated by Gettings (1988). He speculated that the residual thermal effects of an intrusives of late Miocene age or younger could cause shallowing of the brittle-ductile transition of 3 kilometers or more at the present and thus provide an area of possible stress amplification or concentration to explain the 1886 Charleston seismicity.

Long (1988) used the concept of a change in the properties of the brittle-ductile transition in the crust as the basis for a new hypothesis for major intraplate continental earthquakes. In Long's model the perturbation is caused primarily by the movements of fluids instead of the slower mechanism of thermal conduction. Long's (1988) model is based on a sequence of five phases. In the first phase of a major intraplate earthquake, the hydraulic or thermal properties of a portion of the continental crust at Moho depths is disturbed. Such a disturbance could be induced by the intrusion of a sill or by partial melting. In the second phase the upward migration of fluids or heat from the area of recent disturbance corrodes the strength of the crust near the brittle-ductile transition. As a weakened central zone deforms in response to regional stress during the third phase, stresses

are concentrated in the surrounding rigid crust. The fourth phase is the possible occurrence of a major earthquake when the stress surrounding the weakened central zone exceeds the crustal strength, either because the concentrated stresses are anomalously high or because the dispersing fluids have spread and weakened the crust outside the central zone. The final and fifth phase in the occurrence of a major intraplate earthquake is an extended aftershock sequence which concentrates near the fault plane of the main event.

The hypotheses of Long (1988) and Gettings (1988) are new in their use of a perturbed brittle-ductile transition and have not previously been confirmed by seismic data. In this study Long's (1988) model is tested by examining the stresses surrounding various shapes and sizes of a zone of crustal weakness within a compressed elastic crust. The magnitudes and directions of the principal stresses, which are computed using the finite element technique, are used to ascertain regions of likely seismicity and the relative location of strike-slip, normal and reverse focal mechanism solutions. In this study an attempt will be made to correlate the observed focal mechanism solution distribution for southeastern Tennessee with these computed crustal stresses,

SEISMICITY OF SOUTHEASTERN TENNESSEE

A dominant feature of the seismicity of the southeastern United States during the 1980's is the cluster of earthquakes in southeastern Tennessee. The relocation of over 296 earthquakes reveals a concentration of activity in the approximate center (84.3°W , 35.7°N) of the southeastern Tennessee seismicity (Fig 1) and fewer events in the surrounding elliptical seismic zone. Smaller and less active concentrations are found to the northeast near Maryville (84°W , 35.8°N) Tennessee (see Bollinger et al., 1976) and to the southwest in northwest Georgia (Long et al., 1986). Nearly continuous zones of seismicity extend from the center to the southwestern concentration in Georgia. Continuous linear zones of seismicity may also trend northwest across the seismic zone. One such alignment is located at the southwestern edge of the central cluster.

The directions of first motion and SV/P amplitude ratios were used to determine 41 single-event and two composite (two event) focal mechanism solutions for earthquakes in southeastern Tennessee and northern Georgia. The pertinent data for each event are listed in Table 1. The average location precision for two standard deviations is 5 km in depth and 3 km distance. Events were in the magnitude range of 1.7 to 3.9. The statistical estimate of confidence was developed by (Zelt, 1988) as an extension to the method of focal mechanism determination proposed by Guinn and Long, 1977. The significance is the probability that the first motions are not a random distribution.

The significance is based on the number of points, a test of the uniformity of the distribution of data points, the quality of the first motions and a Chi-square estimate of the goodness-of-fit. A confidence level of 0.9 suggests a probability of 0.10 that the observed first motions could be the result of random readings.

Over half of the focal mechanism solutions are strike slip and consistent with the 14 focal mechanisms reported by Johnston et al., 1985, and Teague et al., 1986. Of the remaining, eight are strike slip with a normal or reverse component, six are normal and five are reverse with a strike slip component. The measure of confidence of the focal mechanism solutions verify that for southeastern Tennessee and northwestern Georgia, solutions with large normal and reverse components exist with the same confidence level as the dominant strike-slip focal mechanism solutions. The depths of focus range from just below the base of the Paleozoic sediments at 8 km to 28.8 km and their average depth is 15 km. Figure 1 shows the distribution of these events with depth in a northeast-southwest profile. The average focal depth for strike-slip earthquakes is below the average at 17.3 ± 4.6 km. The average depth of earthquakes with normal or reverse focal mechanism solutions occurred near the average depth.

The central seismic zone (Fig. 1 and 2) is sampled by 18 focal mechanism solutions. Fourteen of these 18 events are either dominantly strike-slip or have a large strike-slip component. The dip of the B axis can be used as a measure of the deviation of the focal mechanism from pure strike slip. The dips of the null-axes (Fig 3), indicate that the most prominent zone of near-vertical dip, corresponding to pure strike-slip regimes, is the central cluster of the central seismic zone near 35.55N and 84.35W. This central cluster is flanked by regions of low B-axis dips, thus regions of normal or reverse components in their focal mechanisms. The two events that are anomalous in the central zone are shallow. Events further to the west and to the south-southwest are also nearly pure strike slip, but there are insufficient events to define anomalous focal mechanisms surrounding these events.

Focal mechanisms with prominent normal or reverse components are found near the outer edges of the central seismic zone. In order to determine which of the low B-axis dip regions corresponds to normal or reverse faulting, the dip of the tension axis was subtracted from the dip of the pressure axis for each solution (Fig. 4). This difference can range from -90 , corresponding to a pure reverse fault, to $+90$, corresponding to a pure normal fault. Values close to zero correspond to strike-slip mechanisms or near-vertical movement on vertical faults. The central cluster is dominated by strike slip faulting with reverse faulting. The northeast and southwest edges of the central zone are dominated by strike slip faulting with components of normal faulting. The general pattern of focal mechanisms in the cluster

of activity in southeastern Tennessee consists of earthquakes with reverse faulting in a central zone flanked by zones of normal faulting.

FINITE ELEMENT MODELS

Stress modeling in this study is based on the second order, multivariate finite element equations, outlined in Chapter 4.5 of Reddy (1984), with special emphasis on the plane elastic deformation of a linear elastic solid. The finite element technique divides the model space into a mesh of triangular elements which can approximate the physical properties of an arbitrarily complex two-dimensional media. The plates in this study are modeled using plane stress formalism in which the thickness is small compared to the dimensions in the plane. The meshes used in this study consisted of about 250 elements. The material types used are all isotropic. No body forces are applied and the model solutions are for elastic material properties. All stress magnitudes are based on a regional lithospheric stress of 5 MPA. Other values of stress can be obtained by scaling the computed stresses.

The intent of the finite element modeling is to estimate the distribution of stress at one instance during the third phase of Long's (1988) mechanism for major intraplate earthquakes. The distortion of weak crustal rock within a more rigid elastic crust is simulated in this study by assigning a lower Young's modulus to the weak zone. The weak zones are given circular and elliptical cross sections because these are expected to be similar to sills and other intrusive bodies. We considered smooth shapes appropriate for modeling the dispersion of fluids, a possible mechanism for weakening the crust. Two zones of weak material are used to simulate the geometry suggested by the focal mechanisms in the crustal volume of southeastern Tennessee.

The boundary conditions are designed to simulate a plate under compression. The left boundary is constrained to zero displacement. A normal force applied to the right boundary was tapered near the corner, producing minor irregularity in the stress field at the right edge. The side boundaries are constrained to zero normal displacement but are free to move tangential to the boundary. For the vertical cross section, one side boundary was made a free surface with no stress. Also, the elastic constants were set to a function of depth, leading to some irregularity in the stress field near the right boundary.

The average compressive stress of the entire grid is used to simulate crustal equilibrium without zones of weakness. When this average compressive stress is subtracted from the compressive stress of each individual point, changes in the form of plate extension and compression initiated by crustal weakening

can be estimated in the rigid plate. In evaluating stresses available for earthquakes occurring above the plate, changes in compressive stress in the plate may be more important than absolute values in establishing patterns of normal or reverse components in the faulting.

Single Large Circle

A single large circular zone provides a simple model for a weak zone in the lower crust (Fig 5). The universally compressive stress in both principal stress axis directions (Fig 6) is consistent with the boundary conditions and applied regional stress. The principal stresses exhibit changes in direction and magnitude near the boundary of the weak zone. Stresses vary by 50 percent near the boundary of the rigid crustal material and are 240 percent higher than in the material used to model the weak zone. The stresses can be divided into their deviatoric and dilatational components. The deviatoric stresses (Fig. 7) describe the stress available for shear failure in earthquakes. The regional compression and boundary conditions require extension perpendicular to the applied stress and compression parallel to the applied stress. Fig. 7 also shows little change in the directions of principal stress within the weak zone. The magnitude of deviatoric stress within the weak zone is only about 40 percent of the deviatoric stress on the boundary of the weak zone and is determined by the arbitrary choice of reduced values of the elastic constants used to simulate the weakened rock.

The changes in dilatation provide a measure of the extension and compression of the plate surrounding a transient weak zone. Fig. 8 represents the dilatation at each point with the dilatation of the entire grid subtracted. The geologic analogy would be the weakening of a portion of the crust, which is in an equilibrium state and a measure in change in compression or extension of the plate induced by the weak zone. The stresses indicate two zones of compression which are situated on the sides of the weak zone normal to the applied stress. The magnitude of the change is approximately twice the regional average. The increased dilatation of the weak zone should not be construed as extension because the change in material properties controls the stress. Instead, compression and hence thrust faulting would be expected in the remaining strong rocks above the deformed weak zone. The extension relative to a plate of uniform stress exists outside the weak zone on the sides in line with the applied stress. The extensional zones above the plate would be zones where normal faulting components would be expected in earthquake focal mechanisms. The compressional zones would be zones where earthquakes would exhibit components of reverse faulting.

In the central zone, the stress levels must decrease in parallel with the strength and are controlled by the distortion

of the surrounding plate. Normally, compression is in line with the regional stress and extension is normal to the applied stress. Consequently, any earthquakes occurring within the weak zone would have a vertical null axis and a strike slip focal mechanism.

Two Adjacent Circles

The stress model for two adjacent circles was chosen to be able to interpret the interaction of a system of sills or other types of weak zones within the crust and to model multiple weak zones delineated by focal mechanisms in southeastern Tennessee. The general properties of the stress field are similar to those of the single large circle. These general properties include the compression perpendicular to the applied stress and the relative extension on the edges of the weak zone parallel to the applied stress. The notable differences relate to increases in stress contrast that are proportional to the fraction of the total width of the model that contains the weaker material. For two circles aligned parallel to the maximum compressive regional stress (Fig 9), 10 km wide separation zone between the two circles is not a zone of stress concentration. The small separation allows a continuous weak zone of low stress from one circle to the other. Two circles aligned parallel to the regional stress, therefore, behave like a single irregularly shaped weak body.

For two circles aligned perpendicular to the applied stress, the finite element model predicts stresses similar to those for circles in line with the stress, except that the stress zone separating the two circular zones shows stress concentrations about 300 percent larger than in the surrounding elastic plate. In the deviatoric stress (Fig. 10) the elastic material separating the circles amplifies the applied stress instead of being absorbed in the weak zone as it is in the case of the circles aligned with the regional stress. The increased stress within the separation is explained by the direct application of the applied stress to the narrow zone of strong rock separating the two circles. Fig. 10 shows a distinct central zones for each weak zone surrounded by zones of higher stress. The patterns of stress are thus distinctly different in the vicinity of the weak zones and depend on the orientation of the complex weak zone in the regional stress.

Two circles located along a diagonal (45 degrees) relative to the applied stress show zones of deviatoric stress concentrations at the boundary of the circles including the zone separating the two circles. The stresses are of the same magnitude found for the other two-circle models. The deviatoric stresses (Fig. 11) show that two circular weak zones oriented diagonally to the applied stress remain independent zones of weakness and do not merge into a continuous weak zone. However, the deviatoric stresses on the connecting bridge are on the order of 100 percent

greater than the average stress. This increase is significant in that it suggests that irregularities within the central weak zone can generate significantly anomalous deviatoric stresses. Also, the diagonal orientation creates large intermediate zones of neither compressive nor extensional character immediately next to the circular weak zones. This can be seen to the right of the top circular weak zone and to the left of the bottom circular weak zone in Fig. 11. The diagonally aligned circles concentrate stresses between the two weak zones and provides a complex pattern of extensional and compressional zones.

Also, an ellipsoidal zone in various orientations was examined to simulate a continuous linear weak zone in an applied stress. The results are similar to those of the two adjacent circles with the exception that stress concentrations on the edges could be 50 percent greater. An ellipsoidal zone could represent perturbation of the strength of a fault zone by fluids. The deviatoric stresses for an ellipsoidal zone with its major axis parallel to the applied stress show negligible contrast with the surrounding stronger crust beside the weak zone. Stress concentrations appear only along the boundaries, particularly at the ends, of the ellipsoidal weak zone with its major axis perpendicular to the direction of applied stress with magnitudes similar to those of the two adjacent circles.

Crustal Perturbation in Vertical Profile

A perturbation of the strength of the lower crust leading to elastic or viscous deformation affects the stresses in the shallow crust. In order to evaluate the influence on stress above the weak zone, a vertical profile was examined. The surface sedimentary layers were added to assess the effects of sediments on stress in this shallow crust (Fig. 12). The model for the vertical profile differs from the model for crustal inclusions examined previously in that the top of the sediments is a free surface and the weak lower crust is simulated with lower elastic constants similar to those in the central weak zone. Also, the cross section is a two dimensional approximation to the three dimensional geometry of a shallowing of the brittle-ductile transition zone. The deviatoric stress (Fig. 13) shows a concentration of shear stress above the zone of perturbation. The deviatoric stresses are about 200 percent higher over a weakened crust than in the surrounding crust. The 200 percent increase is comparable to the largest shear stress observed in the analysis of stress amplification in a horizontal plate; the two weak zones at a diagonal to the applied stress. The direction and magnitude of the principal stress axes favor earthquakes on reverse faults above the weak zone. The low stress levels in the sediments show that low-velocity sedimentary basins are largely insulated from the stresses in the crust. The deeper sedimentary basins could contribute to the amplification of crustal stress by constricting the thickness of the stress

channel. A large abrupt change in crustal structure can thus concentrate stress in one area, which in this case is the zone between the sediments and the top of the weak zone.

CONCLUSIONS AND DISCUSSION

The combined inferences from stresses computed for a horizontal plate and a vertical cross section are that the focal mechanisms above the plate will exhibit stronger components of reverse and normal faulting than earthquakes in the plate. The orientation of principal axes and hence the inferred focal mechanisms is controlled by the central zone of weakened lower crust (fig. 15). In the weak zone of the horizontal plate the focal mechanisms should be strike slip. Stress concentrations at the edge of the weak zone can cause deviations of up to 30 degrees in the orientation of the principal axes. Above the weak zone, thrust or reverse motions are inferred. Above the plate surrounding the weak zone the distortion in the plate predict a pattern of extension perpendicular to the direction of greatest compressional regional stress near the edges of the weak zone parallel to the regional stress. Reverse faulting is expected near the edges of the weak zone normal to the regional field.

In southeastern Tennessee a pattern of earthquake focal mechanisms is observed that can be modeled by a mid-crustal weak zones as illustrated in figure 15. Two weak zones oriented at 45 degrees to the regional compressional stress give a better fit, but more focal mechanisms are needed to confirm the details. The factors that support a crustal weak zone are as follows:

- 1) The pattern of seismicity defines a concentration of activity in a central zone surrounded by lower levels of seismicity. The seismic zone is elongated to the northeast and southwest.

- 2) In the central zone the earthquakes below 15 km uniformly have strike slip focal mechanisms with northeast-southwest trending compressional axes. The stress model suggests that the stress directions in the weak zone should deviate only slightly from the regional stress field and that the null axis should be vertical.

- 3) The shallow events above the weak zone show large thrust components. The stress model for a vertical section predicts amplification above the weak zone.

- 4) All of the earthquakes in the central zone show some thrust component in agreement with the models showing compression in and above the weak zone.

- 5) The focal mechanisms for events surrounding the central

zone depend on their position relative to the applied regional stress. Events on the axis parallel to the regional stress show a normal component in the predominantly strike slip focal mechanisms, in agreement with the finite element stress model. The few events on the axis perpendicular to the regional stress show a thrust component. The decrease in seismicity on the axis perpendicular to the regional stress is consistent with the increased stress required to cause failure in a compressive regime.

The stress model and the observed seismicity in southeastern Tennessee may correspond to phase 3 of Long's (1988) five-phase hypothesis for major intraplate earthquakes. In phase 3 the weakened central zone is being deformed by regional compressive stress and the surrounding elastic crust is bearing the load no longer supported by the central zone. The regional compressive stress is required since without a regional stress the deformation of the central zone would not create the deviatoric stresses for the earthquakes. A local weakening of the crust by a perturbation of its hydraulic or thermal properties is required in order to trigger the events in zones where the crust is normally stronger and to allow concentration of the seismicity in limited seismic zones such as in southeastern Tennessee. In this model the seismicity exists by virtue of a decrease in strength, and not simply because a weak zone exists.

Variations in the P-axis orientation has sometimes been ascribed to the preferential failure of preexisting planes of weakness in a uniform stress field. The uniformity we observe for focal mechanisms in the central zone argues for a direct response to the direction of regional stress. The variations in focal mechanisms for shallow events and those in the surrounding elastic plate fit a pattern. Although existing faults may contribute to the scatter in our focal mechanisms in these zones, the general pattern is that predicted by stress models for a weakness in a plate subjected to regional stress.

The zone of weakness can be generated by perturbations in the hydraulic properties and/or thermal properties of the lower crust. Figure 15a is a simplified conceptual diagram showing the strength of the crust in tensional and compressive tectonic environments. A temperature increase (Fig. 15b) predicts a shallowing of the brittle-ductile transition. An increase in fluid content in the lower crust would create a localized decrease in the frictional strength. The change is more pronounced than that caused by a thermal perturbation and is also more pronounced in zones of crustal extension. In the southeastern Tennessee seismicity, the zones of predicted extension are those exhibiting the greater level of seismicity suggesting that a hydraulic perturbation is the more likely explanation for the seismicity. Also, the greater time and energy required to effect a thermal perturbation favor an

explanation based on fluid movement.

The important conclusions from this analysis are as follows:

1) The focal mechanisms of earthquakes in southeastern Tennessee fit a pattern predicted by stress modeling of a zone of weakness in the lower crust.

2) The different orientations of focal mechanisms can be explained by inhomogeneity in stress.

3) The seismicity in southeastern Tennessee can be explained by a perturbation in the fluid properties of the lower crust.

ACKNOWLEDGMENTS

This research was supported primarily by the Nuclear Regulatory Commission, Office of Nuclear Regulatory Research. Supplemental support was provided by the Corps of Engineers, Savannah District, and the Tennessee Valley Authority. Computer time was provided by the School of Geophysical Sciences and the Advanced Computational Methods Center at the University of Georgia through the Supercomputing Support Group of the Office of Computing Services at the Georgia Institute of Technology.

REFERENCES

- Aggarwal, Y.P. and L.R. Sykes, 1978. Earthquakes, faults and nuclear power plants in southern New York, Science, 200, pp. 425-429.
- Bollinger, G.A., 1973. Seismicity of the southeastern United States, Bull. Seism. Soc. Am., 63, pp. 1785-1808.
- Bollinger, G.A., C.J. Langer and S.T. Harding, 1976. The Eastern Tennessee Earthquake Sequence of October through December, 1976, Bull. Seism. Soc. Am., Vol. 66, No. 2, pp. 525-547.
- Bollinger, G.A. and R. Wheeler, 1988. The Giles County, Virginia, seismic zone--Seismological results and geological interpretations, U.S. Geological Survey Professional Paper, 1355, U.S. Government Printing Office, Washington, D.C., 85pp.
- Bott, M.H.P. and N.J. Kusznir, 1984. The origin of tectonic stress in the lithosphere, Tectonophysics, Vol. 105, pp. 1-13.
- Byerlee, J., 1978. Friction of rocks, Pure and Applied Geophysics, 116, pp. 615-626.
- Campbell, D.L., 1978. Investigation of the stress concentration mechanism for intraplate earthquakes, Geophysical Research Letters, Vol. 5, No. 6, pp. 477-479.
- Chen, W.-P. and P. Molnar, 1983. Focal depths of intracontinental and intraplate earthquakes and their implications for the thermal and mechanical properties of the lithosphere, J. Geophys. Res., Vol. 88, pp 4183-4214.
- Copersmith, K. J., 1988. Temporal and spatial clustering of earthquake activity in the central and eastern United States, Seismological Research Letters, Vol. 59, No. 4, pp299-304.
- Dewey, J.W., 1985. A review of recent research on the seismotectonics of the southeastern seaboard and an evaluation of hypotheses on the source of the 1886 Charleston, South Carolina, earthquakes, NUREG/ CR-4339.
- Fleitout, L. and C. Froidevaux, 1982. Tectonics and topography for a lithosphere containing density heterogeneities, Tectonics, Vol. 1, pp. 21-56.
- Fleitout, L. and C. Froidevaux, 1983. Tectonic stress in the lithosphere, Tectonics, 2, pp. 315-324.
- Fox, F.L., 1970. Seismic geology of the eastern United States, Assoc. Eng. Geologists Bull., 7, pp. 21-43.

Gettings, M.E., 1988. Variation of depth to the brittle ductile transition due to cooling of a mid-crustal intrusion, Geophysical Research Letters, Vol. 15, No. 3, pp. 213-216.

Guinn, S.A. and L.T. Long, 1977. A computer method for determination of valid focal mechanism solutions using P-wave first motions, Earthquake Notes, Vol. 48, No. 4, pp. 21-33.

Johnston, A.C., D.J. Reinbold, and S.I. Brewer, 1985. Seismotectonics of the Southern Appalachians, Bull. Seism. Soc. Am., Vol. 75, pp. 291-312.

Kane, M.F., 1977. Correlation of major eastern earthquake centers with mafic/ultramafic basement masses, U.S. Geol. Survey Prof. Paper 1028-0.

Kuang, Jian, L.T. Long, and J.C. Mareschal, 1989. Intraplate seismicity and stress in the southeastern United States, Tectonophysics, No. 170, pp. 29-42.

Long, L.T., 1976. Speculations concerning Southeastern Earthquakes, mafic intrusions, gravity anomalies, and stress amplification, Earthquake Notes, Vol. 47, No. 3, pp. 29-35.

Long, L.T. and J.W. Champion, Jr., 1977. Bouguer Gravity Map of the Summerville-Charleston, South Carolina, Epicentral Zone and Tectonic Implications, Geol. Survey Prof. Paper 1028-K.

Long, L.T., 1988. A model for major intraplate continental earthquakes, Seismological Research Letters, Vol 59, No. 4, pp 273-278.

Long, L.T., R.E. White, and J. Dwyer, 1986. The Charleston earthquake Hypotheses - A classification by fundamental tectonic processes, Proceedings of the Third U. S. National Conference on Earthquake Engineering, August, 24-25, 1986, Charleston, South Carolina, pp 25-32.

Long, L.T., K.-H. Zelt, J-S. Liow, R. Propes, J. Shand, D. Reinbold and B. Schechter. 1986. The North Georgia Earthquake of October 9, 1984, Earthquake Notes, Vol. 57, No. 3, pp 77-82.

Mareschal, J.C. and Jian Kuang, 1987. Intraplate Stresses and Seismicity: The role of topography and density heterogeneities, Tectonophysics, Vol. 132, pp. 153-162.

McKenzie, D.P., 1969. The relationship between fault plane solution for earthquakes and the directions of principal stresses, Bull. Seism. Soc. Am., Vol. 59, pp. 591-601.

McKeown, F.A., 1978. Hypothesis: Many earthquakes in the

central and southeastern United States are causally related to mafic intrusive bodies, Jour. Research U.S. Geol. Survey, Vol. 6, No. 1, pp. 41-50.

Meissner, R. and J. Strehlau, 1982. Limits of stresses in continental crusts and their relation to the depth-frequency distribution of shallow earthquakes, Tectonics, Vol. 1, No. 1, pp. 73-89.

Oudenhoven, M.S., C.O. Babcock, and W. Blake, 1972. A method for the prediction of stresses in an isotropic inclusion or orebody of irregular shape, U.S. Bureau of Mines, Report of Investigations 7645, 36 pp.

Prowell, D.C. and B.J. O'Connor, 1978. Belair fault zone: Evidence of tertiary fault displacement in eastern Georgia, Geology, Vol. 6, pp. 681-684.

Rankin, D.W., 1976. Appalachian salients and recesses: Late Precambrian continental breakup and the opening of the Iapetus Ocean, J. Geophys. Res., 81, pp. 5605-5616.

Reddy, J.N., 1984. An Introduction to the Finite Element Method, McGraw Hill Company.

Reinhardt, J., D.C. Prowell and R.A. Christopher, 1984. Evidence for Cenozoic tectonism in the southwest Georgia Piedmont, Geol. Soc. Am. Bull., Vol. 95, pp. 1176-1187.

Richardson, R.M., S.C. Solomon and N.H. Sleep, 1979. Tectonic stress in the plates, Rev. Geophys. Space Physics, 17, pp. 981-1019.

Sbar, M.L. and L.R. Sykes, 1973. Contemporary compressive stress and seismicity in eastern North America: an example of intraplate tectonics, Bull. Geol. Soc. Am., 84, pp. 1861-1882.

Solomon, S.C., R.M., Richardson, E.A., Bergman, 1980. Tectonic Stress Models and Magnitudes, J. Geophys. Res., 85, pp. 6086-6092.

Sykes, L.R., 1978. Intraplate seismicity, reactivation of preexisting zones of weakness, alkaline magmatism, and other tectonism postdating continental fragmentation, Rev. Geophys. Space Phys., 16, pp. 621-688.

Talwani, P, 1988. The intersection model for intraplate earthquakes, Seismological Research Letters, Vol. 59, No. 4, pp 305-310.

Teague, A.G., G.A. Bollinger, and A.C. Johnston, 1986. Focal Mechanism analyses for eastern Tennessee earthquakes (1981-

1983), Bull. Seism. Soc. Am., Vol. 76, No. 1, pp. 95- 109.

Turcotte, D.L. and Gerald Schubert, 1982. Geodynamics, Applications of Continuum Physics to Geological Problems, John Wiley & Sons, New York, 450 pp.

Zelt, Karl-Heinz, 1988. Investigation of the cause of earthquakes in southeastern Tennessee and northern Georgia using focal mechanisms and models of crustal stress, Ph.D. Thesis, Georgia Institute of Technology, Atlanta, Georgia, 231 pp.

Zoback, M.L. and M.D. Zoback, 1980. State of stress in the conterminous United States, J. Geophys. Res., Vol. 85, pp. 6113-6156.

Zoback, M.D., 1983. Intraplate earthquakes, crustal deformation and in situ stress, U.S. Geol. Survey, Open file Report 83-843, pp. 169- 178.

TABLE I Earthquake locations and focal mechanisms.

Date YrMoDa	Origin Time	Lat. North	Long. West	Dur. Mag.	Depth km	# of pts.	Sig.	Tension az.	Pressure dip	Null az.	Null dip	P-T		
820130	12:39	35.80	83.94	2.8	18.8	9	0.76	38	47	221	43	130	1	-4
820224	12:10	35.72	84.29	1.3	20.4	8	0.69	189	7	283	27	86	62	20
820905	10:11	35.21	84.51	3.2	8.4	12	0.86	138	2	229	24	44	66	22
820924	21:57	35.68	84.24	3.2	14.0	12	0.78	161	25	257	14	14	61	-11
821214	06:35	35.29	84.17	2.4	9.1	11	0.81	312	8	51	47	215	42	39
821215	02:27	35.75	84.22	2.1	19.2	9	0.65	252	57	13	18	112	26	-39
830118	05:09	35.58	84.27	2.3	11.2	11	0.71	335	49	71	6	166	40	-43
830129	18:08	36.12	83.74	2.1	20.7	10	0.91	322	31	220	20	102	52	-11
830304	14:03	35.60	84.34	2.3	8.0	7	0.71	53	20	150	17	277	63	-3
830316	09:13	35.22	84.55	2.6	16.9	6	0.71	327	8	234	16	83	72	8
830405	03:17	35.54	84.19	2.1	18.8	7	0.96	176	16	266	3	6	74	-13
830526	12:30	35.67	84.27	2.5	14.6	12	0.88	146	4	54	19	247	71	15
831016	22:02	35.86	84.55	2.5	19.8	12	0.84	348	24	82	9	191	64	-15
840207	06:32	35.65	84.64	1.8	20.4	7	0.71	19	2	289	1	172	88	-1
840525	10:15	35.60	84.62	2.0	24.1	11	0.87	319	34	110	53	219	14	19
840830	16:26	35.55	84.35	3.1	21.1	16	0.96	142	12	59	3	315	78	-9
840830	16:41	35.55	84.35	2.4	18.0	7	0.99	331	7	239	16	84	72	9
841009	11:54	34.77	85.19	3.5	15.0	22	0.78	298	6	29	7	168	81	1
841107	09:31	35.59	84.64	2.0	18.7	14	0.71	308	40	199	21	88	43	-19
850309	14:29	35.03	85.03	2.5	9.7	12	0.68	8	6	277	8	134	80	2
850312	13:04	35.87	83.57	2.0	25.6	12	0.82	311	7	218	16	64	72	9
850410	10:53	35.72	84.06	2.3	22.0	11	0.53	14	24	226	62	110	13	38
850420	04:21	35.48	84.56	2.5	9.4	13	0.78	20	1	151	89	290	1	88
850712	18:20	35.20	85.15	3.0	19.6	10	0.60	123	17	216	9	333	71	-8
850815	17:31	35.67	83.95	1.8	12.5	8	0.78	100	3	190	2	314	86	-1
850924	00:01	35.68	84.05	1.7	19.1	9	0.88	140	10	233	16	19	71	6
851220	15:15	34.93	84.76	2.9	9.3	7	0.68	329	0	236	81	59	9	81
860107	01:26	35.60	84.76	3.1	17.5	24	0.95	107	11	198	4	308	78	-7
860127	06:44	35.88	83.65	2.6	15.0	11	0.83	289	8	21	17	175	71	9
860419	07:40	35.19	85.51	3.0	21.0	27	0.91	183	9	280	35	81	53	26
860423	07:18	34.79	85.30	1.8	19.1	8	0.60	120	2	24	70	211	20	68
860519	23:46	35.53	84.54	2.6	9.7	14	0.67	284	11	16	15	159	71	4
860602	07:46	35.43	84.50	2.5	18.6	14	0.87	132	32	31	17	277	53	-15
860624	19:22	35.98	83.94	2.8	28.8	14	0.67	131	1	40	41	222	49	40
860711	14:26	34.93	84.99	3.8	20.7	30	0.98	329	18	60	3	159	72	-15
860719	12:31	34.94	84.97	1.9	10.6	10	0.66	349	40	226	32	112	33	-8
860807	12:36	35.49	84.54	2.5	14.9	11	0.49	285	15	25	32	174	54	17
860819	20:51	36.26	85.01	2.9	20.0	13	0.73	112	20	244	62	15	19	42
861115	12:08	35.88	83.82	2.0	16.4	9	0.70	172	2	81	7	278	83	5
870112	18:56	35.50	84.25	2.1	14.8	9	0.85	320	23	121	65	227	7	42
870222	10:35	36.39	84.21	2.8	19.0	14	0.81	314	2	44	1	161	88	-1
870327	01:26	35.60	84.76	3.9	17.5	35	0.99	323	4	53	6	199	83	2
870901	23:02	35.51	84.40	3.2	16.9	17	0.99	304	20	41	18	170	63	-2

The significance measure is based on the number of points, the distribution of data points, quality of first motions and SV/P ratios, and a Chi-square estimate of goodness-of-fit.

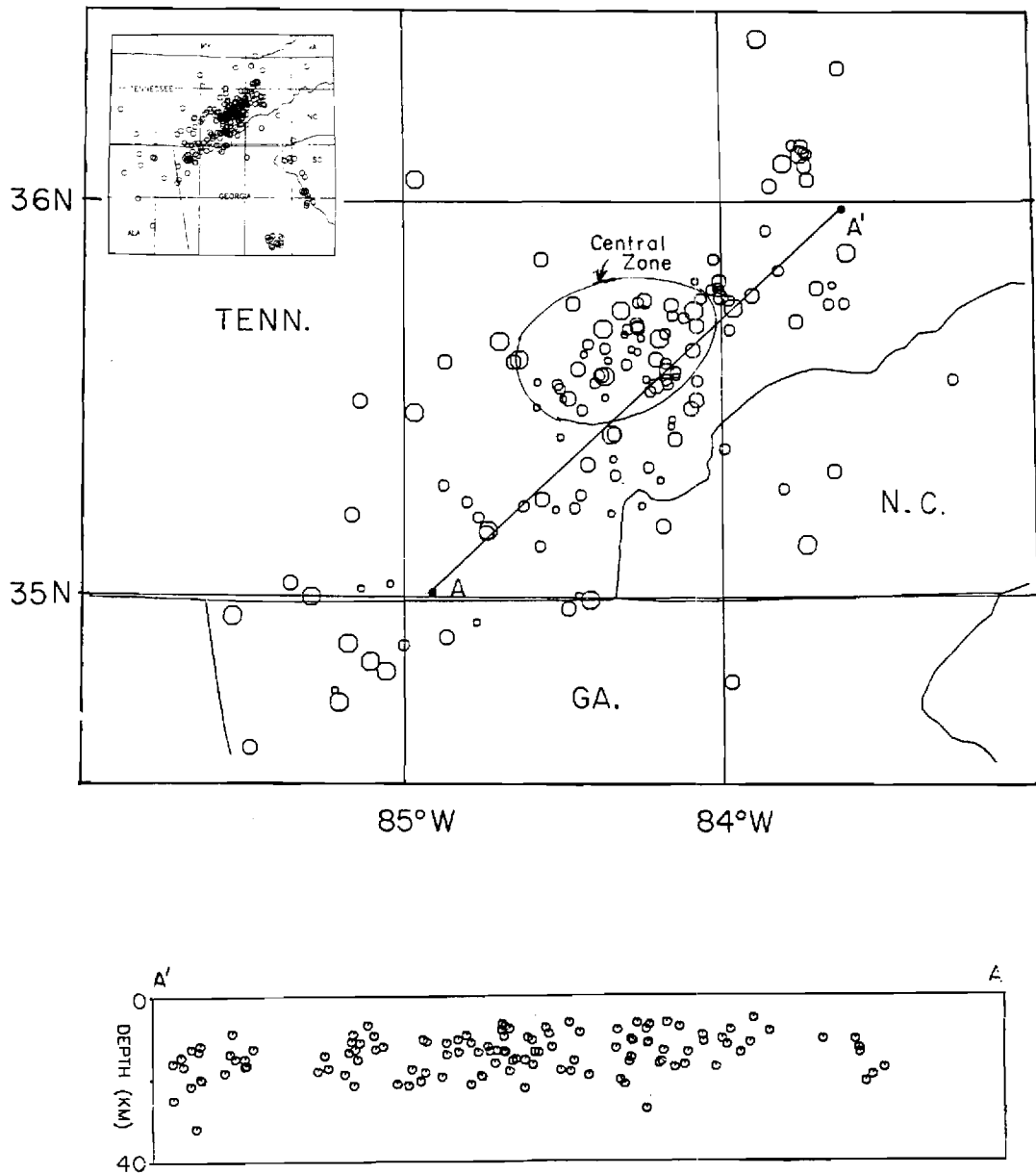


Figure 1. Seismicity of southeastern Tennessee. The events shown have been relocated with station corrections applied and represent a select subset of the observed data in southeastern Tennessee.

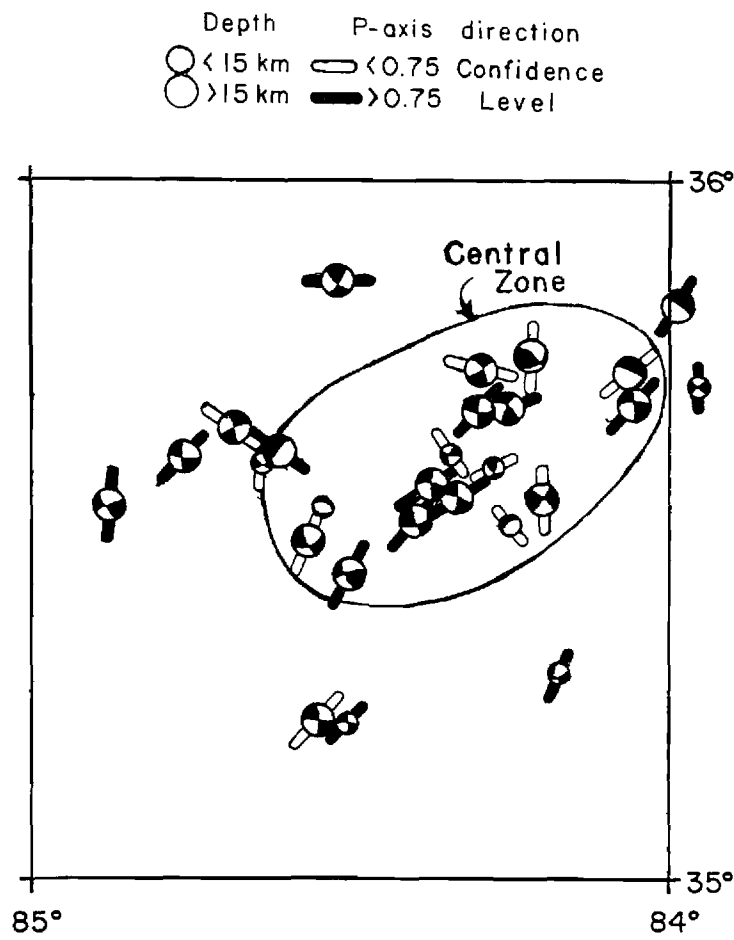


Figure 2. Focal mechanism solutions and epicenters in the central zone. The bar indicates the horizontal projection of the P-axis. Events with confidence levels above 0.75 are solid.

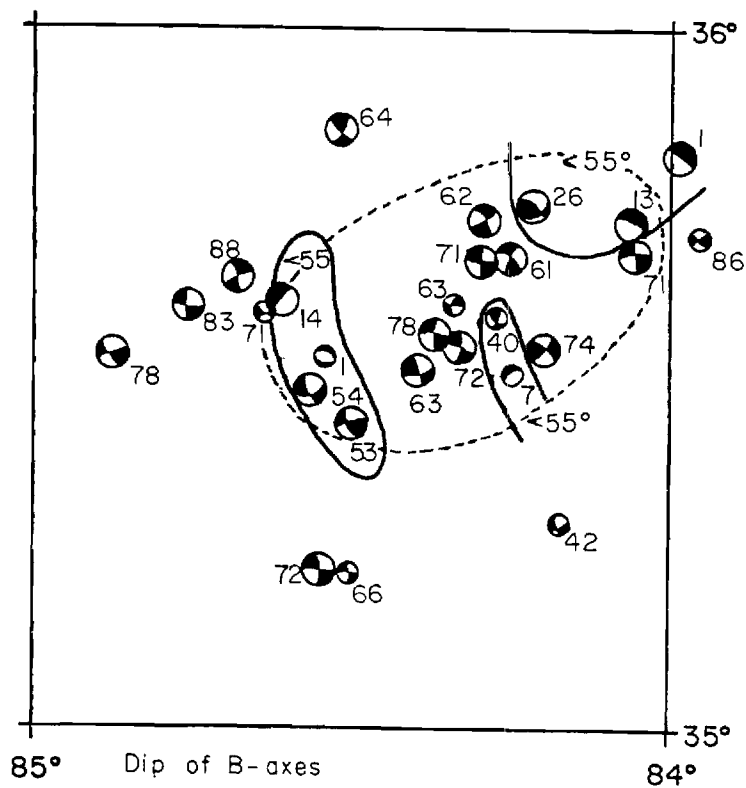


Figure 3. Dip of the B axis of the focal mechanism solution for the central zone. The dip of the B axis indicates deviation from pure strike slip motion.

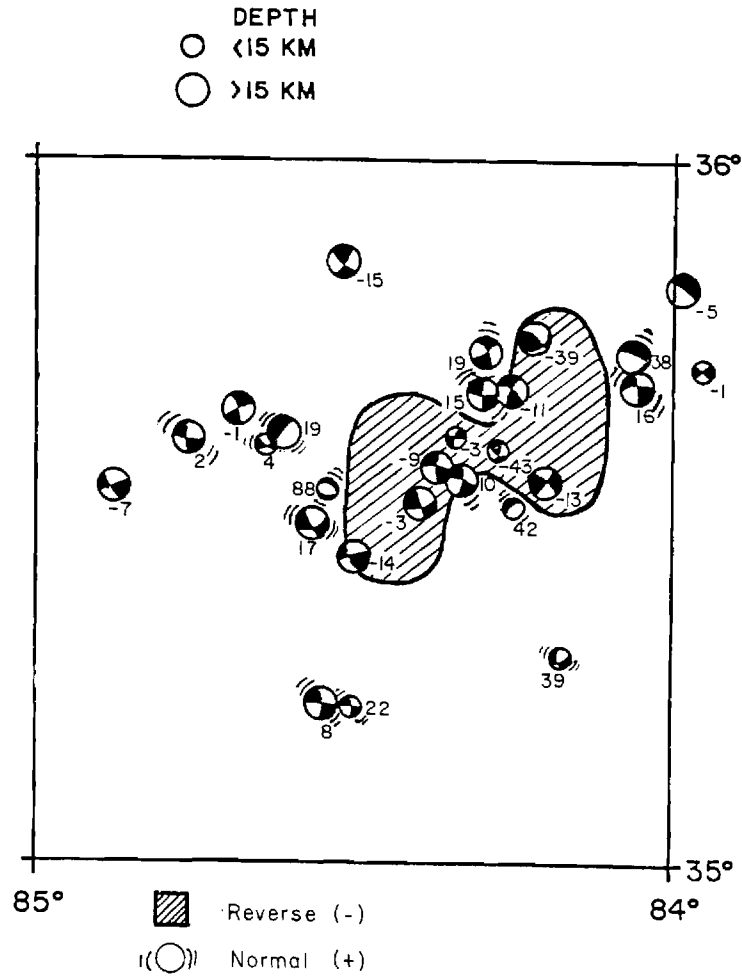


Figure 4. Difference between the dip of the tension axis and the dip of the pressure axis. Negative values suggest reverse faulting and positive values suggest normal faulting components in the predominant strike slip focal mechanisms.

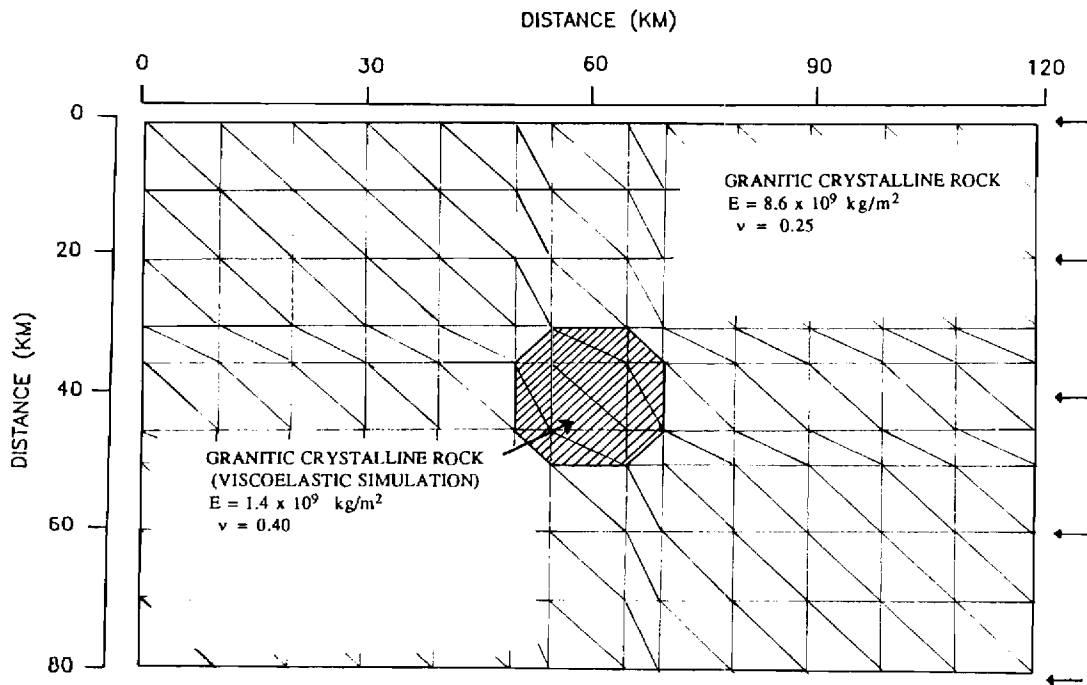


Figure 5. Model for a single circular zone of weakening in a horizontal crustal plate.

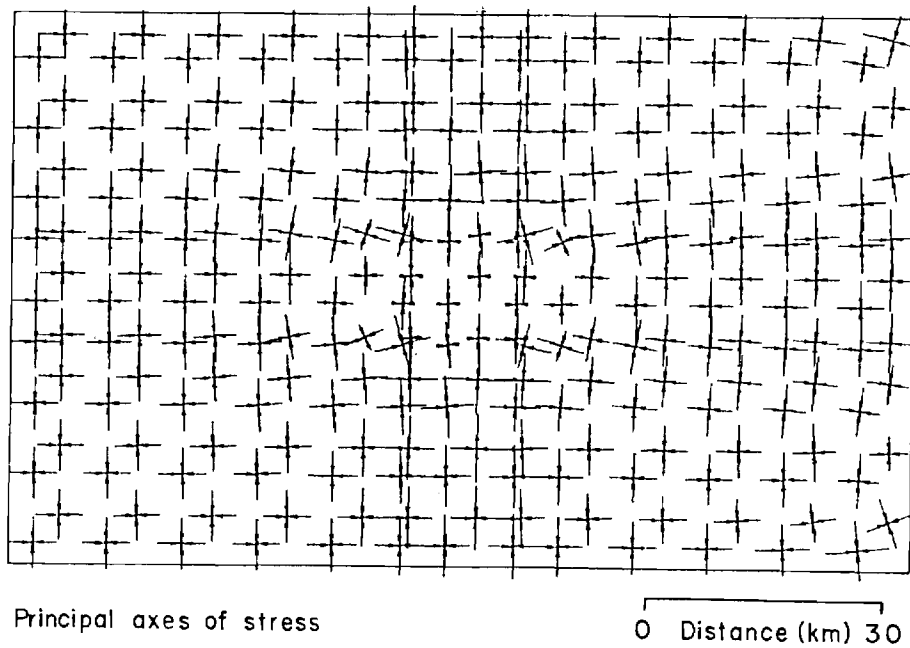


Figure 6. Stress surrounding a weak circular zone in a horizontal crustal plate. Arrows indicate principal stress directions and magnitudes. The force applied to the right boundary was tapered at the edges, leading to some irregularity in the stress directions along the right edge.

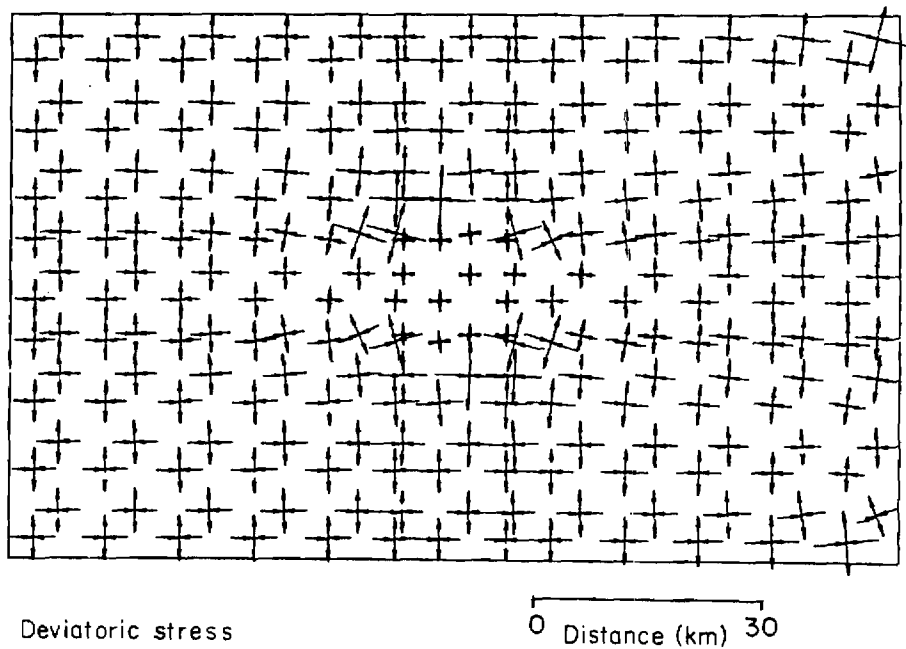


Figure 7. Deviatoric stresses surrounding a weak zone in a horizontal crustal plate. Contours are in MPa.

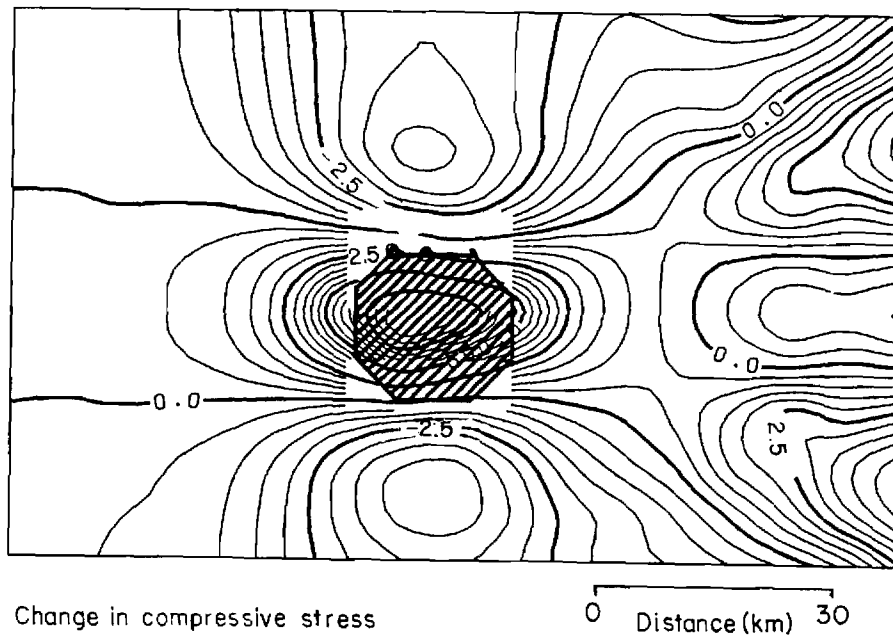


Figure 8. Dilatation surrounding a weak zone in a horizontal crustal plate.

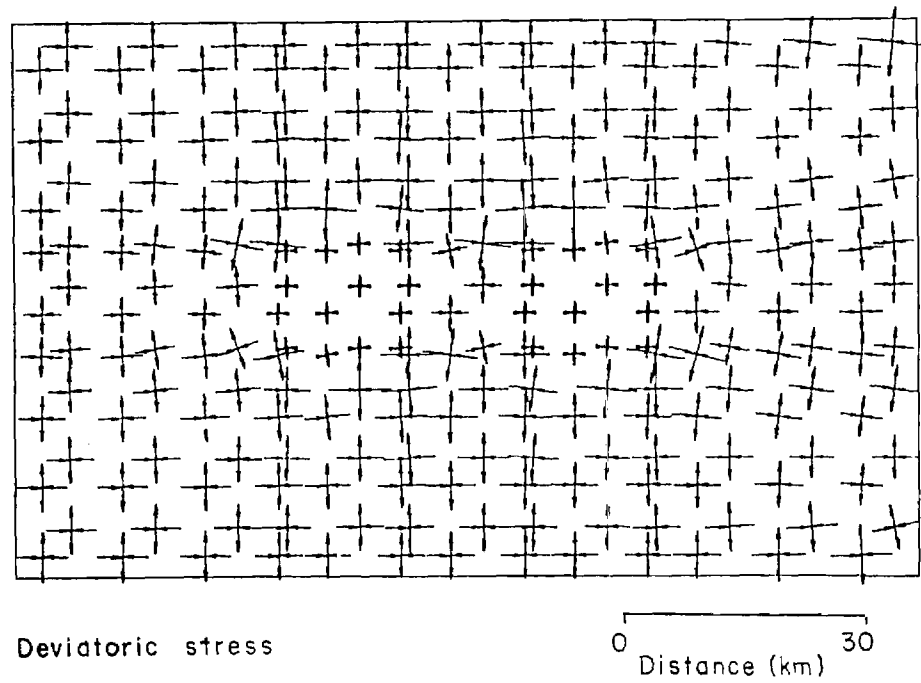


Figure 9. Deviatoric stress for two circular zones of weakened crust aligned parallel to the applied stress.

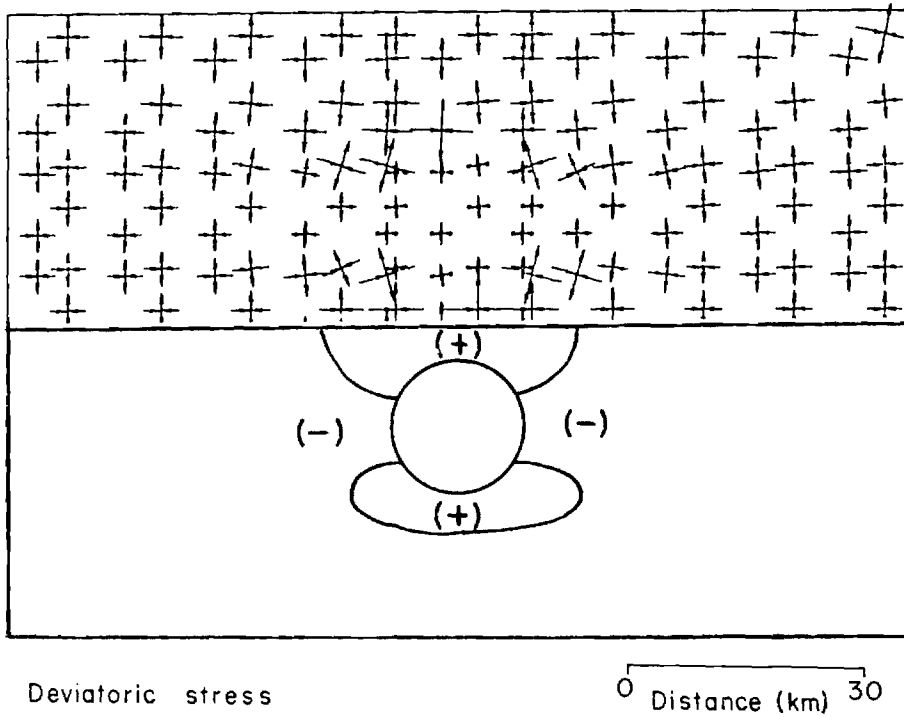


Figure 10. Deviatoric stress for two circular zones of weakened crust aligned perpendicular to the applied stress.

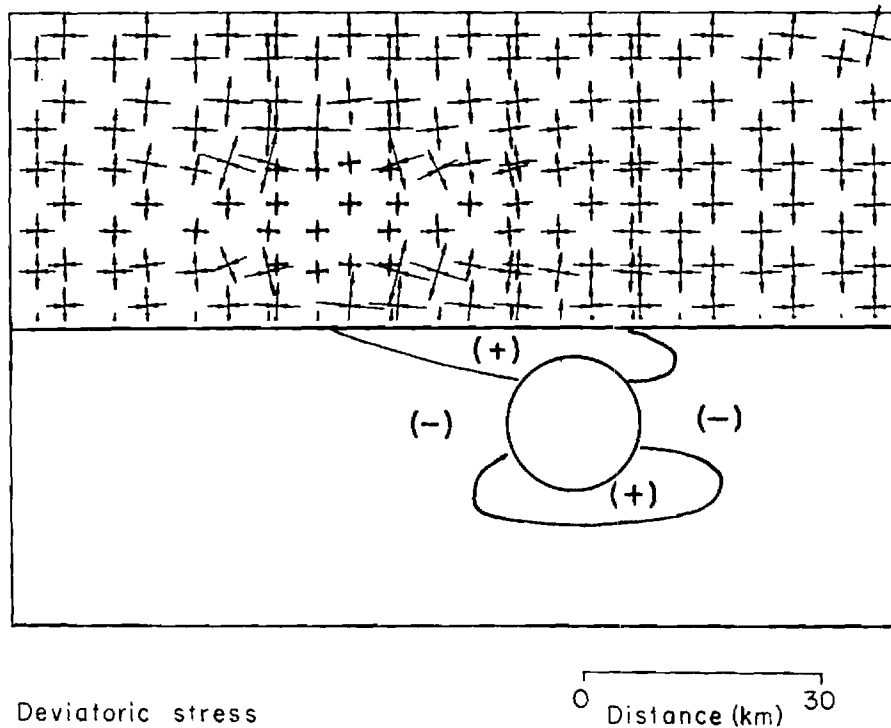


Figure 11. Deviatoric stress for two circular zones of weakened crust aligned at 45 degrees to the direction of applied stress.

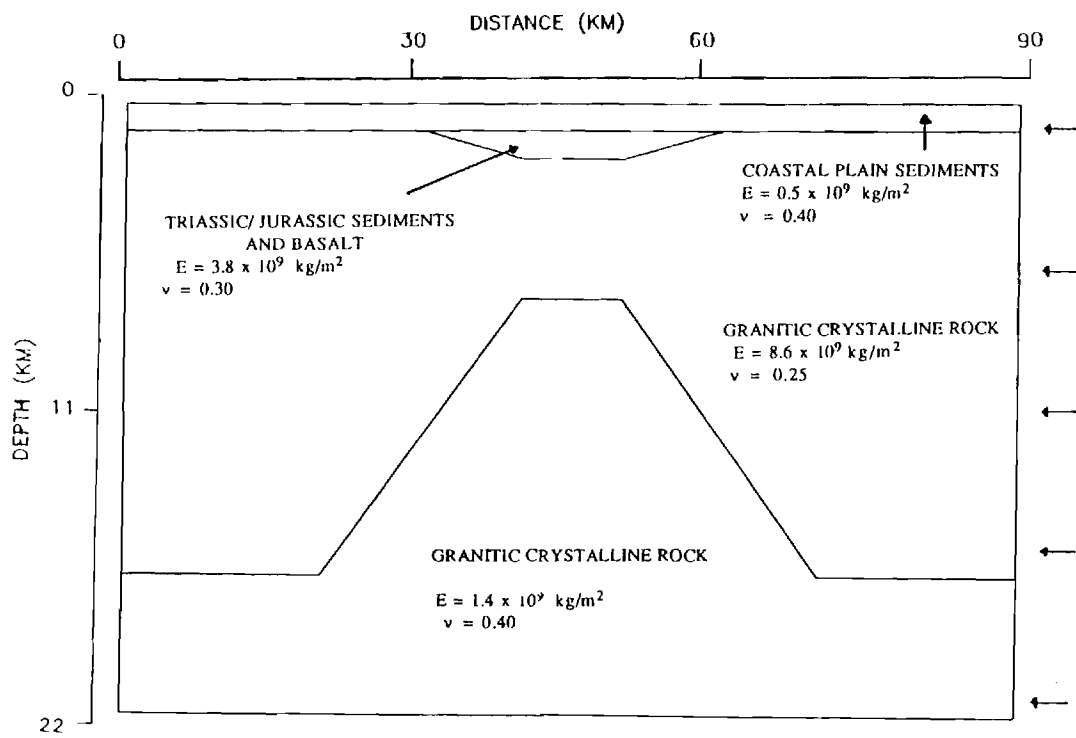


Figure 12. Geologic model for a vertical profile across a zone of weakness in the crust.

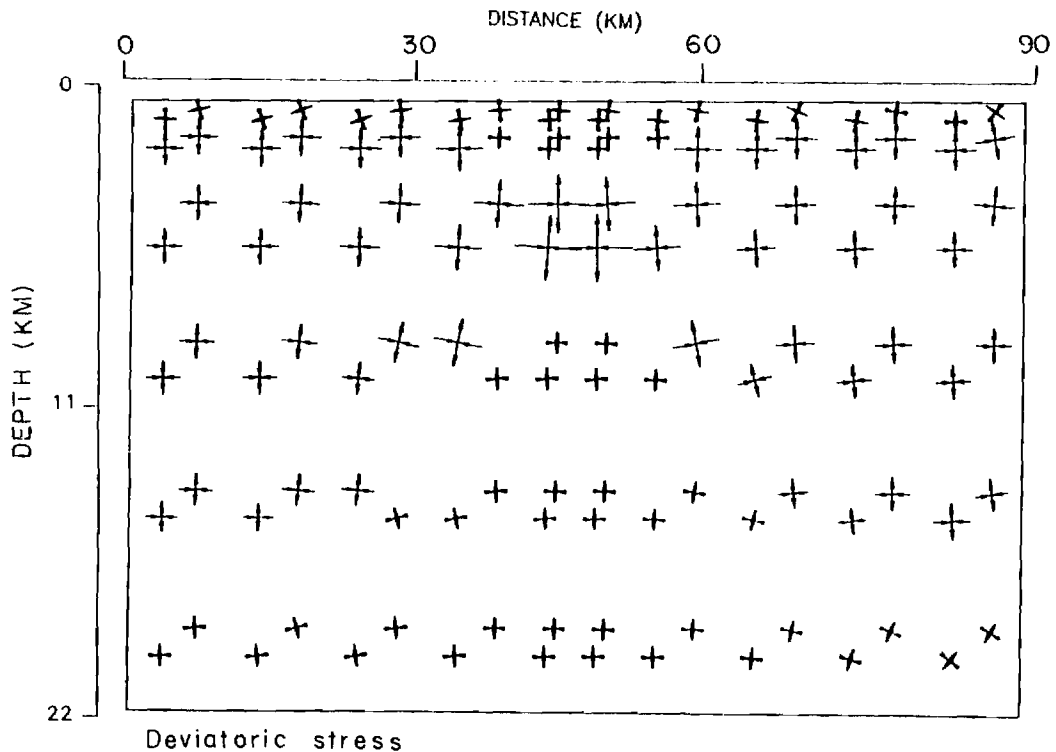


Figure 13. Deviatoric stress in a vertical section across a zone of weakness in the crust. See figure 12 for the model parameters. The top boundary is a free surface. Weak material is simulated across the bottom as well as in the weak zone. Forces applied to the right side were constant so that the differential response of the elastic properties of the shallow and deep crust leads to some irregularity in the stresses near the right boundary.

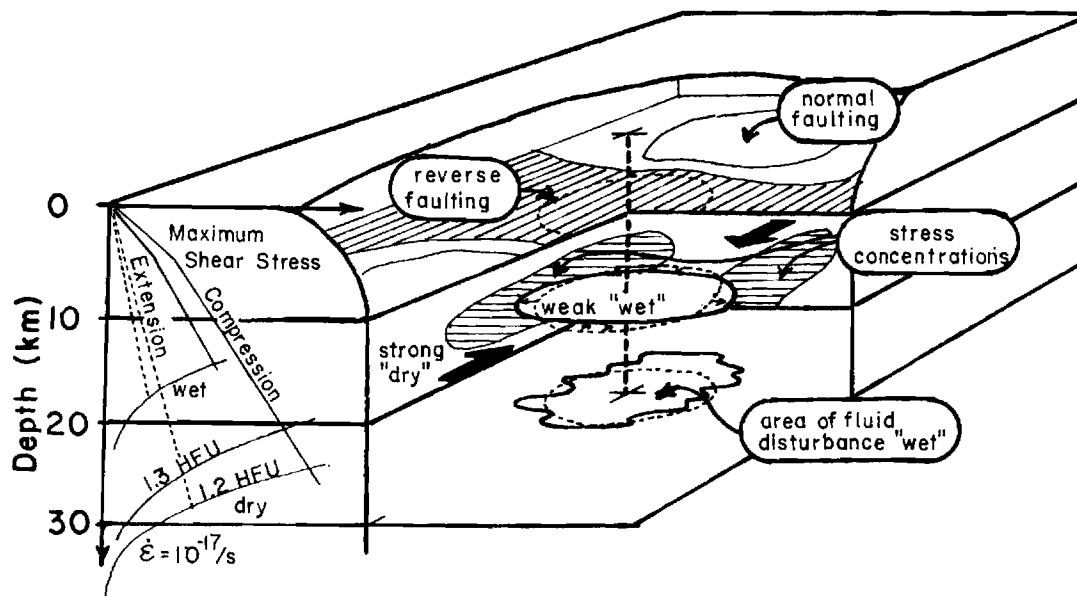


Figure 14. Model for focal mechanisms surrounding a zone of weakness in the lower crust.

NRC FORM 335 (2-84) NRCM 1102, 3201, 3202		U.S. NUCLEAR REGULATORY COMMISSION		1. REPORT NUMBER (Assigned by TIDC, add Vol. No., if any)	
SEE INSTRUCTIONS ON THE REVERSE		BIBLIOGRAPHIC DATA SHEET		NUREG/CR-5258, Vol. 4	
				3. LEAVE BLANK	
2. TITLE AND SUBTITLE		4. DATE REPORT COMPLETED		MONTH	
Georgia/Alabama Regional Seismographic Network Final Report, August 1985-October 1990		November		YEAR	
		1990		6. DATE REPORT ISSUED	
5. AUTHOR(S)		MONTH		YEAR	
L. T. Long		November		1990	
		8. PROJECT/TASK/WORK UNIT NUMBER		9. FIN OR GRANT NUMBER	
7. PERFORMING ORGANIZATION NAME AND MAILING ADDRESS (Include Zip Code)		D1598		11a. TYPE OF REPORT	
School of Earth and Atmospheric Sciences Georgia Institute of Technology Atlanta, Georgia 30332		11a. Technical		b. PERIOD COVERED (Inclusive dates)	
		August 1985-October 1990		12. SUPPLEMENTARY NOTES	
10. SPONSORING ORGANIZATION NAME AND MAILING ADDRESS (Include Zip Code)		11a. Technical		13. ABSTRACT (200 words or less)	
Division of Engineering Office of Nuclear Regulatory Research U.S. Nuclear Regulatory Commission Washington, DC 20555		August 1985-October 1990		Data from the Georgia/Alabama network have contributed to a better understanding of the seismicity in the Southeast. Based on these data, a new theory explaining intraplate earthquakes was developed. The theory predicts that a decrease in strength of the lower crust (e.g. through a change in the fluid regime) leads to weakening and deformation of the stress channel in the mid-crustal zone. The weakening and stress concentration may lead to major earthquakes. Earthquake focal mechanisms in southeastern Tennessee are consistent with such a model. Conclusions reached from this and other studies suggest that major earthquakes have happened or could happen in southeastern Tennessee.	
		14. DOCUMENT ANALYSIS -- a. KEYWORDS/DESCRIPTORS		15. AVAILABILITY STATEMENT	
b. IDENTIFIERS/OPEN ENDED TERMS		Seismicity Georgia Induced Seismicity Alabama Earthquake Models Tennessee		Unlimited	
		16. SECURITY CLASSIFICATION		(This page)	
		17. NUMBER OF PAGES		Unclassified	
		18. PRICE		(This report)	
				Unclassified	

THIS DOCUMENT WAS PRINTED USING RECYCLED PAPER.

**UNITED STATES
NUCLEAR REGULATORY COMMISSION
WASHINGTON, D.C. 20555**

OFFICIAL BUSINESS
PENALTY FOR PRIVATE USE, \$300

SPECIAL FOURTH-CLASS RATE
POSTAGE & FEES PAID
USNRC
PERMIT No. G-67

6